

**UCSF**

**UC San Francisco Electronic Theses and Dissertations**

**Title**

Design of DNA nanoparticulates for convection enhanced delivery to the brain

**Permalink**

<https://escholarship.org/uc/item/8955999t>

**Author**

MacKay, John Andrew

**Publication Date**

2005

Peer reviewed|Thesis/dissertation

Design of DNA Nanoparticulates for Convection Enhanced Delivery to the Brain

by  
John Andrew MacKay  
S.B., Massachusetts Institute of Technology, 1999

DISSERTATION

Submitted in partial satisfaction of the requirements for the degree of

DOCTOR OF PHILOSOPHY

in the

Joint Graduate Group in Bioengineering

in the

GRADUATE DIVISIONS

of the

UNIVERSITY OF CALIFORNIA SAN FRANCISCO

and

UNIVERSITY OF CALIFORNIA BERKELEY

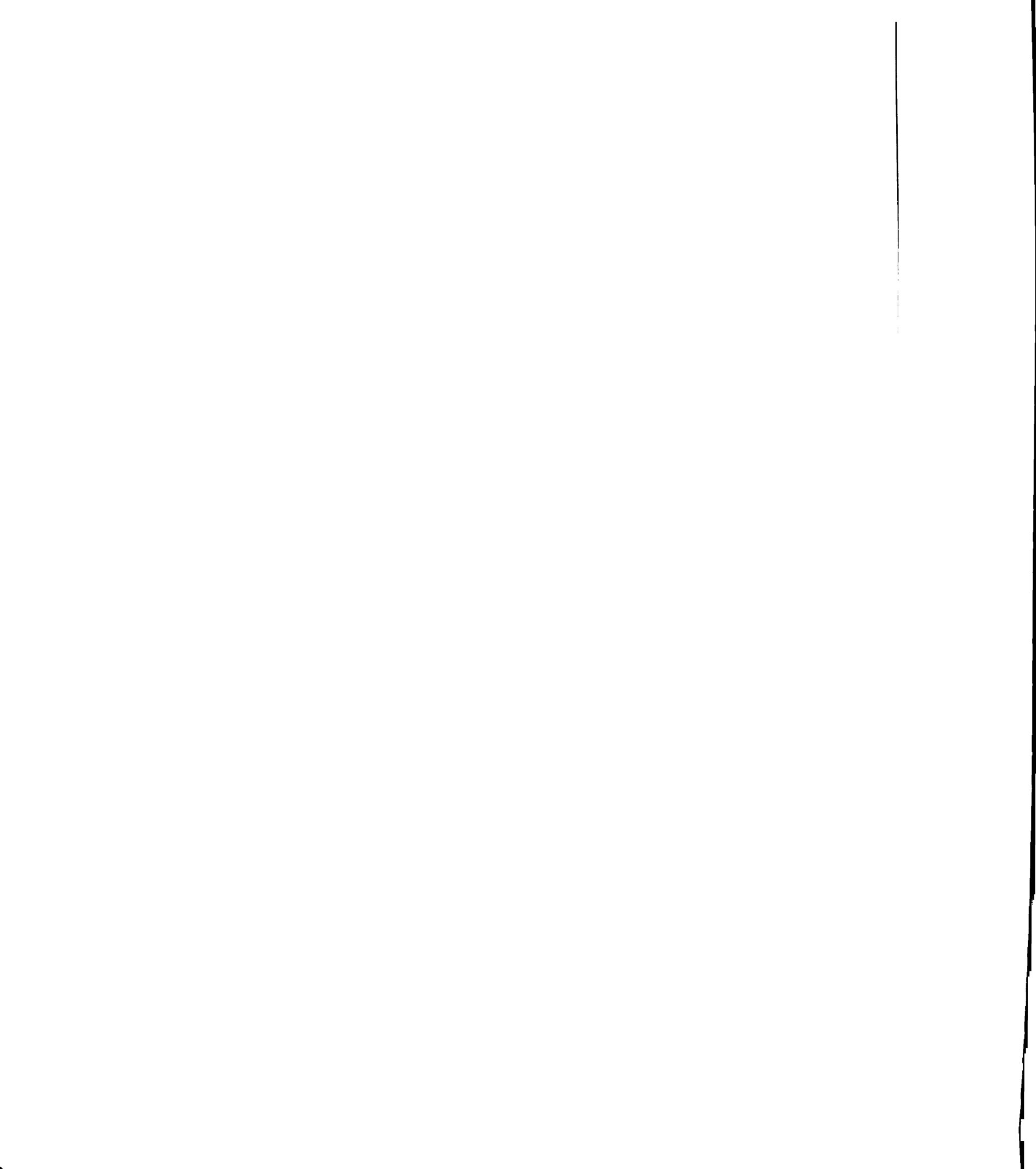


11007 1 1007 1



**Copyright 2005**  
**By**  
**John Andrew MacKay**

11007 1 10 2005



**Dedicated to my wife, Adrienne,  
who inspires me each day  
to enjoy life.**

Many people have  
described in this  
providing me with  
experience. I would  
as my co-mentor

I want to acknowledge  
committee and my  
Prof. Verkman. It  
been possible.

I especially want  
work, including  
collaborating on  
and Dr. J. Sperndt  
PEG-lipid conjugates  
the confocal microscope  
containing particles  
cationic lipid. Dr.  
for formulating the  
collection of TAT  
of microscopy, scanning  
proofreading, and  
Lamborn for advice,  
Tihan for neuropathology,  
Santos for instruction,  
remaining members  
Park, V. Platt, E. Johnson

This work was carried out  
BR01EB002047, and was  
generously supported

Lastly, thank you to  
science.

## ACKNOWLEDGEMENTS

Many people have generously contributed their time and advice to the work and analysis described in this dissertation. In particular, I want to thank Prof. Francis C Szoka Jr. for providing me with mentorship, fresh ideas, and the benefit of his experimental experience. I would also like to extend special thanks to Prof. Dennis F Deen for serving as my co-mentor and introducing me to the field brain tumor research.

I want to acknowledge the faculty members kind enough to serve on my oral examination committee and my dissertation committee, Prof. Bankiewicz, Prof. Schaffer, Prof. Healy, Prof. Verkman, and Prof. Kroetz. Without their guidance this project would not have been possible.

I especially want to thank those who have contributed to the formation of this body of work, including Dr. X Guo for first synthesizing the pH sensitive lipid, POD, and for collaborating on the kinetic characterization of POD liposome collapse, Dr. W Chuang and Dr. J Sperinde for their mentorship in the synthesis of the TATp-lipid and TATp-PEG-lipid conjugates, Dr. R Eliaz and Dr. L Uyechi for instruction and assistance with the confocal microscope, Dr. J Choi for optimizing the formulation of pH sensitive DNA-containing particles, Dr. Z Huang for preparing both POD and a disulfide reducible cationic lipid, Dr. W Li for optimization of bioresponsive DNA-containing particles and for formulating the reduction sensitive particles, E Dy for assistance with animals and the collection of TAT liposome kinetics data, E Fricovsky and A MacKay for the preparation of microscopy sections, G Huynh for assistance with animal experiments and proofreading, and S Grube for collecting content release data. I am also indebted to Dr. K Lamborn for advice regarding the statistical evaluation of the radii of distribution, Dr. T Tihan for neuropathology expertise, and Dr. T Ozawa, Dr. M Papadopoulos, and R Santos for instruction in surgical technique. It has been a pleasure to work with all the remaining members of the group, thank you to M Gundry, J Park, R Nagatani, R Cohen, J Park, V Platt, E Johansen, Dr. M Rashkin, Dr. D Ruhela, Dr. V Sidarov, and Dr. X Wen.

This work was carried out with funding provided by NIH CA-85356, NIH NS42927, NIH 8R01EB002047, and NIH R01CA107268. The Howard Hughes Medical Institute generously supported my graduate education in the form of a predoctoral fellowship.

Lastly, thank you to my family and grandparents for always strengthening my curiosity in science.



## Design

Novel treatment  
brain tumors.  
central nervous  
optimization and

To test this hypothesis  
binding to cells and  
barriers to nanoparticle  
delivery (CED). To  
stabilize fusogenic  
of PODS2000 (PEG)  
liposomes conform to  
surface coverage stability  
surface induces passive  
internalization, a peptide  
aqueous interface or surface  
binding and internalization

# **Design of DNA Nanoparticulates for Convection Enhanced Delivery to the Brain**

by John Andrew MacKay

## **ABSTRACT**

Novel treatments, such as gene therapy, are urgently needed for patients with primary brain tumors. My hypothesis is that barriers to gene therapy using nanoparticles in the central nervous system (CNS) can be overcome by a combination of nanoparticle optimization and delivery directly into the brain.

To test this hypothesis I synthesized and characterized molecules to increase nanoparticle binding to cells and enhance DNA escape from the endosome. I also characterized CNS barriers to nanoparticle distribution infused by a procedure called convection enhanced delivery (CED). To enhance non-viral gene delivery, low pH sensitive PEG lipids that stabilize fusogenic liposomes were characterized. The kinetics of pH-triggered collapse of PODS2000 (PEG=2000Da) and PODS750 (PEG=750Da) phosphatidylethanolamine liposomes conform to a “minimum surface shielding” model, whereby a critical PEG surface coverage stabilizes the bilayer. Below about 2.5% POD, the exposure of a PE surface induces particle collapse and promotes transfection. To increase cell internalization, a peptide (TATp) was attached to liposomes, either at the phospholipid-aqueous interface or separated by a PEG linker. Both TATp lipids promote cell surface binding and internalization.

When infused by

Neutral liposomes

neutral liposomes

elimination of a

distribution of flu

least two days. F

nanoparticle distr

nanoliposomes c

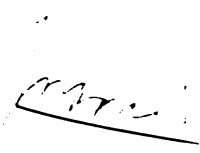
following CED to

designed non-viral

within the CNS and

a strategy to contro

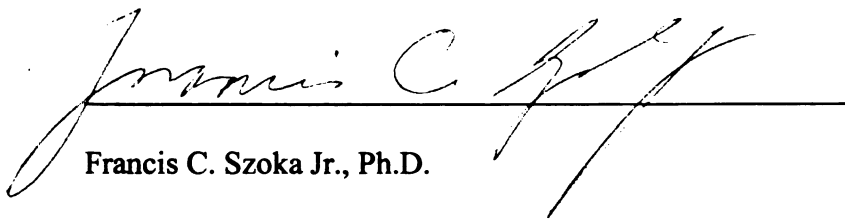
Thesis Committee C



Francis C. Szoka Jr.

When infused by CED, liposome distribution depends upon diameter and surface charge. Neutral liposomes accumulate in perivascular cells within the brain. These cells eliminate neutral liposomes from the interstitial fluid with a  $9.9 \pm 2.0$  hr half-life as determined by elimination of a degradable radiolabeled lipid and by analysis of the time dependent distribution of fluorescence. A non-biodegradable lipid remains within these cells for at least two days. Positive surface charge (10% by mole lipid) dramatically reduces nanoparticle distribution from the infusion site. Incorporation of TATp-PEG-lipid into nanolipoparticles containing DNA, increased binding to and transfection of tumor cells following CED to an intracranial tumor. These results support my hypothesis that better designed non-viral gene vectors will overcome limitations to distribution and transfection within the CNS and suggest that optimization of CED using nanoparticulates will require a strategy to control particle binding and clearance by cells within the CNS.

Thesis Committee Chairman



Francis C. Szoka Jr., Ph.D.

PRELIMINARY

- List of Tables
- List of Figures
- List of Abbreviations

CHAPTER 1:

- 1.1 Introduction
- 1.2 Overcoming Barriers
  - 1.2.1 Barrier 1: ...
  - 1.2.2 Barrier 2: ...
  - 1.2.3 Barrier 3: ...
  - 1.2.4 Barrier 4: ...
  - 1.2.5 Barrier 5: ...
- 1.3 Formulation
- 1.4 Summary

CHAPTER 2:

- 2.1 Introduction
- 2.2 Methods
  - 2.2.1 Materials
  - 2.2.2 Formation of ...
  - 2.2.3 Liposome ...
  - 2.2.4 Determination of ...
  - 2.2.5 Statistical analysis
- 2.3 Results
  - 2.3.1 Effect of PEG ...
  - 2.3.2 Effect of pH ...
  - 2.3.3 Stabilization of ... near-critical ...
  - 2.3.4 Determination of ...
  - 2.3.5 POD Derivatives

## TABLE OF CONTENTS

### PRELIMINARY PAGES:

List of Tables	xi
List of Figures	xii
List of Abbreviations	xiv

### CHAPTER 1: **Design of DNA Nanoparticulates for Improved Intracellular Transport for Use in Convection Enhanced Delivery to the Brain**

1.1	Introduction	1
1.2	Overcoming barriers for non-viral gene therapy in the CNS	2
1.2.1	Barrier 1: Protection of the DNA	3
1.2.2	Barrier 2: Localize delivery to the CNS	3
1.2.3	Barrier 3: Cell-binding and internalization	5
1.2.4	Barrier 4: Endosomal escape	6
1.2.5	Barrier 5: DNA transport to the nucleus	7
1.3	Formulation of the ideal non-viral particle	7
1.4	Summary	10

### CHAPTER 2: **Optimization of Nanoparticulates: The Kinetic Characterization of a pH Sensitive Lipid (POD)**

2.1	Introduction	11
2.2	Methods	12
2.2.1	Materials	12
2.2.2	Formation of liposomes	13
2.2.3	Liposome leakage assay	14
2.2.4	Determination of the duration of lag phase	15
2.2.5	Statistical analysis using the “Minimum Surface Shielding” model	18
2.3	Results	19
2.3.1	Effect of PEG chain length on Leakage	20
2.3.2	Effect of pH on content leakage	23
2.3.3	Stabilization of POD liposomes with near-critical amount of pH insensitive lipids	25
2.3.4	Determination of $t_{lag}$ for PODS750 and PODS2000	27
2.3.5	POD Derivatives follow the “minimum surface shielding” model	29

2.3.6 Effect of

2.3.7 Determination

2.4 Discussion

2.5 Conclusion

## CHAPTER 3:

3.1 Abstract

3.2 Introduction

3.3 Methods

3.3.1 Materials

3.3.2 Preparation

3.3.3 Preparation

3.3.4 Preparation

3.3.5 Osmotic pressure

3.3.6 Acute toxicity

3.3.7 Section preparation

3.3.8 Confocal microscopy

3.3.9 Data analysis

3.3.10 Statistical analysis

3.4 Results

3.4.1 Liposome characterization

3.4.2 Elimination of

3.4.3 Validation of

3.4.4 Comparing

3.4.5 Positive surface

3.4.6 Particle size

3.4.7 Effect of polymer

3.4.8 Effect of excipient

3.5 Discussion

3.5.1 Effects of particle

3.5.2 Long duration

3.5.3 Fate of nanoparticles

3.6 Conclusion

2.3.6	Effect of membrane permeability of buffer on content release	32
2.3.7	Determination of hydrolysis rate and minimum stabilization percentage	35
2.4	Discussion	36
2.5	Conclusions	43

**CHAPTER 3: Convection Enhanced Delivery: Liposome Distribution in Brain after Modulation of Particle Charge, Particle Diameter, and Presence of Steric Coating**

3.1	Abstract	44
3.2	Introduction	45
3.3	Methods	46
3.3.1	Materials	46
3.3.2	Preparation of liposomes	47
3.3.3	Preparation of nanolipoparticles	48
3.3.4	Preparation of radiolabeled liposomes	50
3.3.5	Osmotic pump infusion	50
3.3.6	Acute stereotactic infusion	52
3.3.7	Section preparation and macroscopic imaging	52
3.3.8	Confocal microscopy	53
3.3.9	Data analysis	54
3.3.10	Statistical analysis	55
3.4	Results	56
3.4.1	Liposome co-infusion into the rat brain	57
3.4.2	Elimination of liposomes from the brain	61
3.4.3	Validation of co-infusion measurements	63
3.4.4	Comparing co-infused particle radii of distribution	66
3.4.5	Positive surface charge restricts particle distribution by CED	68
3.4.6	Particle size restricts distribution by CED	71
3.4.7	Effect of polyethylene glycol steric shielding	73
3.4.8	Effect of excess liposomes	73
3.5	Discussion	74
3.5.1	Effects of particle composition on CED	75
3.5.2	Long duration CED in small animal models	79
3.5.3	Fate of nanoparticles infused into the human brain	80
3.6	Conclusion	82



## CHAPTER 4:

- 4.1 Abstract
- 4.2 Introduction
- 4.3 Methods
  - 4.3.1 Calculations
  - 4.3.2 Mathematical models
  - 4.3.3 Estimation of parameters
  - 4.3.4 Estimation of model errors
- 4.4 Results
  - 4.4.1 Determination of model parameters
  - 4.4.2 Positive and negative results
  - 4.4.3 Enhancement of model results
- 4.5 Discussion
- 4.6 Conclusion

## CHAPTER 5:

- 5.1 Abstract
- 5.2 Introduction
- 5.3 Methods
  - 5.3.1 Materials
  - 5.3.2 Synthesis and purification
  - 5.3.3 Preparation of samples
  - 5.3.4 In vitro uptake
  - 5.3.5 Formation of aggregates
  - 5.3.6 Incorporation of dyes
  - 5.3.7 Implantation of samples
  - 5.3.8 Convection enhanced delivery
  - 5.3.9 Macroscopic imaging
  - 5.3.10 Fluorescence imaging
- 5.4 Results
  - 5.4.1 Properties of liposomes
  - 5.4.2 Validation of imaging techniques

**CHAPTER 4: Convection Enhanced Delivery: A Mathematical Model with First Order Binding**

4.1	Abstract	83
4.2	Introduction	83
4.3	Methods	88
4.3.1	Calculation of the Peclet number	88
4.3.2	Mathematical model of CED with first order elimination	88
4.3.3	Estimation of binding constant from fluorescence microscopy	89
4.3.4	Estimation of elimination constant from radiolabel half-life	89
4.4	Results	90
4.4.1	Determination of a binding constant for neutral liposomes	90
4.4.2	Positive charge increases the binding constant of liposomes	93
4.4.3	Enhancement of distribution by adding excess liposomes	95
4.5	Discussion	96
4.6	Conclusion	97

**CHAPTER 5: Optimization of Nanoparticulates: Synthesis and Characterization of an HIV TAT peptide Ligand to Promote Cell Internalization**

5.1	Abstract	98
5.2	Introduction	99
5.3	Methods	100
5.3.1	Materials	100
5.3.2	Synthesis and purification of TATp and TATp lipids	101
5.3.3	Preparation of liposomes	105
5.3.4	In vitro uptake of TATp modified radiolabeled liposomes	107
5.3.5	Formation of bioresponsive NLP	108
5.3.6	Incorporation of TATp into NLP	109
5.3.7	Implantation of U87-MG tumors in athymic rat brains	110
5.3.8	Convection enhanced delivery by acute stereotactic infusion	110
5.3.9	Macroscopic imaging	111
5.3.10	Fluorescence microscopy	112
5.4	Results	113
5.4.1	Properties of liposomes for radiolabel assays	114
5.4.2	Validation of high salt washing	115

- 5.4.3 Lipos
- 5.4.4 TATp
- 5.4.5 Effect
- 5.4.6 2000 L
- 5.4.7 Lipos
- 5.4.8 DNA
- 5.4.9 Conve

5.5 Discus

5.6 Conclu

## APPENDIX A

A.1 Abstract

A.2 Introduct

A.3 Other per

A.4 Promising

A.5 Mechanis

A.6.1 Applicatio

A.6.2 Applicatio

A.6.3 Applicatio

A.6.4 Applicatio

A.6.5 Applicatio

A.6.6 Applicatio

A.7 Conclusions

## REFERENCES

5.4.3	Liposome binding is dependent upon method of chemical attachment	118
5.4.4	TATp modified liposomes internalize at low temperature	120
5.4.5	Effect of TATp surface density on liposome binding	121
5.4.6	2000 Da PEG can shield binding and uptake of TATp liposomes	121
5.4.7	Liposome size does not affect kinetics of binding	123
5.4.8	DNA NLP bind and transfect more efficiently after TATp modification	123
5.4.9	Convection enhanced delivery of TATp nanoparticles to the rat brain	125
5.5	Discussion	128
5.6	Conclusion	132

**APPENDIX A: Review: HIV TAT Protein Transduction Domain Mediated Cell Binding and Intracellular Delivery of Nanoparticles**

A.1	Abstract	133
A.2	Introduction	134
A.3	Other peptides with properties similar to TATp	136
A.4	Promising aspects of TATp research	136
A.5	Mechanism	137
A.6.1	Applications: Polymers	140
A.6.2	Applications: Complexes	141
A.6.3	Applications: Shell Cross-Linked Nanoparticles	142
A.6.4	Applications: Nanoparticles	143
A.6.5	Applications: Liposomes	145
A.6.6	Applications: Phage	148
A.7	Conclusions	149
	<b>REFERENCES</b>	<b>151</b>

Table 2-1.

Table 2-2.

Table 3-1.

Table 3-2.

Table 3-3.

Table 5-1.

Table A-1:

Co

me

## LIST OF TABLES

Table 2-1.	PODS750: Comparison of predicted and observed lag times	28
Table 2-2.	PODS2000: Comparison of predicted and observed lag times	29
Table 3-1.	Compositions and characteristics of polymers and particles used in CED experiments	49
Table 3-2.	Disposition of radiolabeled liposomes following convection enhanced delivery	62
Table 3-3.	Summary of radii of distribution by fluorescent markers	67
Table 5-1.	Compositions and characteristics of polymers and particles used in TATp binding experiments	106
Table A-1:	Comparison of multi-valent cationic peptide modifications of nanoparticles	135

- Figure 1-1. S
- Figure 1-2. Lu  
D
- Figure 2-1. D
- Figure 2-2. PC
- Figure 2-3. pH
- Figure 2-4. pH
- Figure 2-5. La
- Figure 2-6. Eff
- Figure 2-7. PO  
"m
- Figure 2-8. Pred
- Figure 3-1. Con  
to fl
- Figure 3-2. Illus  
distr
- Figure 3-3. Effect
- Figure 3-4. Influe  
on lip
- Figure 3-5. Comp
- Figure 4-1. Predic
- Figure 4-2. Calcul
- Figure 5-1. Struct
- Figure 5-2. High su

## LIST OF FIGURES

Figure 1-1.	Structure of POD	7
Figure 1-2.	Idealized formation of a PEG shielded non-viral DNA nanolipoparticle	9
Figure 2-1.	Determination of lag time ( $t_{lag}$ ) by the derivation method	17
Figure 2-2.	POD liposome leakage is PEG chain length dependent	22
Figure 2-3.	pH-dependent leakage of POD liposomes at 37°C	24
Figure 2-4.	pH-insensitive PEG-lipid stabilizes POD liposomes	26
Figure 2-5.	Lag time is a function of the initial percent POD	31
Figure 2-6.	Effect of buffer on PODS2000 pH-dependent leakage	34
Figure 2-7.	PODS750 and PODS2000 follow the “minimum surface shielding model”	41
Figure 2-8.	Prediction of time to burst for PODS2000 liposomes	42
Figure 3-1.	Comparison of the distribution of fluorescent liposomes to fluorescent 10 kD dextran after co-infusion using CED	59
Figure 3-2.	Illustration of data analysis of fluorescence distribution in brain sections	65
Figure 3-3.	Effect of surface charge on liposome distribution after CED	69
Figure 3-4.	Influence of particle diameter, PEG lipids, and excess lipid on liposome distribution after CED	72
Figure 3-5.	Comparison of particles co-infused by CED	76
Figure 4-1.	Prediction of liposome concentration profile	92
Figure 4-2.	Calculated elimination rate constants for different liposomes	94
Figure 5-1.	Structures of TATp ligands	104
Figure 5-2.	High salt washes remove surface bound TATp liposomes	117



Figure 5-3. E  
t

Figure 5-4. E  
d

Figure 5-5. T

Figure 5-6. C  
to

## LIST OF FIGURES (Continued)

Figure 5-3.	Effect of temperature and concentration on the binding kinetics of TATp liposomes.	119
Figure 5-4.	Effect of TATp density, PEG shielding, and particle diameter on binding kinetics	122
Figure 5-5.	TATp-PEG-lipid enhances particle binding and transfection	124
Figure 5-6.	Convection enhanced delivery of TATp modified particles to the rat brain	127

H-Chol: t  
1-BPE: 1  
A: c  
e  
A: 11  
ANTS: 8  
AUC: a  
C: c  
C: c  
CAT: c  
CED: c  
CF-PE: 1.  
Chol: ch  
CLIO: cro  
CNS: cer  
CSF: cer  
DOPE: 1.2  
DiD: 1.1  
DiO: 3.3  
DiI: 1.1  
DOPE: 1.2  
DOTAP: 1.2-  
Dox: dox  
DPX: p-xy  
DPTAP: 1.2-  
DSPC: 1.2-  
DSPG: 1.2-  
DSTAP: 1.2-  
FACS: fluor  
FITC: fluor  
GFP: green  
HEPES: (hydr  
HIV: huma  
HSPG: hepar  
k. Chap  
LLV: Chap  
NLP: large  
Pe: DNA  
PE: Peclet  
PEG: diacyl  
PEG-DSG: polyeth  
PEG-DSPE: 1,2-dis  
1,2-dis

## LIST OF ABBREVIATIONS

<sup>3</sup> H-Chol:	tritiated cholesteryl hexadecyl ether
<sup>125</sup> I-BPE:	iodinated benzamidine phosphatidylethanolamine
A <sub>c</sub> :	critical POD mole percentage needed to stabilize a phosphatidyl ethanolamine liposome
A <sub>o</sub> :	initial mole percentage of POD in the bilayer
ANTS:	8-aminonaphthalene-1,2,3-trisulfonic acid;
AUC:	area under the curve
C <sub>(r,t)</sub> :	concentration
C <sub>infusion</sub> :	concentration at the point of infusion
CAT:	chloramphenicol acetyltransferase
CED:	convection enhanced delivery
CF-PE:	1,2-dioleoyl-sn-glycero-3-phosphoethanolamine-n-(carboxyfluorescein)
Chol:	cholesterol
CLIO:	cross-linked iron-oxide
CNS:	central nervous system
CSF:	cerebrospinal fluid
DOPE:	1,2-dioleoyl-phosphatidylethanolamine
DiD:	1,1'-dioctadecyl-3,3,3',3'- tetramethylindodicarbocyanine perchlorate
DiO:	3,3'-dioctadecyloxacarboxyanine perchlorate
DiI:	1,1'-dioctadecyl-3,3,3',3'- tetramethylindodicarbocyanine perchlorate
DOPE:	1,2 dioleoylphosphatidylethanolamine
DOTAP:	1,2-dioleoyl-3-trimethylammonium-propane
Dox:	doxorubicin
DPX:	<i>p</i> -xylenebis(pyridinium) bromide
DPTAP:	1,2-dipalmitoyl-3-trimethylammonium-propane
DSPC:	1,2-distearoyl-sn-glycero-3-phosphocholine
DSPG:	1,2-distearoyl-sn-glycero-3-phosphoglycerol
DSTAP:	1,2-distearoyl-3-trimethylammonium-propane
FACS:	fluorescence activated cell sorting
FITC:	fluorescein isothiocyanate
GFP:	green fluorescent protein
HEPES:	(hydroxyethyl)piperazine- <i>N</i> -2-ethanesulfonic acid
HIV:	human immunodeficiency virus
HSPG:	heparan sulfate proteoglycans
<i>k</i> :	Chapter 2: hydrolysis rate constant of POD [M <sup>-1</sup> sec <sup>-1</sup> ] Chapter 4: cell uptake rate constant [sec <sup>-1</sup> ]
LUV:	large unilamellar vesicles
NLP:	DNA containing nanolipoparticle
Pe:	Peclet number
PE:	diacyl phosphatidyl ethanolamine
PEG:	polyethylene glycol
PEG-DSG:	1,2-distearoyl-sn-glycero-3- (polyethyleneglycol)2000
PEG-DSPE:	1,2-distearoyl-sn-glycero-3-phosphoglycerol-N-(polyethyleneglycol)2000

## LIST OF ABB:

POD:	5
PODS750:	F
PODS2000:	F
PODS5000:	F
POPC:	1
POPE:	1
Rh-PE:	1
	ri
q:	v
r:	ra
<i>r<sub>max</sub></i> :	ra
<i>r<sub>min</sub></i> :	ra
<i>r<sub>use</sub></i> :	ou
SCK:	sh
SPLP:	st
SUV:	sm
<i>t</i> :	ha
TAR:	tran
TAT:	tran
TATp:	TA
<i>t<sub>lag</sub></i> :	lag
TRIS:	trist
XS:	ind
•:	extra

## LIST OF ABBREVIATIONS (Continued)

POD:	polyethylene glycol -diortho ester-distearoyl glycerol
PODS750:	polyethylene glycol 750-diortho ester-distearoyl glycerol
PODS2000:	polyethylene glycol 2000-diortho ester-distearoyl glycerol
PODS5000:	polyethylene glycol 5000-diortho ester-distearoyl glycerol
POPC:	1-palmitoyl-2-oleoyl-sn-glycero-3-phosphatidylcholine
POPE:	1-palmitoyl-2-oleoylphosphatidylethanolamine
Rh-PE:	1,2-dipalmitoyl-sn-glycero-3-phosphoethanolamine-N-(lissamine rhodamine B sulfonyl)
$q$ :	volumetric flowrate [ $\mu\text{L min}^{-1}$ ]
$r$ :	radius from tip of infusion cannula
$r_{50\% AUC}$ :	radius, where 50% of the area under the curve is reached
$r_{50\% max}$ :	radius, where intensity is half of the maximum intensity
$r_{wave}$ :	outer radius reached by wave of convection
SCK:	shell cross linked
SPLP:	stabilized plasmid lipid particle
SUV:	small unilamellar vesicles
$t_{1/2}$ :	half-life for elimination of radiolabel from brain
TAR:	trans activator response element
TAT:	trans-acting transcriptional activator
TATp:	TAT derived basic peptide
$t_{lag}$ :	lag time until particle collapse begins
TRIS:	tris(hydroxymethyl)aminomethane
XS:	indicates excess liposomes
$\phi$ :	extracellular fraction in brain

## **CHAPTER 1:**

### **Design of DNA Nanoparticulates for Improved Intracellular Transport for Use in Convection Enhanced Delivery to the Brain**

#### **1.1 Introduction**

The hypothesis of my research is that biological barriers to nucleic acid delivery in the central nervous system (CNS) can be overcome by local delivery directly into the brain (Chapters 3,4) and by design of molecules that exploit aspects of cellular trafficking pathways (Chapters 2,5). This goal required the determination of distribution barriers and elimination properties when nanoparticles are infused directly into the CNS. It also required the synthesis and characterization of small molecules designed to increase binding to cells and enhance escape from the endosome subsequent to internalization.

Primary brain tumors affect 17,000 patients a year in the United States alone [American Cancer Society 2002]. The mortality rate for those diagnosed with brain tumors is high, so there is a strong need for improved treatments. The clinical goal of this research is to develop a non-viral gene therapy for primary brain tumors, which may also have application to many other types of metastatic cancer found in the brain [Kaye and Laws 1995]. Proposed non-viral gene therapies involve expressing a 'suicide' gene within the tumor. Such therapies include cytokines (example: IL-12), inducers of apoptosis (example: BAX), or enzymes capable of converting non-toxic drug to chemotherapeutic drug (example: cytosine deaminase converts 5-fluorocytosine to 5-fluorouracil). Additionally, the use of tumor specific promoters may enable gene therapy to kill only

tumor cells, without affecting normal tissue. As an example, the uncontrolled growth of tumor creates poorly oxygenated regions within the tumor. Cells under low oxygen up-regulate DNA sequences with hypoxia response elements (HRE) before the promoter. In gene therapy studies, the incorporation of HRE into the promoter of a suicide gene enables tumor specific expression [Ruan *et al.* 2001]. While many suicide gene approaches have shown promise, the therapeutic applications of gene therapy remain limited by the inability to safely deliver and express the gene within a tumor. Thus, the goal of this thesis was to develop techniques that enable efficient and widespread non-viral gene delivery.

## **1.2 Overcoming barriers for non-viral gene therapy in the CNS**

Cationic DNA lipoplex, a commonly used *in vitro* non-viral vector, has not been designed to enable *in vivo* transfection. The high density positive charge (50% by mole lipid) on cationic lipoplexes that makes them effective *in vitro*, causes rapid elimination from systemic circulation and local toxicity *in vivo*. Recent efforts to boost non-viral transfection have been driven by the view that viral behaviors can be imitated by a DNA-containing liposome [Kaneda 2000]. Viruses have evolved optimized strategies for overcoming the barriers to transfection. Thus, by mimicking specific viral properties, including cell-surface binding and endosomal escape, it may be possible to boost the efficiency of non-viral DNA particles.

Within this section, the main barriers to *in vivo* non-viral gene therapy have been organized as follows: 1. The DNA must be formulated into a protected particle prior to



delivery; 2. The particle must target/localize within the CNS; 3. The particle must bind and internalize into a target cell within the CNS; 4. The particle must release its DNA to the cytoplasm and bypass DNase degradation in a lysosome; and 5. The DNA must be trafficked into the nucleus to enable gene expression.

### *1.2.1 Barrier 1: Protection of the DNA*

*In vivo* non-viral DNA delivery requires the formulation of a small particle, not unlike a virus, with a protective coat around a plasmid. The purpose of the coat is to protect the DNA from both intracellular and extracellular DNase activity. In this project, liposomes have been used as the platform for coating DNA. Liposomes are self-assembling vesicles that can be modified simply by mixing in other lipidated molecules. The DNA containing nanolipoparticles (NLP) discussed in this thesis, are composed primarily of phospholipids similar to those found in biological membranes and are relatively non-toxic and non-immunogenic when administered into patients. To encapsulate DNA, modifications were made to a detergent dialysis technique based upon the Stabilized Plasmid Lipid Particle (SPLP) [Mok *et al.* 1999, Tam *et al.* 2000]. SPLP are small, PEG-shielded particles. SPLP circulate for a prolonged period in the body and do not induce an inflammatory response [Tam *et al.* 2000]. SPLP have not produced robust transfection *in vivo*, but the addition of functionalized molecules may improve this formulation greatly.

### *1.2.2 Barrier 2: Localize delivery to the CNS*

In order to transfect, non-viral vectors must be delivered to the *in vivo* site of action. One approach is systemic administration, which requires that the particle circulate for long

times in the b  
obstacles assoc  
penetration of  
difficulties asso  
focused on a m  
enhanced delive

CED therapy co  
and a pump tha  
systemic admini  
delivery duration  
(diffusion control  
such as the brain  
millimeters [Bobo  
chance of being sc  
to cover a tumor.  
distribution is limite

Within animal mode  
Low flowrates, from  
the brain volume in r  
and monkeys [Lieber  
been successfully us

times in the blood before binding to a target site via a targeting ligand. There are obstacles associated with this type of administration, including clearance to the liver and penetration of the blood brain barrier. For this research project, I chose to bypass the difficulties associated with targeting the CNS via systemic administration. Instead I focused on a more straightforward, localized approach, a technique called convection enhanced delivery (CED).

CED therapy consists of an infusion cannula placed stereotactically in the parenchyma and a pump that pushes solutions through the tissue for an extended period. Unlike systemic administration, CED enables control over drug location, concentration, and delivery duration. CED is potentially superior to direct injection in small volumes (diffusion controlled) because macromolecules and nanoparticles placed in a dense tissue, such as the brain or solid tumor, tend to diffuse only short distances, on the order of millimeters [Bobo *et al.* 1994, Lonser *et al.* 2002]. Thus, direct injection has a poor chance of being scaled up for humans where drug must travel at least several centimeters to cover a tumor. Alternatively, CED appears highly scalable because the volume of distribution is limited only by the duration of flow and the flowrate.

Within animal models, CED has been successful at delivering a variety of compounds. Low flowrates, from 0.1 to 0.5  $\mu\text{L}$  per min, can deliver proteins to greater than 30% of the brain volume in rats [Chen *et al.* 1999, Groothuis *et al.* 1999], cats [Bobo *et al.* 1994] and monkeys [Lieberman *et al.* 1995, Lonser *et al.* 1999 and 2002]. Recently, CED has been successfully used to distribute adeno-associated virus (30 nm in diameter) into

similar volu

2001]. In ac

al. 2004]. S

DNA partic

targeted del

NLP (Chap

### 1.2.3 Barriers

In order to g

binding and

prevent cell

impossible. S

immunodeficien

(TAT). This pep

array of molecu

internalization. F

Appendix A. In C

based on TATp. in

tumors. The TATp

internalization both

similar volumes of the brain [Bankiewicz *et al.* 2000, Hamilton *et al.* 2000, Nguyen *et al.* 2001]. In addition, liposomes have been delivered by CED [Mamot *et al.* 2004, Saito *et al.* 2004]. So it appears that prolonged infusion should enable the distribution of non-viral DNA particles throughout large volumes of brain and tumor. Thus, to overcome the targeted delivery barrier, I have investigated CED of liposomes (Chapter 3,4) and DNA NLP (Chapter 5) in hopes of optimizing a new gene therapy treatment for brain tumors.

### 1.2.3 Barrier 3: Cell-binding and internalization

In order to gain entry to a target cell, a non-viral vector must have a mechanism for binding and internalization. PEG shielded NLP have been specifically designed to prevent cell binding; furthermore, without cell-surface binding, transfection is impossible. So I prepared a peptide cell-binding ligand, based on a human immunodeficiency virus (HIV) protein, called trans-acting transcriptional activator (TAT). This peptide, RKKRRQRRR (TATp), has been successfully linked to a wide array of molecular and nanoparticulate cargo in order to enable nonspecific cell internalization. For an extensive review of TATp modified nanoparticulates refer to Appendix A. In Chapter 5, I synthesized and characterized two cell-binding ligands, based on TATp, incorporated these into NLP, and delivered these to rat intracranial tumors. The TATp ligand was remarkably efficient at promoting cell binding and internalization both *in vitro* and *in vivo*.

#### 1.2.4 Barrier 4: Endosomal escape

Non-viral access to the cytosol is mediated by the endosome membrane, the typical downstream path of internalization for cell-surface bound particles. This occurs as the cell membrane pinches inward to surround the particle and create a vesicle, the endosome. In the early endosome, the pH rapidly drops 1-2 units within 10 min [Sonawane *et al.* 2002] prior to further trafficking of the endosome to the lysosome, so escape must occur soon after internalization. Many of the details that enable a liposome to escape from the endosome have been discussed in detail [Drummond *et al.* 2000]. To use this pH drop as a trigger for particle collapse, Guo and Szoka [2001] introduced a pH sensitive ortho ester PEG-lipid (POD) (Fig. 1-1) that stabilizes a naturally unstable phosphatidylethanolamine bilayer. The ortho ester chemistry employed to prepare POD is well suited for *in vivo* applications because it can stabilize liposomes for hours at neutral pH; however, at pH 5.0 acid hydrolysis removes the PEG shield and promotes particle collapse within minutes, enabling gene transfer in cell culture [Choi *et al.* 2003]. These kinetics are ideal for creating a particle that can remain stable during convection through the brain for several hours at pH 7.4, but collapses rapidly following internalization to a cell via an endosome with low pH. Thus, to maintain stability and overcome the barrier of endosomal escape, I characterized the collapse properties of liposomes stabilized by POD (Chapter 2).

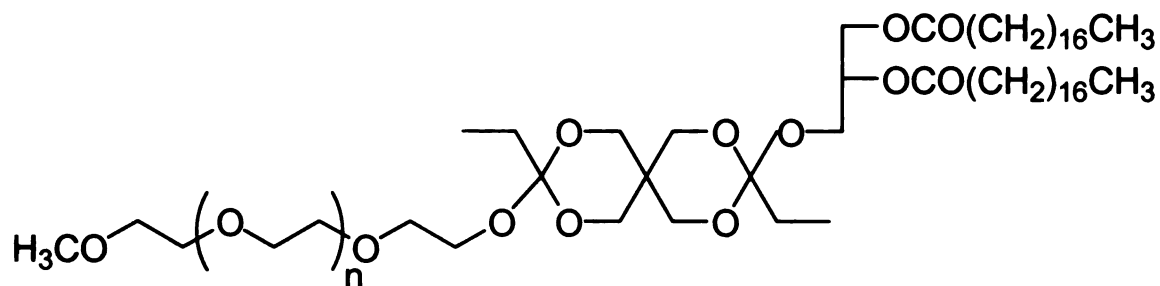


**Figure 1-1. Structure of POD.** To the left is a polyethyleneglycol polymer ( $n=43$ ) and to the right is a distearoyl glycerol lipid anchor. These two pieces are linked by an acid labile diorthoester linker. Cleavage of one orthoester removes the PEG, allowing phosphatidylethanolamine bilayers to change phase to a hexagonal aggregate.

### 1.2.5 Barrier 5: DNA transport to the nucleus

The fifth barrier to non-viral DNA delivery is transporting DNA into the nucleus, for expression. This barrier is beyond the scope of these studies; although, it is possible that the great increase in efficiency of cell internalization and endosomal rupture will produce enhancement of transfection even without optimizing a solution for this barrier.

### 1.3 Formulation of the ideal non-viral particle

Figure 1-2 illustrates the formulation of a nanolipoparticle (NLP), containing plasmid DNA. The NLP is formed by dissolving both lipid and DNA components in either a detergent or alcohol:water mixture. A fraction of the lipid is cationic, so these lipids bind to the anionic phosphate backbone of the DNA. To initiate particle formation, the detergent or alcohol is removed by dialysis. During this process, the cationic lipids remain bound to the DNA by electrostatic interactions. Hydrophobic interactions hold together the lipids, and bilayers form around the DNA. This process forms liposomes

with a minimum diameter of 60 nm, determined empirically. The optimized process is more than 90% efficient at encapsulating the DNA.

Prior to particle formation (Fig. 1-2), PEG lipids can be incorporated into the lipid mixture, sterically preventing cell-membrane binding. Alternatively, POD (Chapters 2,5) can be incorporated to yield a pH sensitive NLP. For a reduction sensitive NLP, a disulfide reducible cationic lipid can be employed. Incorporation of a disulfide reducible cationic lipid allows removal of surface positive charge after particle formation. Disulfide reducible cationic lipid could also enhance transfection by releasing DNA once access to the cytosol is achieved (Chapter 5). Finally, DNA can be functionalized with a peptide sequence, such as a motor protein or nuclear localization sequence, which will eventually carry the DNA from the cytoplasm to the nucleus.

After particle formation (Fig. 1-2), the surface of the particle has residual cationic charge. This cationic charge can contribute to cell binding and internalization, even when shielded by PEG lipids (Chapter 3). If a disulfide reducible cationic lipid is used, then the surface positive charge can be replaced by disulfide exchange to neutral or negatively charged headgroups. To re-initiate particle binding, a targeting ligand can be incorporated by attaching it first to the end of a PEG-lipid. These PEG-lipids form micelles that can insert into the bilayer of previously formed particles. This ligand can be either receptor specific or nonspecific, such as TATp (Chapter 5).

1007 1 2011



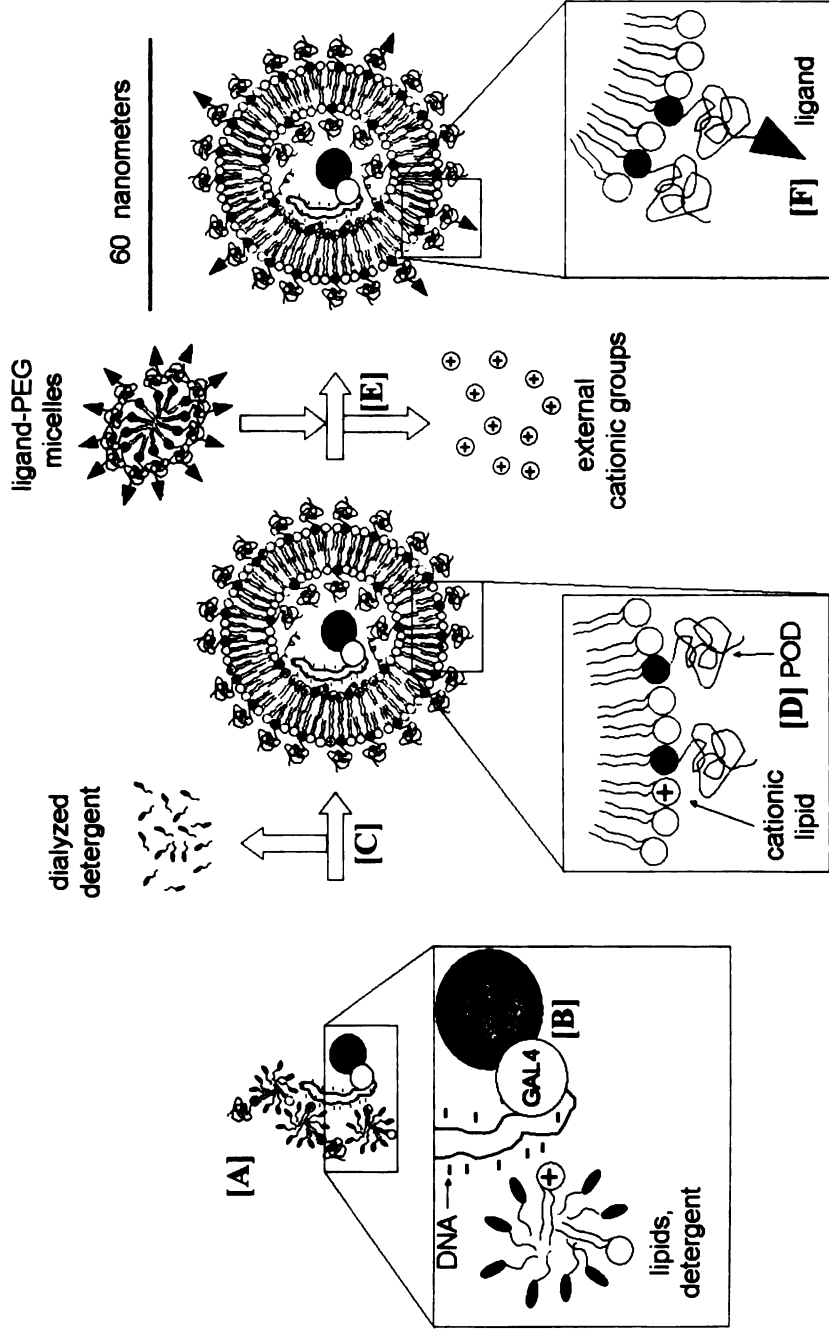


**Figure 1-2. Idealized formation of a PEG shielded non-viral DNA nanolipoparticle (NLP).** [A] The DNA is attracted to cationic lipids within detergent micelles, that may carry other neutral lipids. [B] A nuclear targeting protein is bound to the DNA, by a GAL4 DNA binding domain that uses molecular motor proteins within the cell. [C] Dialysis removes detergent, allowing the formation of small plasmid-containing particles. The resulting bioresponsive particle is functionalized as desired: [D] A pH sensitive PEG lipid (POD) hydrolyzes within the endosome to promote delivery to the cytoplasm; [E] Residual positive charge, used for compacting DNA, is eliminated through the reduction of a disulfide cationic lipid; furthermore, this may eliminate nonspecific binding to negatively charged extracellular matrix and proteoglycans; [F] Ligands attached to PEG lipid micelles, such as TATp, are diffused into the preformed particle to boost target cell binding.

UNIVERSITY OF MICHIGAN

#### 1.4 Summary

The goal of this project has been to investigate *in vivo* the transfection efficiency of DNA containing nanolipoparticles (NLP) following convection enhanced delivery (CED). To do so, I made use of both a cell binding ligand (TATp) to gain entry to the cell and a pH sensitive lipid (POD) to release DNA from the endosome. By using CED, I was able to sidestep the problem of systemic clearance following intravenous injection. For therapeutic use, this vector could carry one of several suicide genes that could potentially target and kill tumor cells, such as cytosine deaminase, thymidine kinase, or Bax. Success in developing a vector that can be infused throughout brain tumors could have an immediate clinical impact.

11007 11007 11007

## CHAPTER 2:

### Optimization of Nanoparticulates: The Kinetic Characterization of a pH Sensitive Lipid (POD)

#### 2.1 Introduction

In this study, I have mathematically characterized a series of novel pH sensitive lipids, polyethyleneglycol-orthoester-distearoylglycerol lipid (POD). These lipids contain polyethyleneglycol (PEG) chains (MW = 750, 2000, and 5000 Da) that stabilize phosphatidylethanolamine (PE) in a bilayer. Under physiological conditions, unsaturated PE ensembles prefer a hexagonal phase and cannot maintain a stable bilayer; however, the presence of small fractions of PEG lipids can stabilize PE in a bilayer. Here I characterize liposomes loaded with an aqueous space marker ANTS/DPX and assay for content release as a function of pH, buffering agent, PEG molecular weight, and the presence of a pH insensitive PEG lipid [Guo *et al.* 2003, Li *et al.* 2005].

When acid-catalyzed hydrolysis lowers the mole percentage of POD on the liposome surface to a critical level, the liposomes destabilize and transition to hexagonal phase aggregates. The instability of these liposomes occurs in 2 phases: a lag phase and a burst phase. During the lag phase, few of the liposomal contents are released. The burst phase occurs when the surface density of the PEG lipid has reached a critically low level, and the bilayer to hexagonal phase conversion occurs with concomitant liposome content release. I further developed a kinetic “minimum surface shielding” model that can fit liposome content release profiles and used the model to predict the behavior of POD

functionalized liposomes. The burst phase occurs when the surface density of the PEG lipid has reached a critically low level. Using nonlinear regression, this level was estimated to be  $2.3 \pm 0.6$  mole% for PODS2000 (2000 Da PEG) and  $2.8 \pm 0.7$  mole % for PODS750 (750 Da PEG). Liposomes formed with PODS5000, (5000 Da PEG) lipids could not be analyzed by the model because they did not have distinct lag and burst phases, presumably because 5000 Da PEG lipids induce nonspecific leakage of contents. This kinetic model can be used to predict the bioresponsive properties of POD modified liposomes *in vivo*.

I then investigated whether pH-*insensitive* PEG lipid was capable of preventing POD induced leakage. Interestingly, vesicles containing 4 mole % of a pH-*insensitive* PEG-lipid conjugate and 10% POD did not leak contents or collapse at any pH. Vesicles containing 3 mole % of a pH-*insensitive* PEG-lipid only released about half of their contents and then stopped leaking. Also investigated was the impact of membrane permeability of the buffer on burst kinetics. It was found that a membrane permeable acetate buffer had only a minor impact on the lag time before burst phase compared to membrane impermeable phosphate, glucuronate, and citrate buffers at pH 6.0.

## 2.2 Methods

### 2.2.1 Materials

The pH sensitive PEG-lipid conjugates (PODS750, PODS20000, and PODS5000) were synthesized within our group as previously described [Guo *et al.* 2001, Li *et al.* 2005], using PEG of 750 Da, 2000 Da, and 5000 Da respectively. Briefly, 2 mmole of

polyethyleneglycol monomethyl ether was dried by azeotropic distillation with 50 ml anhydrous toluene under argon. A small amount of toluene was left with the residue, which was then cooled to 50°C, followed by the addition of 2 mmole diacyl glycerol in 20 ml anhydrous tetrahydrofuran (THF). 3,9-bisethylidene-2,4,8,10-tetraoxaspiro[5,5]undecane (2 mmol) was melted by heat gun and transferred into the THF solution. Then, 50 µl anhydrous THF solution of *p*-toluenesulfonic acid (0.6 mg/ml) was added and the reaction mixture was stirred at 40°C under argon for 2 hrs. The reaction was stopped by adding 0.5 ml triethylamine and 20 ml methanol. The final product was purified with a silica gel flash column. Yields after purification ranged from 15% to 33.3%. Structures were confirmed by mass spectrometry and <sup>1</sup>H-NMR analysis [Guo *et al.* 2004].

PEG-distearoyl glycerol conjugate (PEG-DSG) [Shimada *et al.*, 1995] was a generous gift from Dr. A. Suginaka (NOF Corp., Tokyo, Japan). Dioleoylphosphatidylethanolamine (DOPE), 1-palmitoyl-2-oleoylphosphatidylethanolamine (POPE), and dipalmitoylphosphatidylethanolamine-lissamine rhodamine B (Rh-PE) were purchased from Avanti Polar Lipids (Birmingham, AL). 8-Aminonaphthalene-1,2,3-trisulfonic acid (ANTS) and *p*-Xylenebis(pyridinium) bromide (DPX) were purchased from Molecular Probes, Inc. (Junction City, OR). MilliQ water (Millipore Inc, Bedford, MA) was used to prepare all the aqueous buffers. All other chemical reagents and solvents were purchased from Sigma (St. Louis, MO) or Fisher (Tustin, CA).

### 2.2.2 Formation of liposomes

Liposomes were prepared by the freeze-thawing method based on the procedure of Monnard and coworkers [1997]. A chloroform solution of POD, PEG-DSG, POPE

and/or DOPE in desired molar ratio (10  $\mu$ mole total lipid) was added to a clean glass tube. Chloroform was evaporated under reduced pressure (27 mm Hg) at room temperature to form a lipid film and then placed under high vacuum for 1 hr to remove residual chloroform. Liposomes for leakage assays were hydrated in a pH 8.5 buffer including the ANTS fluorophore (50 mM), a DPX quencher (50 mM), and HEPES buffer (5 mM). To detach lipid from the glass the film was agitated intermittently with a vortex for about 20 min. Hydrated liposomes were sealed under argon and frozen in liquid nitrogen. The solution was melted in a water bath at room temperature. This freeze thawing cycle was repeated 10 times. The solution was then extruded 5 times through a 0.2  $\mu$ m polycarbonate membrane (Nucleopore Corp., Pleasanton, CA) with a hand-held extruder (Avestin, Ottawa, Canada). The extruded vesicles were separated from the unencapsulated material using a Sephadex G-75 column with a pH 8.5 elution buffer composed of HEPES (5 mM) and NaCl (145 mM), pH 8.5. All liposomes had zeta average diameters ranging from 170 to 200 nm and a polydispersity index of less than 0.2, as measured by a Malvern Zeta1000 Dynamic Light Scattering Instrument (Southborough, MA). There was no significant difference in the encapsulation volume among vesicles prepared with POD, PEG-DSG or a mixture of the two.

### 2.2.3 Liposome leakage assay

The ANTS/DPX fluorescence assay [Ellens *et al.*, 1984] was used to measure the content release of the liposomes. Measurements were made using a Spex Fluorolog fluorometer (Model FL1/2, Jobin Yvon, Inc., Edison, NJ, USA). Excitation was at 370 nm (4.5 nm bandpass) and the 90° emission signal was recorded at 520 nm (18 nm bandpass). At time

zero, G-75 purified liposomes (10-20  $\mu$ l) were injected into a cuvette containing 2-3 mL of stirred buffer at 37 °C. Leakage assays were carried out with a cuvette concentration of 1 to 25  $\mu$ M lipid, as required for assay sensitivity. The time to burst phase is not dependent upon lipid concentration (Figure 2-6B). One data point of fluorescence intensity was collected each second except for pH 7.0 and 7.4, where measurements were taken every 30 min and the samples were incubated in dark between the measurements to minimize the exposure of the sample to the excitation light source. The initial intensity was defined as 0% contents leakage. To define 100% contents leakage, 50-200  $\mu$ L of 1% C<sub>12</sub>E<sub>8</sub> detergent was added to the cuvette at the termination of the experiment to release all of the dye. Several buffers were utilized at different pH, acetate (50 mM sodium acetate, 100 mM NaCl), phosphate (50 mM sodium phosphate, 100 mM NaCl), glucuronate (50 mM glucuronic acid, 100 mM NaCl), and citrate (50 mM citric acid, 100 mM NaCl). Buffers were titrated by the addition of NaOH or HCl. The pH and buffering agent are indicated on each figure. Data are plotted as a percentage of content released, calculated using the following equation:

$$\text{Content Leakage} = 100\% * [(F_{\text{time}} - F_{\text{background}})/(F_{\text{maximum}} - F_{\text{background}})] \quad \text{Eq. 2-1}$$

Where  $F_{\text{time}}$  is fluorescence as a function of time,  $F_{\text{background}}$  is determined immediately after the injection of liposomes into the cuvette, and  $F_{\text{maximum}}$  is determined at the end of each assay following lysis with detergent.

#### 2.2.4 Determination of the duration of lag phase

In previous studies on POD/DOPE vesicles [Guo *et al.* 2001], the duration of the lag phase ( $t_{\text{lag}}$ ) for each leakage assay was determined by a visual estimation of the

intersection point of two lines: a line tangent to the trace of the lag phase and a line tangent to the steepest slope of the burst phase. For this analysis, I developed a mathematical derivation method to reduce bias. Since slow leakage during the lag phase and fast leakage during the burst phase are reflected, respectively, by a shallow slope and a steep slope of the fluorescent trace, the transition point between the two phases can be considered as the point when the change of the leakage rate, or the change of the slope of the fluorescent trace, reaches the maximum. Mathematically, this maximum point is equivalent to the maximum point of the secondary derivative of the fluorescent trace.

To obtain the first and second derivatives from raw fluorescence data (Fig. 2-1A), a window of width ( $t_w$ ) was centered on each time point ( $t$ ). Assuming the data within the window is linear, the derivative was determined for this point by linear regression. At time points later than  $0.5 \times t_w$ , the derivative was obtained for each time point to obtain the first derivative curve (Fig. 2-1B). To account for different leakage kinetics at different pH, the linear window time ( $t_w$ ) was defined as 20% of the time required for 50% leakage. This method scales  $t_w$  between experiments and computes a smooth derivative trace with sharp peaks for all data sets. The analogous method was used to obtain second derivative (Fig. 2-1C) curves from the first derivative curves, using the same  $t_w$  for obtaining the corresponding first derivative curves. The time point where the second derivative reached a maximum was taken as the transition point between the lag phase and the burst phase; the elapsed time between the transition point and  $t_0$  is taken as the lag time ( $t_{lag}$ ).



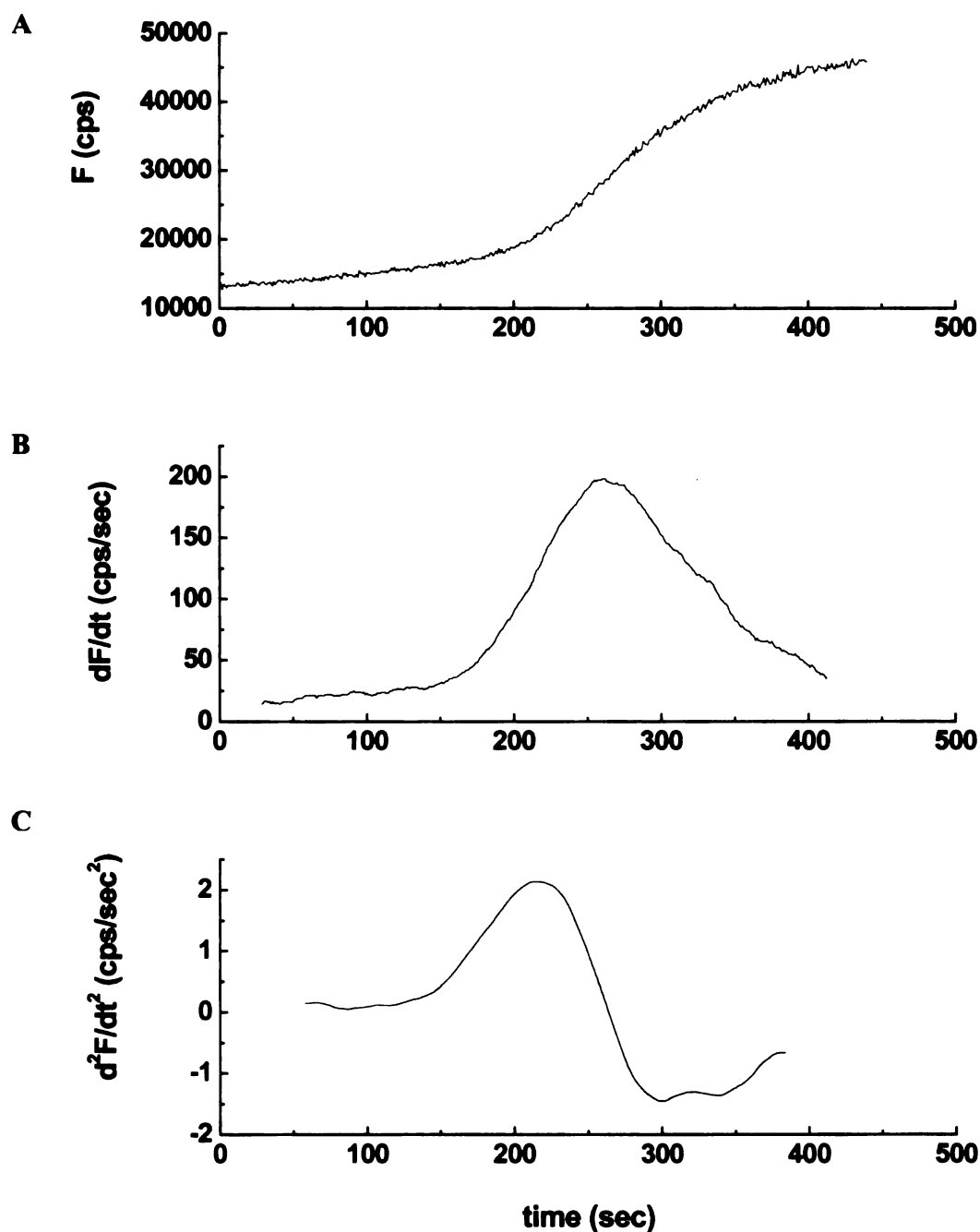


**Figure 2-1. Determination of lag time ( $t_{lag}$ ) by the derivation method.** As an example, the data processing of the leakage of POD/POPE/DOPE (10/50/40, 25  $\mu$ M total lipid concentration) liposome at pH 5.5 is shown. [A] The fluorescent intensity  $F$  (counts per sec) over incubation time. [B] and [C] The first and the second derivatives of the fluorescent trace in [A], respectively. The maximum of  $d^2F/dt^2$  is 2.133 cps/sec<sup>2</sup> at 214 sec and this is defined as  $t_{lag}$ .

### 2.2.5 Statistical analysis using the “minimum surface shielding” model

The hydrolysis of POD on liposome surfaces at a constant pH can be described by the following rate equation:

$$dA / dt = - k [H^+] \quad \text{Eq. 2-2}$$

Where A is the mole percent of intact POD on the liposome surface,  $k$  is a hydrolysis rate constant, and  $[H^+]$  is the concentration of protons. Integrating this equation from  $t = 0$  to  $t$  and  $A = A_0$  to  $A_t$ , I obtain the following exponential solution:

$$A_t = A_0 \text{EXP}(-k[H^+]t) \quad \text{Eq. 2-3}$$

Where  $A_t$  is the percentage of POD on liposome surface at the incubation time  $t$  and  $A_0$  is the percentage of POD at the starting time of incubation. At the transition point between the lag phase and the burst phase, the equation can be written as:

$$A_c = A_0 \text{EXP}(-k[H^+]t_{lag}) \quad \text{Eq. 2-4}$$

where  $A_c$  is the minimum percentage of POD required on liposome surface to stabilize the bilayer structures,  $t_{lag}$  is the duration of lag phase. Solving for  $t_{lag}$ :

$$t_{lag} = \ln A_0 / (k[H^+]) - \ln A_c / (k[H^+]) \quad \text{Eq. 2-5}$$

By substituting the  $[H^+] = 10^{-\text{pH}}$  into the equation and rearranging slightly I get:

$$t_{lag} = \ln(A_0/A_c) 10^{\text{pH}} / k \quad \text{Eq. 2-6}$$

This form of the equation was used to obtain estimates for the parameters of the “minimum surface shielding” Model, i.e., POD hydrolysis rate constant ( $k$ ) and critical percentage of POD ( $A_c$ ). For the PODS750 these parameters were obtained by fitting the observed  $t_{lag}$  in phosphate buffer at pH 5.0, 6.0, and 7.0 (Table 2-1) using nonlinear regression, performed by SPSS™ version 11.5 (Chicago, IL, USA). For PODS2000,

these parameters were obtained by fitting  $t_{lag}$  using the pH 5.0 acetate buffer (Table 2-2).

To fit the complete set of data for PODS750 simultaneously requires a nonlinear multiple regression, so it was important to carefully choose how to fit the data. The error was a strong function of the magnitude of  $t_{lag}$ ; therefore, to prevent the excessive weighting of larger lag times, the regressions were performed using a relative variance model. This is achieved in SPSS™ by minimizing the following user defined loss function:

$$\text{Loss Function} = (\text{RESID}_- / t_{lag})^2 \quad \text{Eq. 2-7}$$

Within the SPSS™ software  $\text{RESID}_-$  is defined the residual difference between the predicted lag time and the observed lag time,  $t_{lag}$ . The loss function was minimized using the sequential quadratic programming method, which allowed bootstrap estimation of the standard errors for  $A_c$  and  $k$ .

### 2.3 Results

POD stabilized liposomes are pH sensitive in a unique manner that is well tuned for use in biological systems. Using an aqueous content release assay, I investigated the pH dependent collapse properties of these liposomes in order to better engineer them into a therapeutic tool for drug and gene delivery. In this process, I developed a “minimum surface shielding model” that explains the observed kinetics of POD liposome collapse.

The content released from POD/PE liposomes consists of 2 phases, a lag phase and a burst phase (Fig. 2-1 A). During the lag phase, the liposomes leak only marginal amounts of their encapsulated dye. The length of the lag phase,  $t_{lag}$ , drops dramatically with a decrease in the pH. Presumably, as the POD is cleaved by acid hydrolysis, PEG is

released from the liposome surface. Eventually, there is not enough PEG to stabilize the liposome, resulting in a burst of liposome leakage until all the contents have been released. During the burst phase, the vesicles coalesce into large aggregates that precipitate out of solution.

I prepared lipid films composed of 50% of POPE, (50- $A_0$ )% of DOPE, and ( $A_0$ )% of PODS750, PODS2000, PODS5000, or PEG-DSG for our studies. These lipid films were easily hydrated and large unilamellar vesicles (LUV) were prepared by freeze-thawing and extrusion. Freeze-thawed POD/POPE/DOPE liposomes possess large encapsulated volumes in the range of 2.5~3.5  $\mu\text{l}/\mu\text{mole}$  lipid [Guo *et al.* 2003]. There were 2 reasons to use LUV in these studies: the encapsulation of larger volumes enabled greater sensitivity of fluorescence, and the existence of multilamellar structures within a particle could complicate the analysis of transition to hexagonal phase. For example, a liposome could collapse because of bilayer-bilayer contact between two of its own lamellae. Thus, these studies reflect the kinetics of collapse for POD liposomes consisting primarily of unilamellar vesicles, and may or may not reflect how multilamellar structures collapse.

### 2.3.1 *Effect of PEG chain length on Leakage*

The presence of PEG is a critical parameter in the stabilization of PE bilayers; therefore, I was interested in determining if PEG length affects the collapse properties of POD stabilized liposomes. Figure 2-2 shows a comparison of POD liposomes injected into pH 6.0 buffer at time zero. The 10% PODS2000 liposome burst occurs at a later time than then the 10% PODS750 and 9% PODS5000, suggesting that these liposomes are less

stable than PODS2000 (Figure 2-2). On a per mole basis, the PODS750 should be expected to provide less steric shielding than the PODS2000. This supports the “minimum surface shielding” model; the PODS750 should have a larger  $A_c$  than the PODS2000. If the lipids are hydrolyzing at the same rate, then the model predicts that the PODS750 liposomes burst first. According to the model, the PODS5000 liposomes should wait even longer than PODS2000 until entering the burst phase. Interestingly, it was possible to form liposomes containing 9% PODS5000, but these particles were unable to retain aqueous contents for any period of time (Fig. 2-2), and since these liposomes did not exhibit a lag time their release kinetics could not be analyzed using the model.

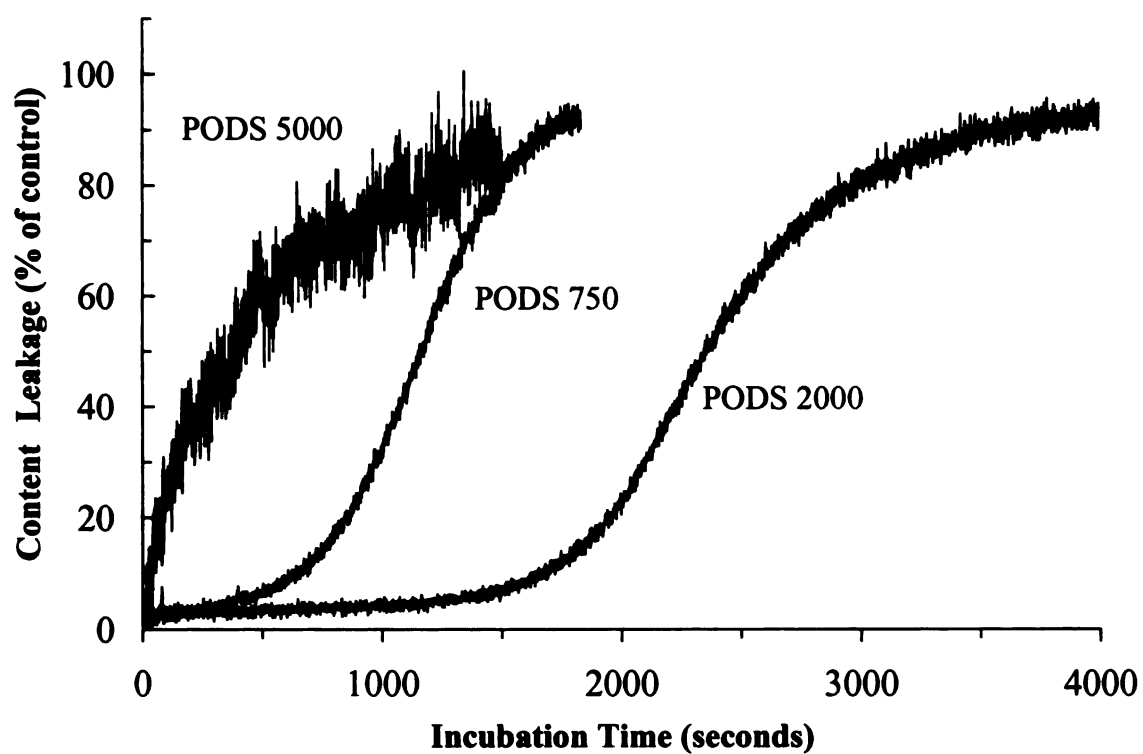


**Figure 2-2. POD liposome leakage is PEG chain length dependent.** Conforming to the minimum shielding model, the PODS750 ( $A_o = 10\%$ ) burst faster than PODS2000 ( $A_o = 10\%$ ). Note that PODS5000 ( $A_o = 9\%$ ) liposomes display excessive nonspecific leakage and  $t_{lag}$  could not be identified using this lipid formulation. Phosphate buffer pH 6.0 at 37°C.

### 2.3.2 *Effect of pH on content leakage*

The “minimum surface shielding” model predicts a 10-fold increase in the  $t_{lag}$  for every 1 pH unit shift (Eq. 2-5), and this is clearly observed for PODS750 (Fig. 2-3A) and PODS2000 (Fig. 2-3B). The x-axes in these figures have been plotted in  $\text{Log}_{10}$  scale so that all of the data can be viewed together. Additionally, the impressive pH sensitivity of the POD compounds and their utility in biological systems is evident. Even at 37°C, in neutral pH, POD liposomes are stable over an hour; however, at pH 5 and below, these liposomes collapse within minutes. Thus, these liposomes can circulate for a long time following i.v. administration. For the purpose of carrying DNA or drugs, these liposomes are naturally suited for targeted collapse in acidic environments such as the interstitial space within a tumor or a cellular endosome.

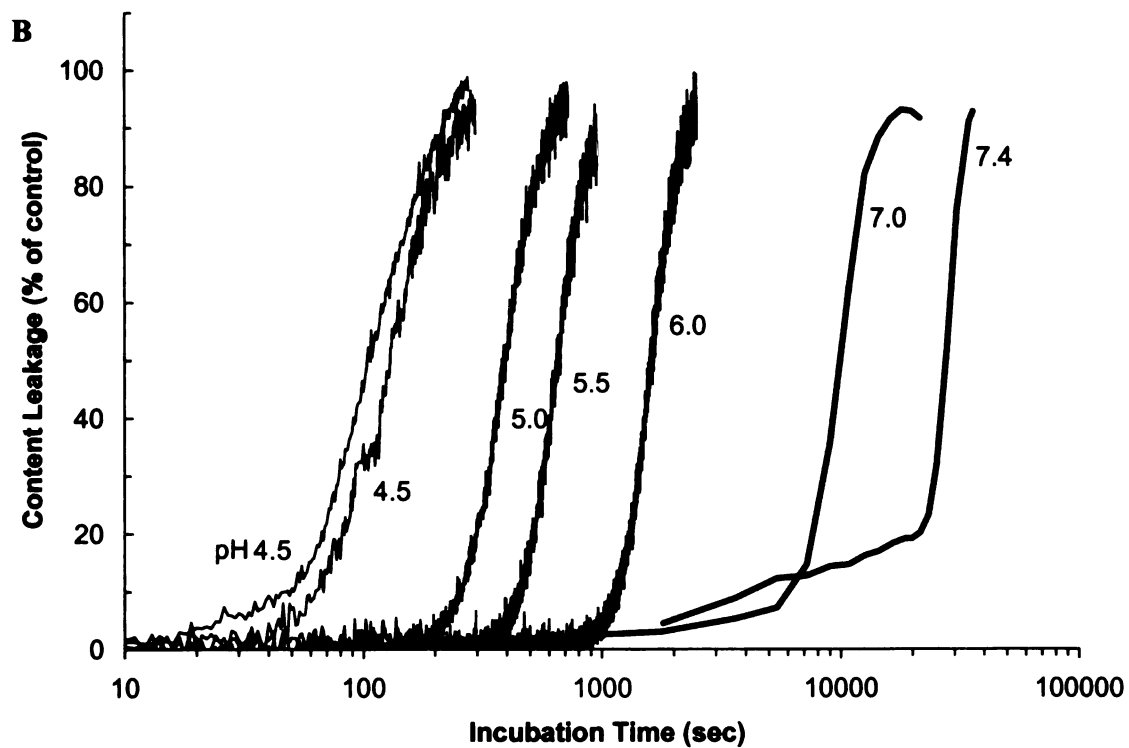
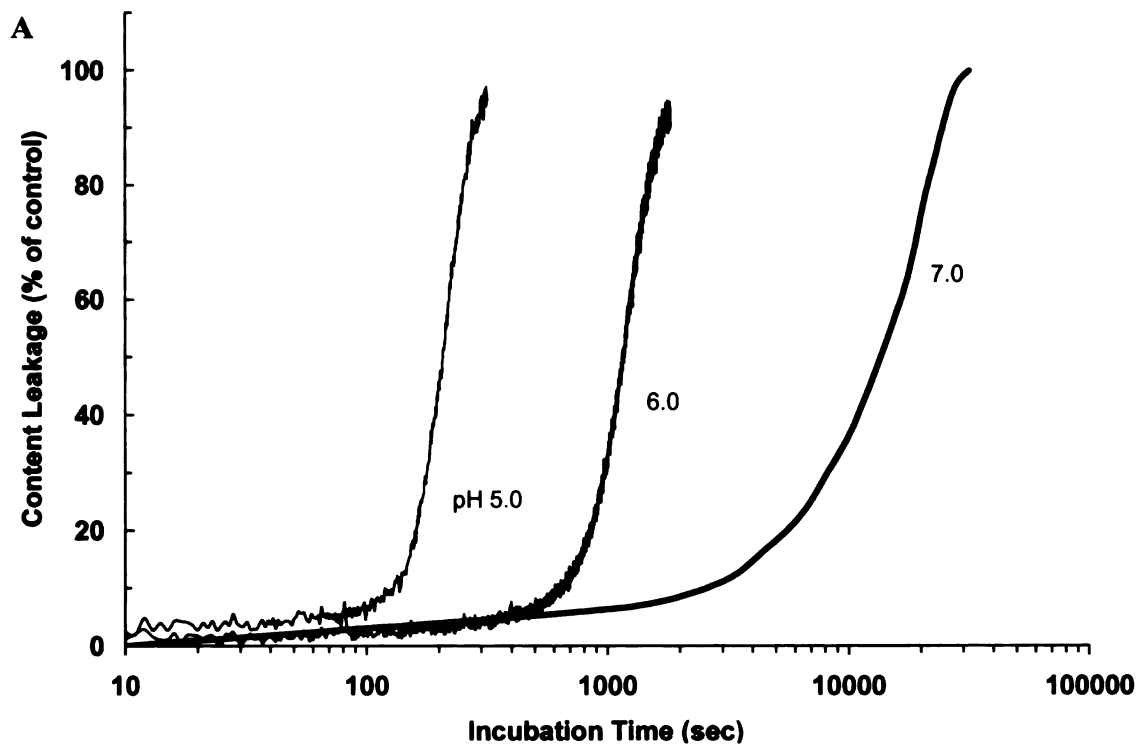


**Figure 2-3. pH-dependent leakage of POD liposomes at 37°C.** [A] PODS750 liposome ( $A_o = 10\%$ ) in phosphate buffer. [B] PODS2000 liposome ( $A_o = 10\%$ ) leakage in acetate buffer (pH 4.5, far left) and phosphate buffer.



1977

1977

1977

1977

1977

1977

1977



1977

1977

1977

1977

1977

1977

1977

1977

1977

1977

1977

1977

1977

1977

1977

1977

1977

1977

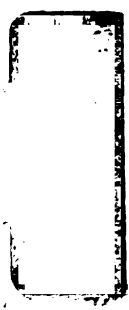
2  
T  
v  
h  
th  
se  
P  
ha  
P  
Lip  
per  
Ve  
wt  
PO  
incl  
resu  
that

### 2.3.3 Stabilization of POD liposomes with near-critical amount of pH insensitive lipids

To confirm an estimate of the critical mole percent,  $A_c$ , of POD required to stabilize the vesicles and to eliminate the possibility that hydrolysis products from the POD (the PEG, linker, or distearoyl glyceride) were responsible for the leakage or collapse, I examined the pH release profile in vesicles composed of POPE/DOPE, containing either the pH-sensitive POD or a pH-insensitive PEG-DSG derivative. The PEG-DSG had a similar Da PEG (2000) as POD, the same hydrophobic anchor distearoyl glycerol and, like POD, had no charge. Thus, PEG-DSG has physical-chemical properties that are analogous to PODS2000.

Liposomes with 10% PODS2000 collapsed efficiently at pH 5.0 either in a membrane permeant acetate buffer (Fig. 2-4A) or a membrane impermeant citrate buffer (Fig. 2-4B). Vesicles composed of 10% PEG-DSG neither leaked contents (Fig. 2-4F) nor collapsed with any buffer tested. In addition, PE vesicles stabilized by 4% PEG-DSG and 10% POD did not leak contents (Figure 2-4E) or collapse at any pH tested. This control was included because one of the breakdown products from POD is distearoyl glyceride. These results confirm that the PE vesicles are stabilized by the PEG coat at all pH values and that hydrolysis products from POD do not cause content release.

1910  
1911  
1912  
1913  
1914  
1915  
1916  
1917  
1918  
1919  
1920



1921  
1922  
1923  
1924  
1925  
1926  
1927  
1928  
1929  
1930  
1931  
1932  
1933  
1934  
1935  
1936  
1937  
1938  
1939  
1940  
1941  
1942  
1943  
1944  
1945  
1946  
1947  
1948  
1949  
1950  
1951  
1952  
1953  
1954  
1955  
1956  
1957  
1958  
1959  
1960  
1961  
1962  
1963  
1964  
1965  
1966  
1967  
1968  
1969  
1970  
1971  
1972  
1973  
1974  
1975  
1976  
1977  
1978  
1979  
1980  
1981  
1982  
1983  
1984  
1985  
1986  
1987  
1988  
1989  
1990  
1991  
1992  
1993  
1994  
1995  
1996  
1997  
1998  
1999  
2000  
2001  
2002  
2003  
2004  
2005  
2006  
2007  
2008  
2009  
2010  
2011  
2012  
2013  
2014  
2015  
2016  
2017  
2018  
2019  
2020  
2021  
2022  
2023  
2024  
2025  
2026  
2027  
2028  
2029  
2030  
2031  
2032  
2033  
2034  
2035  
2036  
2037  
2038  
2039  
2040  
2041  
2042  
2043  
2044  
2045  
2046  
2047  
2048  
2049  
2050  
2051  
2052  
2053  
2054  
2055  
2056  
2057  
2058  
2059  
2060  
2061  
2062  
2063  
2064  
2065  
2066  
2067  
2068  
2069  
2070  
2071  
2072  
2073  
2074  
2075  
2076  
2077  
2078  
2079  
2080  
2081  
2082  
2083  
2084  
2085  
2086  
2087  
2088  
2089  
2090  
2091  
2092  
2093  
2094  
2095  
2096  
2097  
2098  
2099  
2100

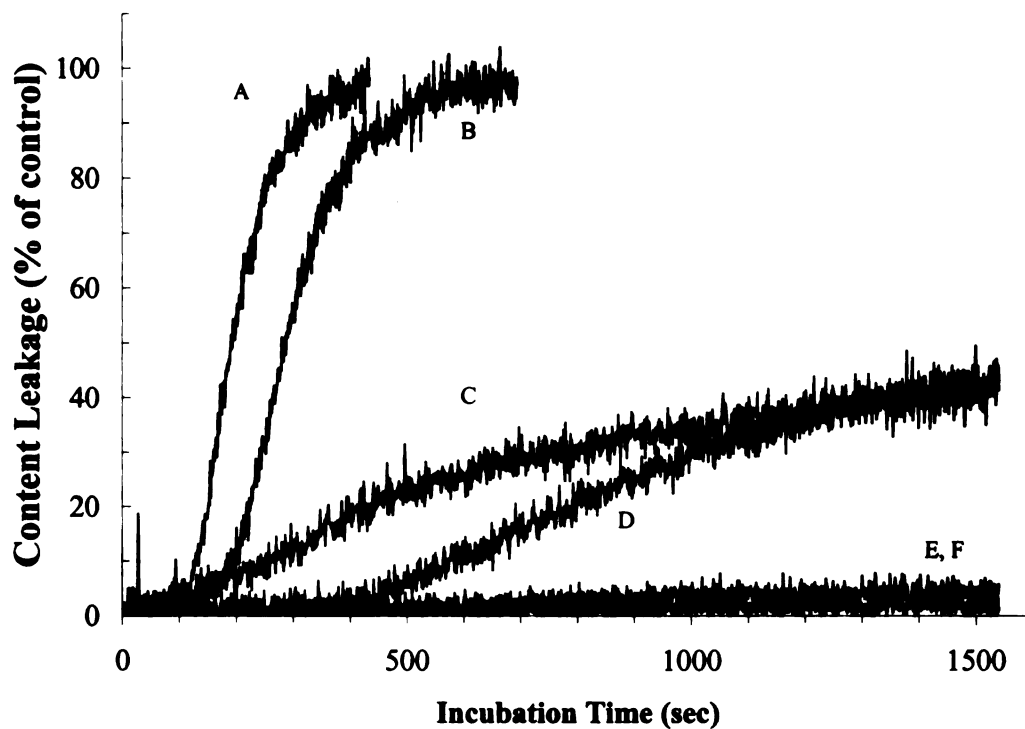


**Figure 2-4. pH-insensitive PEG-lipid stabilizes POD liposomes.** Percentage of leakage over time at pH 5.0 and 5  $\mu$ M lipid. [A] and [B] POD/POPE/DOPE (10/50/40); [C] and [D] PEG-DSG/POD/POPE/DOPE (3/10/50/36); [E] PEG-DSG/POD/POPE/DOPE (4/10/50/36); [F] PEG-DSG/POPE/DOPE (10/50/40); [A], [C],[E],and [F] in acetate buffer; [B]and [D] in citrate buffer.

1870  
1871  
1872  
1873  
1874  
1875  
1876  
1877  
1878  
1879  
1880  
1881  
1882  
1883  
1884  
1885  
1886  
1887  
1888  
1889  
1890  
1891  
1892  
1893  
1894  
1895  
1896  
1897  
1898  
1899  
1900



1901  
1902  
1903  
1904  
1905  
1906  
1907  
1908  
1909  
1910  
1911  
1912  
1913  
1914  
1915  
1916  
1917  
1918  
1919  
1920  
1921  
1922  
1923  
1924  
1925  
1926  
1927  
1928  
1929  
1930  
1931  
1932  
1933  
1934  
1935  
1936  
1937  
1938  
1939  
1940  
1941  
1942  
1943  
1944  
1945  
1946  
1947  
1948  
1949  
1950  
1951  
1952  
1953  
1954  
1955  
1956  
1957  
1958  
1959  
1960  
1961  
1962  
1963  
1964  
1965  
1966  
1967  
1968  
1969  
1970  
1971  
1972  
1973  
1974  
1975  
1976  
1977  
1978  
1979  
1980  
1981  
1982  
1983  
1984  
1985  
1986  
1987  
1988  
1989  
1990  
1991  
1992  
1993  
1994  
1995  
1996  
1997  
1998  
1999  
2000

Interestingly, vesicles stabilized with 3% PEG-DSG and 10% POD did collapse and display burst kinetics in either acetate buffer (Fig. 2-4C) or citrate buffer (Fig.2-4D); however, these 3% PEG-DSG stabilized liposomes only released about 40% of their contents, even after long periods of time. These burst kinetics also scaled with pH as the same effect was found to be true over much longer time periods ( $t_{lag} \sim 12,600$  sec in pH 7.0 citrate buffer), and even at pH 7.0, only 40% of the contents were released before the addition of detergent. This suggests that 4% of 2000 Da PEG is a sufficient lower bound to stabilize the liposomes; however, 3% PEG is extremely close to the critical minimum shielding level,  $A_c$ . Thus, I would expect to calculate an  $A_c$  close to 3% PODS2000.

#### 2.3.4 Determination of $t_{lag}$ for PODS750 and PODS2000

Eq. 2-5 also predicts that the change of  $t_{lag}$  in response to  $A_0$  is relatively small; therefore, a precise determination of  $t_{lag}$  values is needed in order to obtain reasonable estimations of  $k$  and  $A_c$ . Two approaches were taken to improve the data quality for  $t_{lag}$  values. First, all the leakage data in this report were processed by an automated derivation method to remove bias from the determination of  $t_{lag}$  values from the fluorescent traces. Second, concentrated liposome samples were utilized for leakage assays (25  $\mu$ M here versus 5  $\mu$ M in Fig. 2-4) to obtain smoother traces with sharper increase of the fluorescent signal at the burst phase. Thus, POD/POPE/DOPE liposomes containing different mole percentages of POD were prepared by freeze-thawing and their leakage measured at multiple pH. Using the second derivative method, the lag times of POD/POPE/DOPE liposomes with different  $A_0$  are listed for PODS750 in Table 2-1 and and PODS2000 in Table 2-2.

**Table 2-1. PODS750: Comparison of predicted<sup>\*</sup> and observed<sup>\*\*</sup> lag time<sup>\*\*\*</sup>,  $t_{lag}$ , (sec).**

pH <sup>****</sup>	Initial Percentage of PODS750, $A_0$ (mole %)				
	5	7.5	10	15	20
5.0	57 (104)	102 (135)	129 (149)	174 (228)	209 (298)
6.0	562 (535)	977 (698)	1,262 (899)	1,664 (1,362)	1,905 (1,895)
7.0	6,021 -	10,231 (11,170)	13,219 (17,090)	17,429 (20,850)	20,417 (25,300)

<sup>\*</sup> Predicted by the "minimum surface shielding" model;  $k = 963 \pm 183 \text{ sec}^{-1}\text{M}^{-1}$  and  $A_c = 2.8 \pm 0.7\%$ .

<sup>\*\*</sup> The predicted lag times are presented with the observed lag time below in parenthesis.

<sup>\*\*\*</sup> Obtained from the maximum of the second derivative plot of the ANTS/DPX leakage.

<sup>\*\*\*\*</sup> POD/POPE/DOPE ( $A_0/50/(50-A_0)$ ) liposomes were incubated in phosphate buffer at 37°C for  $t_{lag}$  sec until the burst phase was observed.





**Table 2-2. PODS2000: Comparison of predicted\* and observed\*\* lag times\*\*\*,  $t_{lag}$ , (sec).**

pH****	Initial Percentage of PODS2000, $A_0$ (mole %)					
	7	8	9	10	12	14
4.5	26	29	31	34	38	41
	-	-	-	(63)	-	(74)
4.7	41	45	50	53	60	66
	-	-	-	(63)	-	(84)
5.0	81	90	99	106	120	131
	(85)	(94)	(96)	(97)	(117)	(138)
5.5	256	286	313	337	378	413
	(176)	(211)	(223)	(220)	(287)	(332)
6.0	808	904	989	1,065	1,196	1,307
	-	-	-	(1,603)	-	(1,819)
6.3	1,613	1,804	1,974	2,125	2,387	2,608
	-	-	-	(1,645)	-	(2,222)
7.0	8,083	9,044	9,891	10,650	11,962	13,071
	-	-	-	(11,700)	-	(16,560)
7.4	20,303	22,717	24,846	26,750	30,046	32,833
	-	-	-	(21,600)	-	(37,800)

\* Predicted by the "minimum surface shielding" model;  $k=1,390 \pm 232 \text{ s}^{-1}\text{M}^{-1}$ ,  $A_c=2.3 \pm 0.6\%$ .

\*\* The predicted lag times are presented with the observed lag time below in parenthesis..

\*\*\* Obtained from the maximum of the second derivative plot of the ANTS/DPX leakage

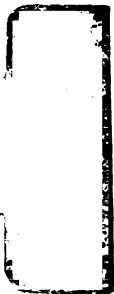
\*\*\*\* POD/POPE/DOPE ( $A_0/50/(50-A_0)$ ) liposomes were incubated in acetate buffer (pH  $\leq 5.5$ ) or phosphate buffer (pH  $\geq 6.0$ ) at the specified pH for  $t_{lag}$  sec until the burst phase was observed.

### 2.3.5 POD Derivatives follow the "minimum surface shielding" model

Having collected  $t_{lag}$  data for a number of initial percentage PEG,  $A_0$ , over a range of pH (Tables 2-1, 2-2), I must prove that the data fits to the predictions of the model. Eq. 2-5 shows that the length of lag time,  $t_{lag}$ , should have a linear relationship with the natural logarithm of the initial percentage of POD on liposome surface. Furthermore, the equation predicts that, by measuring the  $t_{lag}$  of POD/POPE/DOPE liposomes comprising of different  $A_0$  at known pHs, followed by an appropriate regression of the data, one can

1940

1941  
1942  
1943  
1944  
1945  
1946  
1947  
1948  
1949  
1950



1951  
1952  
1953  
1954  
1955  
1956  
1957  
1958  
1959  
1960  
1961  
1962  
1963  
1964  
1965  
1966  
1967  
1968  
1969  
1970  
1971  
1972  
1973  
1974  
1975  
1976  
1977  
1978  
1979  
1980  
1981  
1982  
1983  
1984  
1985  
1986  
1987  
1988  
1989  
1990  
1991  
1992  
1993  
1994  
1995  
1996  
1997  
1998  
1999  
2000  
2001  
2002  
2003  
2004  
2005  
2006  
2007  
2008  
2009  
2010  
2011  
2012  
2013  
2014  
2015  
2016  
2017  
2018  
2019  
2020  
2021  
2022  
2023  
2024  
2025  
2026  
2027  
2028  
2029  
2030  
2031  
2032  
2033  
2034  
2035  
2036  
2037  
2038  
2039  
2040  
2041  
2042  
2043  
2044  
2045  
2046  
2047  
2048  
2049  
2050

deduce the rate constant of POD hydrolysis ( $k$ ), as well as the minimum percentage of POD ( $A_c$ ), that is required to stabilize the liposome. As shown in Figure 2-5, the lag time versus  $\ln(A_0)$  (following Eq. 2-5) gives a linear plot, where the slope contains the kinetic rate constant,  $k$ , and the x-intercept contains an approximation of  $A_c$ . Buffered at pH 5.0,  $t_{lag}$  data from initial POD percentages of 7, 8, 9, 10, 12, and 14% were fit to Eq. 2-6.

As shown in Figure 2-5, the duration of the lag time shows a linear relationship with the natural logarithm of the starting POD mole percentage at pH 5.0 ( $r^2 = 0.945$ ,  $P = 0.001$ ,  $n=6$ ), demonstrating that the “minimum surface shielding” model adequately describes pH-triggered content release of POD/PE liposomes. To estimate the kinetic parameters ( $k$  and  $A_c$ ), nonlinear regression was performed to fit the  $t_{lag}$  data in Figure 2-5 to Eq. 2-6. The parameters derived were  $k = 1,390 \pm 232 \text{ sec}^{-1}\text{M}^{-1}$  and  $A_c = 2.3 \pm 0.6\%$ . The parameters obtained,  $A_c$  and  $k$ , were successfully used to predict the length of the lag phase for PODS2000 liposomes, as shown in Table 2-2.

San Francisco

San Francisco  
LI  
1973  
1973

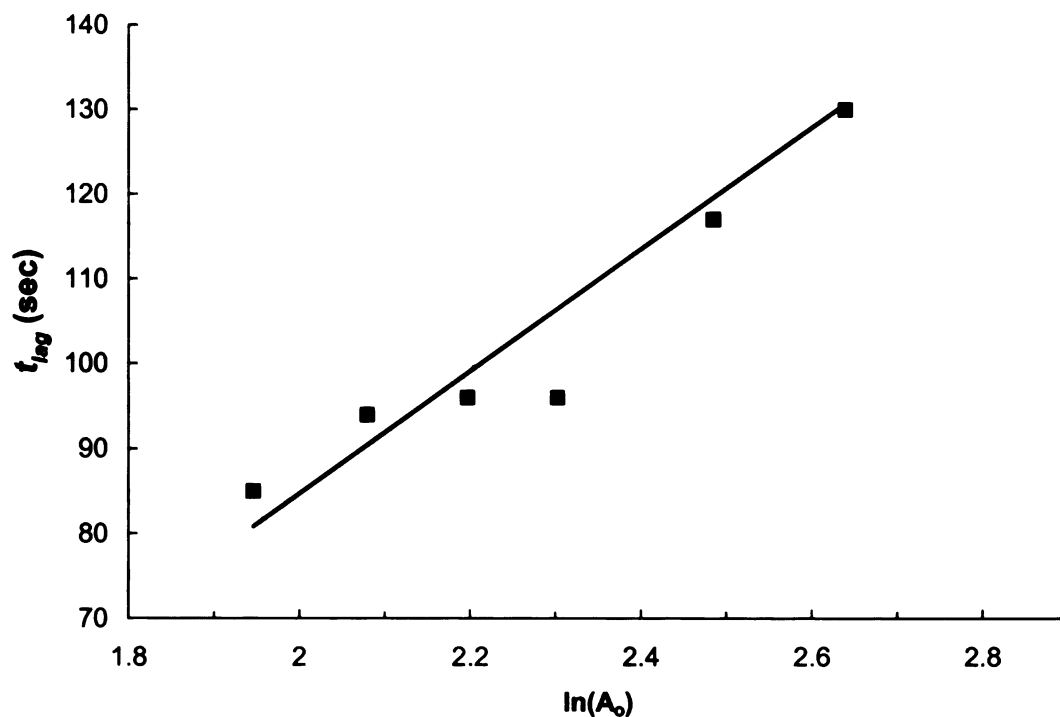


San Francisco  
LI  
1973  
1973  
San Francisco  
LI  
1973  
1973  
San Francisco  
LI  
1973  
1973

San Francisco

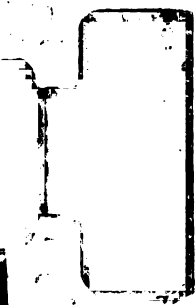
(sec)

Fig  
tim  
log  
197  
0.9



**Figure 2-5. Lag time is a function of the initial percent POD.** Dependence of lag time ( $t_{lag}$ ) of PODS2000/POPE/DOPE ( $A_0/50/(50 - A_0)$ ) liposomes on the natural logarithm of initial mole % of POD,  $A_0$ , in pH 5.0 acetate buffer. Model:  $t_{lag} = \ln(A_0) 10^{pH} / k - \ln(A_c) 10^{pH} / k$ ; Observed:  $k = 1,390 \pm 232 \text{ s}^{-1}\text{M}^{-1}$ ,  $A_c = 2.3 \pm 0.6\%$ ,  $r^2 = 0.949$ ,  $P = 0.001$ .

1950  
1951  
1952  
1953  
1954  
1955  
1956  
1957  
1958  
1959  
1960



1961  
1962  
1963  
1964  
1965  
1966  
1967  
1968  
1969  
1970

1971  
1972  
1973  
1974  
1975  
1976  
1977  
1978  
1979  
1980

1981  
1982  
1983  
1984  
1985  
1986  
1987  
1988  
1989  
1990

1991  
1992  
1993  
1994  
1995  
1996  
1997  
1998  
1999  
2000

2001  
2002  
2003  
2004  
2005  
2006  
2007  
2008  
2009  
2010

2011  
2012  
2013  
2014  
2015  
2016  
2017  
2018  
2019  
2020

2021  
2022  
2023  
2024  
2025  
2026  
2027  
2028  
2029  
2030

v  
v  
r  
a  
b  
d  
c  
w  
T  
a  
(F)

Additional confirmation that the data fits the “minimum surface shielding” model can be determined by plotting the  $\text{Log}_{10}(t_{lag})$  vs. the pH. This is based upon another rearrangement of Eq. 2-6 that gives:

$$\text{Log}_{10}(t_{lag}) = \text{pH} - \text{Log}_{10}(\ln(A_o/A_c)/k) \quad \text{Eq. 2-8}$$

The data in Fig. 2-6A has been plotted according to this transformation so that the relationship between the pH and the  $t_{lag}$  is obvious. Eq. 2-8 predicts that the slope of the regression line fit to this data should be 1, and in Fig. 2-6A, the observed slope was 0.819 with  $r^2 = 0.88$ . Thus, I conclude that the data obtained from PODS2000 liposomes are well described by the model, both with respect to pH and with respect to  $A_o$ .

### 2.3.6 *Effect of membrane permeability of buffer on content release*

Vesicles composed of 10% PODS2000/POPE/DOPE underwent a pH-dependent leakage, which was slightly faster in acetate buffer (Figure 2-4 A) than in citrate buffer, a relatively membrane-impermeant buffer (Figure 2-4 B). The data shown in Figure 2-3B at pH 4.5 was generated in both acetate buffer and phosphate buffer, and phosphate buffer was used for the rest of the traces in Figure 2-3B. Because of these slight discrepancies, I decided to investigate the importance of membrane permeability of the chosen buffer. I used a membrane permeable buffer (acetate), and compared this collapse with membrane impermeant buffers (citrate, glucuronate, and phosphate) (Fig. 2-6).

The lag time for content release measured in acetate buffer was consistently shorter, albeit slightly, than the lag time measured in the less membrane-permeant buffers (Figures 2-6A); furthermore, this was not a function of lipid concentration (Fig. 2-6B).

Handwritten text and markings on the left margin, including the word "LIBRARY" and various numbers and symbols.



Vertical text or markings in the left margin, possibly a date or reference number.



This suggests that either acetate buffer is more effective at reducing the pH in the immediate vicinity of the ortho ester linkage, causing collapse from inter-vesicular bilayer contact on a faster time scale, or acetate, as acetic acid, crosses the bilayer and leads to hydrolysis of POD on the inside monolayer. Removal of PEG by hydrolysis of POD on the inside of the vesicles might lead to more rapid content release. Alternatively, hydrolysis of POD on the inside of oligolamellar vesicles could result in more rapid contents leakage due to membrane contact between the exterior bilayer and interior bilayers (i.e. collapse from within). At present I cannot differentiate between these possibilities.

17  
18  
19  
20  
21  
22  
23  
24  
25  
26  
27  
28  
29  
30  
31  
32  
33  
34  
35  
36  
37  
38  
39  
40  
41  
42  
43  
44  
45  
46  
47  
48  
49  
50  
51  
52  
53  
54  
55  
56  
57  
58  
59  
60  
61  
62  
63  
64  
65  
66  
67  
68  
69  
70  
71  
72  
73  
74  
75  
76  
77  
78  
79  
80  
81  
82  
83  
84  
85  
86  
87  
88  
89  
90  
91  
92  
93  
94  
95  
96  
97  
98  
99  
100

1  
2  
3  
4  
5  
6  
7  
8  
9  
10  
11  
12  
13  
14  
15  
16  
17  
18  
19  
20  
21  
22  
23  
24  
25  
26  
27  
28  
29  
30  
31  
32  
33  
34  
35  
36  
37  
38  
39  
40  
41  
42  
43  
44  
45  
46  
47  
48  
49  
50  
51  
52  
53  
54  
55  
56  
57  
58  
59  
60  
61  
62  
63  
64  
65  
66  
67  
68  
69  
70  
71  
72  
73  
74  
75  
76  
77  
78  
79  
80  
81  
82  
83  
84  
85  
86  
87  
88  
89  
90  
91  
92  
93  
94  
95  
96  
97  
98  
99  
100



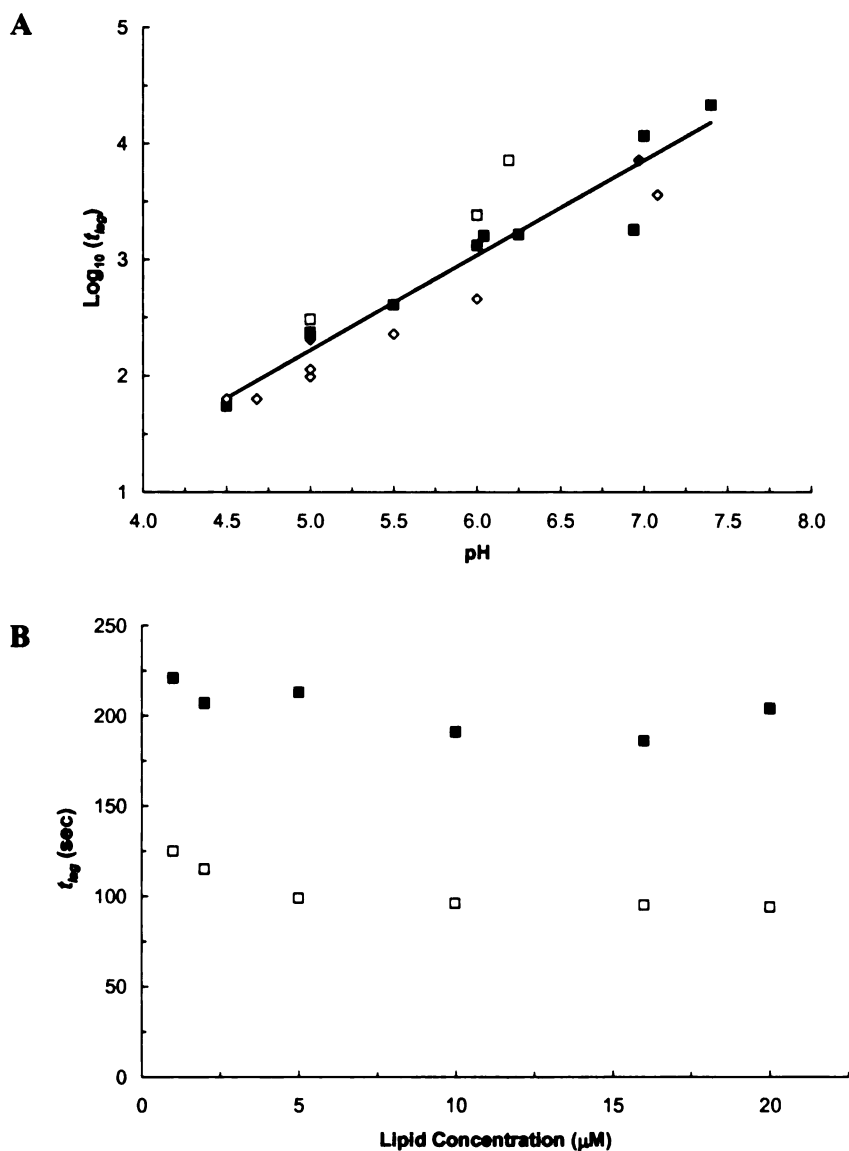


**Figure 2-6. Effect of buffer on PODS2000 pH-dependent leakage.** [A] logarithm of lag time ( $t_{lag}$  in sec) of POD/POPE/DOPE (10/50/40) vesicles at various pH in acetate (◇), citrate (◆), glucuronate (□), and phosphate (■) buffers. Model:  $\text{Log}_{10}(t_{lag}) = \text{pH} - \text{Log}_{10}(\ln(A_o/A_c)/k)$ ; Observed:  $\text{Log}_{10}(t_{lag}) = (0.819 \pm 0.067) \times \text{pH} - (1.881 \pm 0.395)$ ,  $r^2 = 0.88$ . [B] duration of lag phase ( $t_{lag}$ ) of POD/POPE/DOPE (10/50/40) vesicles of different lipid concentrations in pH 5.0 acetate (□) and phosphate (■) buffer.

1940  
1941  
1942  
1943  
1944  
1945  
1946  
1947  
1948  
1949  
1950  
1951  
1952  
1953  
1954  
1955  
1956  
1957  
1958  
1959  
1960  
1961  
1962  
1963  
1964  
1965  
1966  
1967  
1968  
1969  
1970  
1971  
1972  
1973  
1974  
1975  
1976  
1977  
1978  
1979  
1980  
1981  
1982  
1983  
1984  
1985  
1986  
1987  
1988  
1989  
1990  
1991  
1992  
1993  
1994  
1995  
1996  
1997  
1998  
1999  
2000  
2001  
2002  
2003  
2004  
2005  
2006  
2007  
2008  
2009  
2010  
2011  
2012  
2013  
2014  
2015  
2016  
2017  
2018  
2019  
2020  
2021  
2022  
2023  
2024  
2025



1940 1941 1942 1943 1944 1945 1946 1947 1948 1949 1950 1951 1952 1953 1954 1955 1956 1957 1958 1959 1960 1961 1962 1963 1964 1965 1966 1967 1968 1969 1970 1971 1972 1973 1974 1975 1976 1977 1978 1979 1980 1981 1982 1983 1984 1985 1986 1987 1988 1989 1990 1991 1992 1993 1994 1995 1996 1997 1998 1999 2000 2001 2002 2003 2004 2005 2006 2007 2008 2009 2010 2011 2012 2013 2014 2015 2016 2017 2018 2019 2020 2021 2022 2023 2024 2025

1940  
1941  
1942  
1943  
1944  
1945  
1946  
1947  
1948  
1949  
1950  
1951  
1952  
1953  
1954  
1955  
1956  
1957  
1958  
1959  
1960  
1961  
1962  
1963  
1964  
1965  
1966  
1967  
1968  
1969  
1970  
1971  
1972  
1973  
1974  
1975  
1976  
1977  
1978  
1979  
1980  
1981  
1982  
1983  
1984  
1985  
1986  
1987  
1988  
1989  
1990  
1991  
1992  
1993  
1994  
1995  
1996  
1997  
1998  
1999  
2000  
2001  
2002  
2003  
2004  
2005  
2006  
2007  
2008  
2009  
2010  
2011  
2012  
2013  
2014  
2015  
2016  
2017  
2018  
2019  
2020  
2021  
2022  
2023  
2024  
2025

### 2.3.7 Determination of hydrolysis rate and minimum stabilization percentage

Initial study of PODS2000 was performed by nonlinear regression using a single independent variable,  $A_0$ , taken while holding the pH constant at 5.0 (Fig. 2-5). The resulting parameters,  $k = 1,390 \pm 232 \text{ sec}^{-1}\text{M}^{-1}$  and  $A_c = 2.3 \pm 0.6\%$ , were successfully used to predict  $t_{lag}$  over a wide range of pH and  $A_0$  (Table 2-2). In order to fit the data from PODS750, a more sophisticated method based upon multiple nonlinear regression was used. Two independent variables,  $A_0$  and pH, were varied to determine the best fit to predict  $t_{lag}$ .

To perform this type of fit, it was necessary to obtain a balanced data set that uniformly covered both variables. Thus, for PODS750, data (Table 2-1) was collected at every measurable pH and  $A_0$  without taking extra measurements in any one direction as was performed for the PODS2000 liposomes (Table 2-2). This data set was then fit using nonlinear regression. The magnitude of fitted  $t_{lag}$  varied greatly, and the errors increased dramatically as  $t_{lag}$  increased. To reduce this weighting problem and effectively fit all of the data, I defined a 'relative residual'. In this model (Eq. 2-7), the squared standard residual (Observed Value – Predicted Value)<sup>2</sup> is divided by the (Observed value)<sup>2</sup>. The sum of squared relative residuals was then minimized iteratively to obtain an estimate for  $k$  and  $A_c$ . For PODS750 liposomes  $k = 963 \pm 183 \text{ sec}^{-1}\text{M}^{-1}$  and  $A_c = 2.8 \pm 0.7\%$ . The dataset for the PODS2000 liposomes was not balanced appropriately, so this method of fitting could not be applied.



## 2.4 Discussion

The goal for these studies was to mathematically characterize the collapse of liposomes stabilized by a novel pH sensitive lipid based upon a polyethylene glycol polymer conjugated to a diacyl lipid anchor via a diorthoester group (POD). pH insensitive PEG lipids are already important chemicals for the formulation of stable liposomes for therapy, such as Doxil<sup>TM</sup>. The incorporation of PEG lipids provides a steric hindrance that prevents rapid elimination of liposomes given intravenously. The Doxil<sup>TM</sup> formulation of the chemotherapeutic drug Doxorubicin consists of a liposome tightly packed with drug. Upon administration, the liposomes are cleared from the blood with a long half-life of about a day. POD liposomes also have a long elimination half-life [Guo *et al.* 2001]. Because the pH is lower in the tumor environment, it is plausible that these pH sensitive liposomes could be formulated to burst preferentially within tumor vasculature while remaining stable at pH 7.4 in the blood for many hours.

Another opportunity for the use of POD is in the formulation of pH sensitive non-viral DNA delivery systems. Our lab has taken a strong interest in creating a particle that can overcome multiple barriers to DNA delivery, and one of these barriers is entrapment within a cellular endosome following particle uptake into the cell. In the early endosome, the pH rapidly drops 1-2 units within 10 min [Sonawane *et al.* 2002] prior to further trafficking of the endosome to the lysosome -- hence escape must occur soon after internalization. Many of the details that enable a liposome to escape from the endosome have been explicated [Drummond *et al.* 2000]. Thus, DNA loaded nanoparticles





consisting of PE bilayers stabilized by POD make an attractive platform on which to build other functionalities required for *in vivo* non-viral cell transfection.

I have sufficiently characterized the behavior of POD in PE bilayers in the form of an easily understood mathematical model (Eq. 2-6). The model is based on the observation that PE bilayers can be stabilized only under the presence of steric or electrostatic repulsion between adjacent bilayers [Ellens *et al.* 1984, Cullis *et al.* 1991]. PEG polymer can provide this steric force preventing the liposomes from collapsing; however, if not enough PEG-lipid is incorporated, then a stable liposome cannot be formed. Here I start with larger than required amounts of PEG-lipid, POD, and acid hydrolysis cleaved PEG from the bilayer surface until a critical point of no return is reached. At this point, there is a rapid increase in the collapse of the liposomes by particle size measurements [Guo *et al.* 2001], aqueous content release, and lipid mixing [Guo *et al.* 2003]. To characterize this process, I developed a second derivative method for identifying the time until particle collapse,  $t_{lag}$ . Finally, I obtained sufficient data points to estimate the kinetic rate constant,  $k$ , and critical percentage,  $A_c$ , of POD that coincides with the point of collapse.

In Tables 2-1 and 2-2, all the experimentally observed  $t_{lag}$  values of POD/POPE/DOPE vesicles under different conditions are compared with their corresponding predicted values based on the “minimum surface shielding” model, using the estimated  $k$  and  $A_c$ . Given the large ranges of pH and  $t_{lag}$  values, the model provides satisfactory predictions of the experimental data. The relatively poor predictions of  $t_{lag}$  values at pHs lower than 5.0 may be attributed to the following two factors. First, the POD hydrolysis at these low

1860

July 1st  
to Aug 31st  
1860



1860

July 1st  
to Aug 31st

1860

July 1st  
to Aug 31st

1860

July 1st  
to Aug 31st

1860

July 1st  
to Aug 31st

1860

July 1st  
to Aug 31st

1860

pHs is so rapid that it is no longer the rate limiting step of liposomal leakage. The membrane mixing and collapse of the PE bilayers may instead be the major factors that control the content release of the vesicles. Second, the low  $t_{lag}$  values at these pHs may induce additional errors in using the second derivative method to determine the lag time. On this spectrophotometer, data could only be collected once every second. An instrument with a faster acquisition time could acquire more data points during the lag time, and this may help to smooth out noise during the assay. Regardless, this existing data successfully predicts all contents leakage at pH 5.0 and above.

During the fitting process, it was observed that small errors in the measurement of the pH induced large errors in the assumed proton concentration. This had a major impact on fitting datasets where data were taken at many different pH. To reduce this source of variability, it became important to only fit sets of data for which a complete set of  $A_0$  had been surveyed at a given pH. For PODS750 this included all the data at pH 5.0, pH 6.0, and pH 7.0, and for PODS2000 this included the dataset at pH 5.0 and pH 5.5. The parameters obtained from fitting these balanced datasets do an excellent job of predicting other data.

While the model and parameters do a good job of predicting the time to burst for both PODS750 and PODS2000, it was not possible to detect a significant difference between the parameters  $A_c$  and  $k$ . Having used Eq. 2-6 and 2-8 to prove that both  $A_0$  and pH separately impact  $t_{lag}$ , according to the “minimum surface shielding” model, I wanted to collapse all the data to a single plot so I could visually determine sources of error in this

LIBRARY  
UNIVERSITY OF MICHIGAN  
ANN ARBOR MI 48106-1000



LIBRARY  
UNIVERSITY OF MICHIGAN  
ANN ARBOR MI 48106-1000

experiment. To make this illustration, Eq. 2-6 was manipulated to the following form whereby the  $t_{lag}$  was normalized by the  $10^{pH}$ :

$$t_{lag}/10^{pH} = [\ln(A_o) - \ln(A_c)]/k \quad \text{Eq. 2-9}$$

Thus, plotting  $t_{lag}/10^{pH}$  vs.  $\ln(A_o)$  should give a linear plot with the slope equal to  $k^{-1}$  and the x-intercept equal to  $\ln(A_c)$ . The PODS750 data from Table 2-1 are summarized in this linearized plot (Fig. 2-7). The predicted values for PODS750 liposomes are indicated by a dashed line (Fig. 2-7). Additionally, data collected from PODS2000 liposomes (Table 2-2) are presented on this plot along with a best-fit prediction indicated by a solid line.

The fits to these two lines provide information that is hard to visualize during a nonlinear multiple regression (Fig. 2-7). The x-intercept appears to be slightly higher for PODS750 than PODS2000. This is consistent with the thinking that fewer mole percent of a larger polymer are required to achieve the same steric stabilization. The slope of the line for the PODS750 is steeper than the PODS2000, suggesting that the PODS2000 does indeed have a slightly faster hydrolysis rate constant,  $k$ . For a perfect fit to the model, the data from both PODS750 and PODS2000 should lie close to their respective best-fit lines; however, there was clearly some variation around the line. There was no clear trend to these variations though, and I concluded that the error in Fig. 2-7 is associated with small errors in the measurement of the pH that contribute to large deviations when taken to the tenth power and placed in the denominator. An error of 0.1 pH units contributes to about 30% error in the estimate of  $t_{lag}/10^{pH}$ . This is on the order of the error observed around the best-fit lines for both PODS750 and PODS2000 (Fig. 2-7). Thus, to make the best-fit

FRANCESCO

LIBRARY

LIBRARY

LIBRARY

LIBRARY

LIBRARY

LIBRARY

LIBRARY

LIBRARY

LIBRARY

LIBRARY

LIBRARY

LIBRARY

LIBRARY

LIBRARY

LIBRARY

LIBRARY

LIBRARY

LIBRARY

LIBRARY

LIBRARY

LIBRARY

LIBRARY

LIBRARY

LIBRARY

LIBRARY

LIBRARY

possible it would be helpful to determine the exact pH of the prepared buffer at 37°C to an accuracy of several decimal places.

Regardless, the kinetic parameters derived from fitting  $t_{lag}$  data to the model permit prediction of the lag time for POD/POPE/DOPE liposome preparations as a function of pH. Moreover, at any pH, the lag time can be adjusted by altering the initial percentage of POD in the lipid composition. A phase diagram of the iso-time to burst has been prepared in Fig. 2-8. This diagram predicts that a 20% PODS2000 particle kept at 37°C in pH 8.5 should be stable for about 3 days. Thus, these particles may lend themselves to being delivered by implantable pumps without fear of collapse over several days of pumping. Furthermore, a particle given by i.v. administration should also be stable for at least 5 hrs at pH 7.4, whereas a particle depleted of POD *in vivo*, under an environment of pH 5.0 will be stable for only minutes.





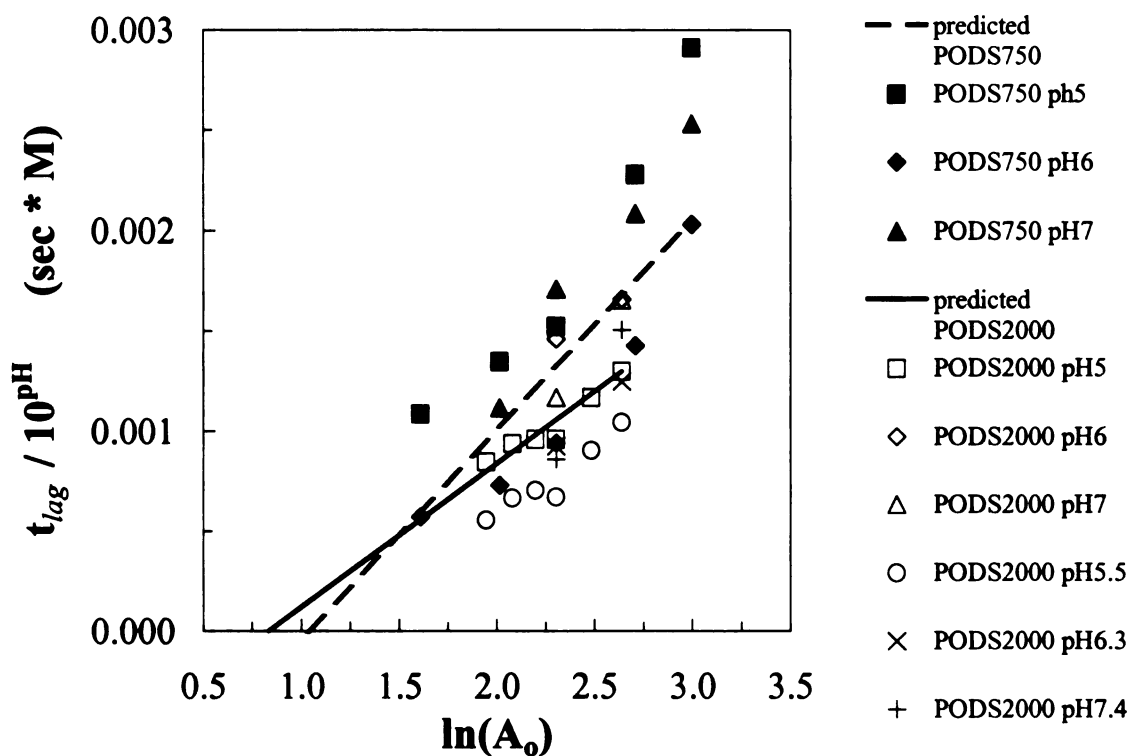


**Figure 2-7. PODS750 and PODS2000 follow the “minimum surface shielding” model.** The lag time,  $t_{lag}$ , was determined over a range of pH and initial percentages,  $A_0$ , for both PODS750 and PODS2000. Data from Table 2-1 are plotted for PODS750 liposomes at pH 5, pH 6, and pH 7. The dashed line indicates the best-fit prediction for PODS750 using  $k = 963 \pm 183 \text{ sec}^{-1} \text{M}^{-1}$  and  $A_c = 2.8 \pm 0.7\%$ . Data from Table 2-2 are plotted for PODS2000 liposomes at pH 5, pH 5.5, pH 6, pH 6.3, pH 7, pH 7.4. The solid line indicates the best-fit prediction for PODS2000 given by  $k = 1,390 \pm 232 \text{ sec}^{-1} \text{M}^{-1}$  and  $A_c = 2.3 \pm 0.6\%$ . This linearized form of the model is as follows:  $t_{lag}/10^{pH} = (1/k) * (\ln(A_0)) - (1/k) * (\ln(A_c))$ . The slope equals  $k^{-1}$  and the x-intercept equals  $\ln(A_c)$ .

San Francisco

Library

of the

City and

County of

San Francisco

California

1912

100

100

100

100

100

100

100

100

100

100

100

100

100

100

100

100

100

100

100

100

100

100

100

100

100

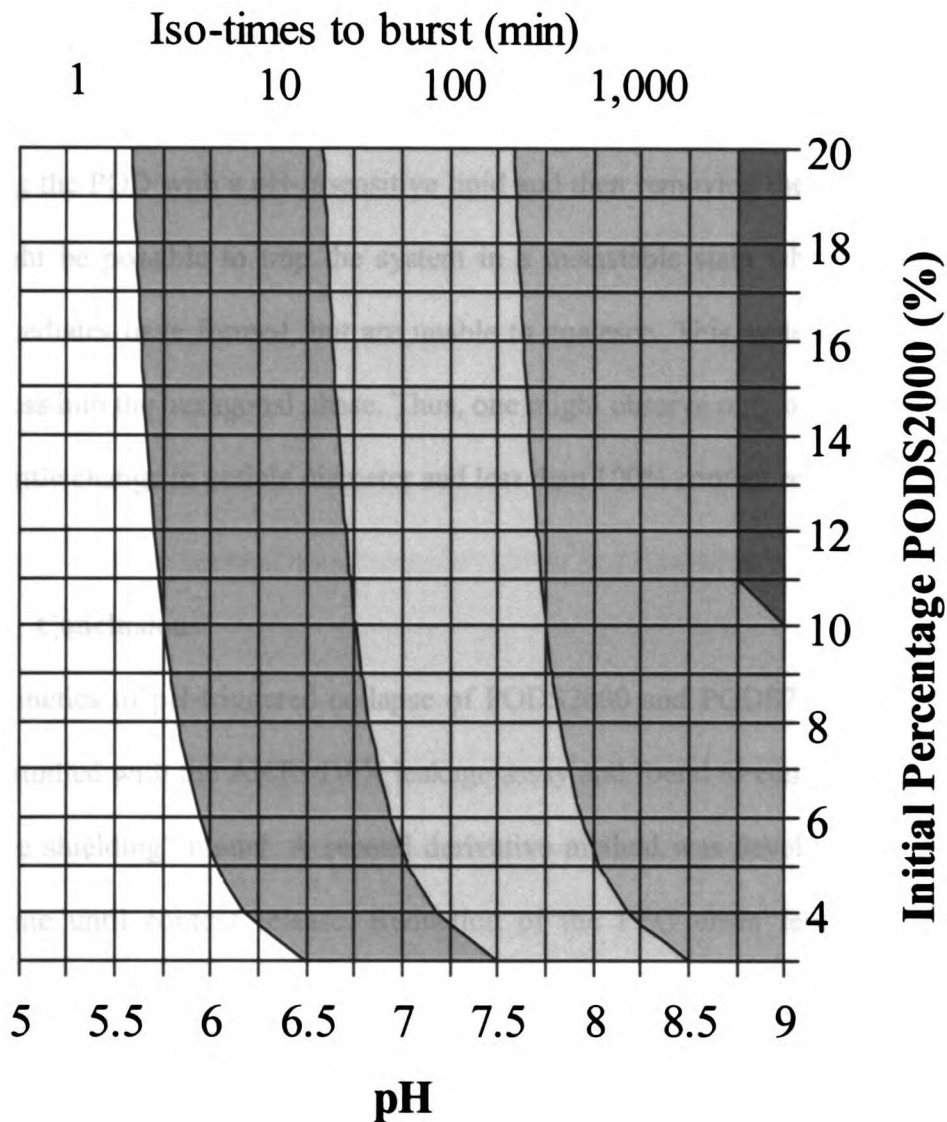


**Figure 2-8. Prediction of time to burst for PODS2000 liposomes.** Phase diagram showing the order of magnitude for the length of time until particle destabilization as a function of pH and initial percentage PODS2000,  $A_0$ . These lines between shaded regions indicate 'iso-times' where it takes the liposomes 1, 10, 100, or 1000 min to burst as indicated at the top of the graph. Data are based upon the "minimum surface shielding" model with  $A_c = 2.3 \pm 0.6$  mole % and  $k = 1,390 \pm 232 \text{ sec}^{-1}\text{M}^{-1}$ .



Lastly, based upon the observation that stable PEG lipids can stabilize all or just a fraction of the ANTS/DPX release (Fig. 2-4), it remains possible that by judiciously mixing the POD with a pH-insensitive lipid and then removing the POD lipid at low pH, it might be possible to trap the system in a metastable state where the early collapse intermediates have formed, but are unable to coalesce. This system might be unable to progress into the hexagonal phase. Thus, one might observe only outer monolayer mixing with little change in vesicle diameter and less than 100% content release.

## 2.5 Conclusions

The kinetics of pH-triggered collapse of PODS2000 and PODS750 PE liposomes have been studied with the ANTS/DPX leakage assay and found to conform to the “minimum surface shielding” model. A second derivative method was developed to determine the lag time until content release. Reduction of the PEG chain length or the use of a membrane permeable buffer both caused a slight decrease in the lag time. The presence of near critical amounts of a stable PEG-lipid partially prevented leakage of PODS2000 liposomes. Nonlinear regression was used to determine parameters of the model whereby a critical PEG surface coverage of  $A_c = 2.3 \pm 0.6$  mole % PODS2000 or  $2.8 \pm 0.7$  mole % PODS750 is required to stabilize the PE bilayer. The rate of hydrolysis,  $k$ , for PODS2000 is  $1,390 \pm 232 \text{ sec}^{-1}\text{M}^{-1}$  and  $963 \pm 183 \text{ sec}^{-1}\text{M}^{-1}$  for PODS750. These values can be used to predict liposome stability as a function of the environmental pH and the initial mole % of POD in the lipid composition.

1000

1000

1000

1000

1000

1000

1000



1000

1000

1000

1000

1000

1000

1000

1000

1000

1000

1000

1000

1000

1000

1000

1000

1000

1000

## CHAPTER 3:

### **Convection Enhanced Delivery: Liposome Distribution in Brain after Modulation of Particle Charge, Particle Diameter, and Presence of Steric Coating**

#### **3.1 Abstract**

We have investigated the role of diameter, charge, and steric shielding on the brain distribution of liposomes infused by convection enhanced delivery (CED) using both radiolabeled and fluorescent-labeled particles. Liposomes of 40 nm and 80 nm diameter traveled the same distance but penetrated significantly less than a 10 kD dextran; whereas 200 nm diameter liposomes penetrated less than 80 nm liposomes. A neutral liposome shielded by polyethylene glycol (PEG; 2 kD; 10% by mole) penetrated significantly farther than an unshielded liposome. Even when shielded with PEG, positive surface charge (10% by mole) significantly reduced the penetration radius compared to a neutral or negatively charged liposome (10% by mole). During CED, liposomes accumulated in a subpopulation of perivascular cells within the brain. A non-degradable lipid radiolabel showed that lipid components remained within these perivascular brain cells for at least 2 days. In contrast, a degradable lipid radiolabel was eliminated from the brain with a  $9.9 \pm 2.0$  hr half-life that may reflect the rate of binding and degradation. To decrease binding, 100-fold molar excess of non-labeled liposomes were co-infused with labeled liposomes, which significantly increased liposome penetration. These studies suggest that optimization of therapeutic CED using particles such as drug-loaded liposomes, polymeric nanoparticles, non-viral DNA complexes, and viruses will require a strategy to overcome particle binding and clearance by cells within the CNS.

12/12/60

12/12/60

12/12/60

12/12/60

12/12/60

12/12/60

12/12/60

12/12/60

12/12/60

12/12/60

12/12/60

12/12/60

12/12/60

12/12/60

12/12/60

12/12/60

12/12/60

12/12/60

12/12/60

12/12/60

12/12/60

12/12/60

12/12/60

12/12/60

12/12/60

12/12/60

12/12/60

12/12/60

12/12/60

12/12/60

12/12/60

12/12/60

12/12/60



### 3.2 Introduction

For many compounds, the blood brain barrier impedes drug delivery to the brain parenchyma so that systemic drug administration is ineffective for treating diseases of the CNS. For life-threatening or highly debilitating diseases, a drug infusion directly into the brain (intra cranial) may be the only feasible route of administration; however, agents directly infused into the brain in a small volume do not readily disperse from their infusion site. Diffusion coefficients are typically too low to allow even small molecule drugs to move more than a few millimeters. Additionally, diffusion requires a high concentration gradient to drive effective drug concentrations over a large distance [Saltzman *et al.* 1999]. Such high drug concentrations often lead to dose limiting neurotoxicity. A straightforward solution is to provide bulk convective flow at the site of infusion, a technique called convection enhanced delivery (CED) [Bobo *et al.* 1994, Groothuis 2000]. Small molecule agents have been administered using CED for the past 5 years [Viola *et al.* 1999, Lonser *et al.* 1999, Groothuis *et al.* 1999, Groothuis *et al.* 2000, Kaiser *et al.* 2000, Mardor *et al.* 2001, Levy *et al.* 2001, Carson *et al.* 2002]. Convective flow is also effective for distributing large macromolecules (MW > 500 Da) [Bobo *et al.* 1994, Lieberman *et al.* 1995, Chen *et al.* 1999, Hamilton *et al.* 2001, Bruce *et al.* 2000, Lonser *et al.* 2002, Sandberg *et al.* 2002a, Sandberg *et al.* 2002b] and nanoparticles, including viruses [Betz *et al.* 1998, Bankiewicz *et al.* 2000, Cunningham *et al.* 2000, Nguyen *et al.* 2001, Hirko *et al.* 2002], magnetic nanoparticles [Kroll *et al.* 1996], liposomes [Polfliet *et al.* 2001, Silva-Barcellos *et al.* 2004, Mamot *et al.* 2004, Saito *et al.* 2004], and non-viral DNA complexes [Ono *et al.* 1990, Roessler *et al.* 1994, Imaoka *et*

10000

10000

10000

10000

10000

10000

10000

10000

10000

10000

10000

10000

10000

10000

10000

10000

10000

10000

10000

10000

10000

10000

10000

10000

10000

10000

10000

10000

10000

10000

10000

*al.* 1998, Thorsell *et al.* 1999, Leone *et al.* 2000, Cao *et al.* 2002, Hirko *et al.* 2002]. Research into CED has progressed such that clinical trials have been initiated for treatment of brain tumors with conventional chemotherapeutic drugs, such as taxol [Mardor *et al.* 2001], and with DNA lipoplex [Voges *et al.* 2003, Voges *et al.* 2004].

A phase I/II clinical trial using CED of cationic DNA lipoplexes was completed with the recommendation that basic research needs to address the interaction between nanoparticle composition and brain/tumor tissue [Voges *et al.* 2003, Voges *et al.* 2004]. This research is a response, in part, to such recommendations [Weyerbrock *et al.* 1999, Voges *et al.* 2004]. Here we show that the ability of liposomes to flow by bulk fluid through living brain tissue is highly dependent upon their physical-chemical characteristics including size, charge, and steric coating. Additionally, a subset of cells in the brain accumulate neutral liposomes and necessitates a strategy to saturate liposome binding if CED is to reach its full potential for disseminating nanoparticle drug carriers through the brain.

### **3.3 Methods**

#### *3.3.1 Materials*

1,2-distearoyl-sn-glycero-3-phosphocholine (DSPC), 1,2-dioleoyl-sn-glycero-3-phosphoethanolamine (DOPE), 1,2-distearoyl-3-trimethylammonium-propane (DSTAP), 1,2-dioleoyl-3-trimethylammonium-propane (DOTAP), 1,2-distearoyl-sn-glycero-3-phosphoglycerol (DSPG), and cholesterol were obtained from Avanti Polar Lipids (Alabaster, AL). 10 kD FITC-dextran-lysine and fluorescent lipid tracers DiO (D-275), DiI (D-282), and DiD (D-307) were purchased from Molecular Probes (Eugene, OR).

San Francisco

LIBRARY  
OF THE  
CITY OF  
SAN FRANCISCO



San Francisco  
LIBRARY  
OF THE  
CITY OF  
SAN FRANCISCO

1874  
112

LIBRARY  
OF THE  
CITY OF  
SAN FRANCISCO

1874  
112

LIBRARY  
OF THE  
CITY OF  
SAN FRANCISCO

1874  
112

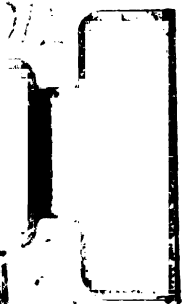
LIBRARY  
OF THE  
CITY OF  
SAN FRANCISCO

1,2-distearoyl-sn-glycero-3-monomethoxy-ether-poly-ethylene glycol (PEG-DSG, Sunbright DSG-20H) was a generous gift from A. Suginaka (NOF Corp., Tokyo, Japan). POD was synthesized in our lab as described elsewhere [Guo *et al.* 2003]. Alzet™ osmotic pumps (200 µL/day) and the Brain Infusion Kit II were purchased from Durect (Cupertino, CA). Green fluorescent protein (GFP) encoding plasmid was a generous gift from Valentis (Burlingame, CA).

### 3.3.2 Preparation of liposomes

For the preparation of liposomes, 10 µmole total lipid was mixed in chloroform and dried in a glass test tube by rotary evaporation under reduced pressure. The lipid film was placed under high vacuum for 4 hrs to remove residual solvent. Liposomes were formed in pH 8.5 Tris-acetate buffered saline (150 mM NaCl, 5 mM Tris base / acetate). The lipid (10 mM) was hydrated at 70°C with intermittent vortexing. ~80 nm liposomes were formed by extrusion (11x) through 80 nm pores in polycarbonate membranes at 60°C. ~200 nm diameter liposomes were formed by (3x) freeze (-20°C)/ thaw (70°C) cycles followed by extrusion (3x) through a 400 nm polycarbonate membrane at 60°C. To prepare ~40 nm small unilamellar vesicles (SUV), hydrated liposomes were sonicated for 1 hr at 65°C in the dark under argon. SUV were separated from larger particles by centrifugation at 20°C for 1 hr at 50,000 RPM in a Beckman Rotor TLA100.3. The supernatant was collected and sterile filtered through 0.45 µm to further remove larger aggregates. After particle formation, the concentration of lipid phosphate was determined by the method of Bartlett [Bartlett 1959]. Particle size and zeta potential, a method for estimating the amount of surface charge, were determined using a Malvern

San Francisco  
California  
Sept 11  
1850



San Francisco  
California  
Sept 11  
1850  
San Francisco  
California  
Sept 11  
1850  
San Francisco  
California  
Sept 11  
1850  
San Francisco  
California  
Sept 11  
1850

San Francisco  
California  
Sept 11  
1850

(Southborough, MA) Zeta3000 Dynamic Light Scattering Instrument and are presented in Table 3-1.

### 3.3.3 Preparation of nanolipoparticles

DNA was encapsulated into a pH-sensitive nanolipoparticle (NLP) using a detergent dialysis method, as described [Li *et al.* 2005], using a pH-sensitive polyethylene glycol di-orthoester (POD) lipid [Guo *et al.* 2003]. Briefly, 200 µg of plasmid DNA encoding GFP was dissolved in 1.5 mL of 5 mM Tris-acetate pH 8.3 and 28 mM n-octylglucopyranoside. Separately, 2.5 µmole of total lipid was dissolved in 1.5 mL of the same buffer, with a lipid composition of DOTAP:DOPE:POD:DiI [50:40:10:0.1]. The DNA solution was added to the lipid solution under stirring, giving a positive / negative charge ratio of 2. The solution was dialyzed against 4 liters of Tris-acetate buffer pH 8.5 for 6 hrs at 20°C with a 10 kD MWCO. The solution was further dialyzed against 3 additional changes (4 L) of Tris-acetate pH 8.5 at 4°C over 2 days. The picogreen assay was used to confirm DNA encapsulation efficiency [Choi *et al.* 2003].

1940

1941

1942

1943

1944

1945

1946

1947

1948

1949

1950

1951

1952

1953

1954

1955

1956

1957

1958

1959

1960

1961

1962

1963

1964

1965

1966

1967

1968

1969

1970

1971

1972

1973



**Table 3-1. Compositions and characteristics of polymers and particles used in CED experiments**

Particle	Color	Composition	Formation	Size* (nm)	Zeta Potential** (mV)
dextran	green	10 kD dextran, FITC labeled, lysine fixable	polymer	-	nd***
40 nm	red	DSPC:Chol:PEG-DSG:DiD [50:40:10:0.1]	sonicated liposome	43.2	nd
80 nm	green	DSPC:Chol:PEG-DSG:DiO [50:40:10:0.1]	80 nm extruded liposome	84±2.1	2.6±1.8
80 nm	red	DSPC:Chol:PEG-DSG:DiD [50:40:10:0.1]	80 nm extruded liposome	85.8±0.8	5.1±1.3
200 nm	red	DSPC:Chol:PEG-DSG:DiD [50:40:10:0.1]	400 nm extruded liposome	197.3±0.6	nd
10% negative	red	DSPG:DSPC:Chol:PEG-DSG:DiD [10:40:40:10:0.1]	80 nm extruded liposome	83.3±9.6	-8.6±2.4
10% positive	red	DSTAP:DSPC:Chol:PEG-DSG:DiD [10:40:40:10:0.1]	80 nm extruded liposome	89.3± 1.1	70.0±2.4
no PEG	red	DPSC:Chol:DiD [60:40:0.1]	80 nm extruded liposome	91.0±2.8	-10.3±2.7
Excess Liposomes	none	DSPG:DSPC:Chol:PEG-DSG:DiD [10:40:40:10:0.1]	80 nm extruded; high pressure	108.3± 0.8	nd
<sup>125</sup> I-BPE Liposomes	none	DSPC:Chol:PEG-DSG [50:40:10] <0.01% <sup>125</sup> I-BPE	80 nm extruded liposome	89.9±1.9	nd
<sup>3</sup> H-Chol Liposomes	none	DSPC:Chol:PEG-DSG [50:40:10] <0.01% <sup>3</sup> H-Chol	80 nm extruded liposome	82.5±0.4	nd
GFP-NLP	red	DOTAP:DOPE:POD:DiI [50:40:10:0.1]	detergent dialysis 2.5 μmole lipid + 200 μg plasmid	110.6±5.5	nd

\* particle diameter measured by light scattering zeta average size, ± indicates standard deviation

\*\* zeta potentials all at low salt 1 mM NaCl, 1 mM Hepes, pH 7.5, ± indicates 95% confidence interval

\*\*\* not determined

FRANCISCO

1850

1851

1852

1853

1854

1855

1856

1857

1858

1859

1860

1861

1862

1863

1864

1865

1866

1867

1868

1869

1870

1871

1872

1873

1874

1875

1876

1877

1878

1879

1880

1881

1882

1850

1851

1852

1853

1854

### 3.3.4 Preparation of radiolabeled liposomes

For radiolabeled liposome biodistribution experiments we synthesized a headgroup iodinated benzamidine phospholipid ( $^{125}\text{I}$ -BPE), as described previously [Abra *et al.* 1982]. Tritiated liposomes were prepared using cholesteryl hexadecyl ether ( $^3\text{H}$ -Chol) purchased from Perkin Elmer (Boston, MA). Radiolabeled lipids (less than 0.01% mole percent of the total lipid) were deposited as a film with other lipid components from a chloroform solution before hydration. Gamma radiation activity was determined using a Perkin Elmer Wizard Gamma Counter (Boston, MA). Tritium radiation activity was measured after solublizing tissues with Perkin Elmer Solvable and diluting into Perkin Elmer liquid scintillation cocktail Ultima Gold, according to the recommendations of the manufacturer. Tritium disintegrations per min were obtained on a Beckman Liquid Scintillation Counter (Fullerton, CA).

### 3.3.5 Osmotic pump infusion

Before implantation, each liposome preparation was diluted to a concentration of 1 mM lipid in TBS. Dextran was diluted to 1 mg/mL. Nanolipoparticles (NLP) were diluted to a DNA concentration of 50  $\mu\text{g}/\text{mL}$ . Infusions were loaded into 200  $\mu\text{L}$  / day Alzet<sup>TM</sup> pumps and delivered by a brain infusion cannula with an outer diameter of 0.36 mm (Durect; Cupertino, CA). It was important to determine what fraction of the 200  $\mu\text{L}$  dose was actually delivered to the parenchyma vs. leaked up the cannula. Leakage along the cannula track is a common problem encountered in small animal models of CED, and large diameter cannula and high flowrate are the two main variables that cause leakage [Chen *et al.* 1999]. Thus, to determine the true flowrate into the brain, both non-



degradable  $^3\text{H}$ -Chol and  $^{125}\text{I}$ -BPE labeled liposomes were infused using the osmotic pump.

Athymic rats were purchased from the National Cancer Institute and cared for at the UCSF Laboratory Animal Resource Center. We adhered to strict protocols as recommended by the National Institute of Health Guide for the Care and Use of Laboratory Animals and as approved by the UCSF Institutional Animal Care and Use Committee. To minimize pain and discomfort, animals were sedated with an intraperitoneal injection of Ketamine (60 mg / kg body weight) and Xylazine (7.5 mg / kg body weight). After anesthesia was attained, an incision was made in the scalp above the bregma and the animal was mounted in a stereotactic frame (Stoelting, Wood Dale IL). A hole was drilled in the skull 3 mm right of the bregma. The 5 mm long infusion cannula was attached to the top of the skull by dental cement and an anchoring screw, and the tip of the cannula was centered within the caudate putamen [Paxinos and Watson 1982]. The loaded pump was inserted into a subcutaneous pocket on the back of the animal. To relieve pain following surgery, animals were given a subcutaneous injection of Buprenorphine (0.05 mg / kg body weight). 24 hrs following pump implantation, animals were sedated and sacrificed. After sedation, animals with fluorescent markers were prepared by perfusion fixation with 200 mL of phosphate buffered saline PBS (100 mM phosphate, 150 mM NaCl, pH 7.4) and 200 mL of 4% paraformaldehyde in PBS. Brains were removed and post-fixed overnight in 4% paraformaldehyde at 4°C.



### 3.3.6 *Acute stereotactic infusion*

To determine the elimination rate of liposomes from the brain, animals were given an acute infusion of radiolabeled liposomes at a peak flowrate of 0.8  $\mu\text{L} / \text{min}$ . Animals were sedated and mounted on a stereotactic frame. To prevent backflow at this higher flowrate [Chen *et al.* 1999] a narrow cannula was prepared from fused silica tubing with an outer diameter of 0.16 mm (Polymicro Technologies, Phoenix, AZ) extending 3 mm from the tip of a 24 gauge needle used for support. This cannula was inserted into the same stereotactic coordinates used for the osmotic pumps. A syringe pump was used to infuse solutions into the brain at an increasing flowrate as follows: 0.1  $\mu\text{L} / \text{min}$  for 5 min, 0.2  $\mu\text{L} / \text{min}$  for 5 min, 0.5  $\mu\text{L} / \text{min}$  for 5 min, 0.8  $\mu\text{L} / \text{min}$  for 30 min for a total volume of 28  $\mu\text{L}$  infused over 45 min [Mamot *et al.* 2004, Saito *et al.* 2004]. The volume infused into the brain was assessed by subtracting the recovered radiolabel in the syringe at the end of the infusion from the amount initially added to the syringe. The infusion cannula was withdrawn over a 5 min period following cessation of infusion. Post infusion, animals were sacrificed at 1, 6, 24, or 48 hrs. Cerebrospinal fluid was sampled in anesthetized animals by surgically exposing and piercing the cisterna magna with a micropipette.

### 3.3.7 *Section preparation and macroscopic imaging*

Fixed brains were suspended in 7% low melting point agarose immediately before sectioning. The entire brain was sliced into 200  $\mu\text{m}$  axial sections using a Vibratome (St. Louis, MO). A cooling stage was used to keep the brain and sections immersed in 4°C





PBS during sectioning. These sections were imaged macroscopically using a fluorescence scanner, the Molecular Dynamics Storm<sup>TM</sup> (Amersham Biosciences; Piscataway, NJ) for both blue fluorescence (excitation = 450 nm; emission > 520 nm) and red fluorescence (excitation = 640 nm; emission > 650 nm). Images (16 bit) were saved as TIFF files for analysis.

### 3.3.8 *Confocal microscopy*

Confocal images were obtained on axial sections of brain that cross the tip of the infusion cannula. All images were taken using LaserSharpe Software on a Biorad 1024 Confocal Scanning Laser Microscope (Hercules, CA) mounted on a Nikon Diaphot 200 microscope. The DiI signal was acquired in photomultiplier 1 with excitation from the 568 nm line of a krypton-argon laser. The DiO or FITC signals were acquired in photomultiplier 2 with excitation from the 488 nm line of a krypton-argon laser, and the DiD signals were acquired in photomultiplier 3 with excitation from the 633 nm line of a helium-neon laser. To allow quantitative image processing, the gain on the photomultiplier signal was set low enough to prevent pixel overexposure in the images. Multiple regions of interest were imaged using a 4x objective lens and saved as 8 bit PIC files at a resolution of 2.5  $\mu\text{m}$  per pixel. Using Image J version 1.3.1\_03 (<http://rsb.info.nih.gov/ij/>), the PIC files were converted to 24 bit RGB TIFF images. The FITC or DiO fluorescence was depicted by the green channel and the DiD or DiI fluorescence was depicted by red. These images were then imported into Adobe Photoshop Version 7.0 (San Jose, CA), overlaid with adjacent images, and saved to a



single 24 bit RGB TIFF file for analysis. Similarly, higher resolution images were acquired using a 40x oil objective at a resolution of 0.25  $\mu\text{m}$  per pixel.

### 3.3.9 Data analysis

A radially directed profile in a region extending from the tip of the cannula outward was extracted from either the confocal microscopy or fluorescence macroscopy images using Image J. When the liposomes reached a ventricle or white matter track, there was often leakage around the periphery of the caudate. For this reason, radial profiles were obtained only in regions of convection through gray matter where staining was uninterrupted. In all cases, the profile was obtained by taking a box of 0.5 mm in height and extending away from the center of the infusion 2-6 mm, based on the distance of particle penetration. This RGB image was separated into both red and green 8 bit TIFFs. For each color box, the plot profile was obtained and the raw data were saved to a Microsoft Excel<sup>TM</sup> (Redmond, WA) spreadsheet for further analysis.

To characterize the extent of particle penetration, two radii were calculated for each profile, the half maximum radius,  $r_{50\% \text{ max}}$ , and the radius of 50% area under the curve (AUC),  $r_{50\% \text{ AUC}}$ . The half maximum radius is an estimate of the farthest extent of particle distribution from the cannula, the radius,  $r_{50\% \text{ max}}$ , where:

$$I_{r_{50\% \text{ max}}} = 0.5 (I_{\text{maximum}} - I_{\text{minimum}}) + I_{\text{minimum}} \quad \text{Eq. 3-1}$$

Where  $I_{r_{50\% \text{ max}}}$  is the intensity halfway between the maximum signal,  $I_{\text{maximum}}$ , and the background signal,  $I_{\text{minimum}}$ . The radius of 50% area under the curve,  $r_{50\% \text{ AUC}}$ , estimates where half of the fluorescent signal has been deposited.  $r_{50\% \text{ AUC}}$  was calculated for each

7/10/50  
MARY  
LIBR  
7/10/50  
LIBR



profile by first subtracting the background signal in unstained gray matter, and then integrating using the trapezoidal rule to obtain the AUC as a function of radius. The maximum AUC near the end of the plot was used to normalize the profile. This normalized percentage AUC and the corresponding raw data are shown for the same brain sections observed either macroscopically by the fluorescence scanner (Fig. 3-2A) or microscopically by the confocal microscope (Fig. 3-2B).

### 3.3.10 Statistical analysis

Statistical analysis was performed using SPSS version 11.5 (Chicago, IL). Average radii of distribution (both  $r_{50\% \max}$  and  $r_{50\% \text{ AUC}}$ ) and standard deviations are provided in Table 3-3. ANOVA was performed using SPSS to identify significant variations in the  $r_{50\% \text{ AUC}}$ . For all profiles without excess liposomes, a two-way ANOVA was performed on the Log ( $r_{50\% \text{ AUC}}$ ) with two independent variables: with variable 1 as animal identification and variable 2 as particle type (7 subgroups: dextran, 40 nm, 80 nm, 200 nm, positive, negative, no PEG). To identify significant differences, a two-tailed Dunnett's test was used to compare each particle to 80 nm control liposomes and the resulting p value for each particle is indicated in Table 3-3. There was no way to provide an internal control for animals that were given excess liposomes; therefore, to compare the effect of excess liposomes a one-way ANOVA (3 groups: 80 nm without excess liposomes, 80 nm with excess liposomes, dextran with excess liposomes) was performed on the Log ( $r_{50\% \text{ AUC}}$ ). To determine significant comparisons the ANOVA was followed by a two-tailed Dunnett's test to compare against 80 nm control liposomes without excess lipid.

LIBRARY

LIBRARY

LIBRARY

LIBRARY

LIBRARY

LIBRARY

LIBRARY

LIBRARY

LIBRARY

LIBRARY

LIBRARY

LIBRARY

LIBRARY

LIBRARY

LIBRARY

LIBRARY

LIBRARY

LIBRARY

LIBRARY

LIBRARY

LIBRARY

LIBRARY

LIBRARY

LIBRARY

LIBRARY

LIBRARY

LIBRARY

LIBRARY

LIBRARY

LIBRARY

LIBRARY

LIBRARY

LIBRARY

LIBRARY

LIBRARY

LIBRARY

LIBRARY

LIBRARY

### 3.4 Results

We have used both radioisotopes and fluorescent labels to better understand the fate of nanoparticulates following convection enhanced delivery (CED) to the rat brain. Confocal imaging immediately revealed that a subset of brain cells rapidly accumulates liposomes (Fig. 3-1). To investigate the effect of these cells following CED, we infused two types of radiolabeled liposomes. The first probe was a headgroup labeled phospholipid  $^{125}\text{I}$ -BPE that is susceptible to degradation [Abra *et al.* 1982], and the second probe was a non-exchangeable, metabolically stable, tritium labeled cholesteryl hexadecyl ether ( $^3\text{H}$ -Chol). One hr after the start of infusion both probes gave identical biodistribution (Table 3-2). Liposomes labeled with the non-degradable  $^3\text{H}$ -Chol radioactive tracer remained in the brain at least two days without a reduction of signal (Table 3-2); however, the  $^{125}\text{I}$ -BPE liposomes rapidly lost signal in the brain with a  $9.9 \pm 2.0$  hr half-life. This indicates that liposome components remained in the brain but underwent degradation.

In addition to acute infusion (Table 3-2), we wanted to deliver particles over longer periods (24 hrs) using an implantable pump. Due to the relatively large diameter of the brain infusion cannula (0.36 mm, 28 Gauge) we became concerned that a significant fraction of the dose was leaking up the cannula tract. It has been reported that 28 Gauge infusion cannula can have extensive leakback [Chen *et al.* 1999]. For this reason we infused radiolabeled liposomes with this pump to validate the efficiency of delivery to the brain. The non-exchangeable  $^3\text{H}$ -Chol labeled liposomes were infused using the 24 hr Alzet<sup>TM</sup> pump, giving  $3.07 \pm 1.04\%$  (n=3) of the infused dose in the brain. By the same

LIBRARY

LIBRARY

LIBRARY

LIBRARY

LIBRARY

LIBRARY

LIBRARY

LIBRARY

LIBRARY

LIBRARY

LIBRARY

LIBRARY

LIBRARY

LIBRARY

LIBRARY

LIBRARY

LIBRARY

LIBRARY

LIBRARY

LIBRARY

LIBRARY

LIBRARY

LIBRARY

LIBRARY

LIBRARY

LIBRARY

LIBRARY



method, the  $^{125}\text{I}$ -BPE labeled liposomes were also infused, giving a similar value of  $4.4 \pm 3.8\%$  ( $n=4$ ) of the infused dose in the brain. This delivery was confirmed with the generous assistance of Dr. Tomoko Ozawa, an expert at the surgical implantation of pumps for brain infusion. Dr. Ozawa performed the implantation in one animal, and after 24 hrs of infusion, 4.0% of the  $^{125}\text{I}$ -BPE labeled liposomes were in the brain. We conclude that this delivery was a function of the Alzet<sup>TM</sup> Brain Infusion Cannula itself, and not the surgeon. With the understanding that leakage would be an unpredictable source of error with the implantable pump, all the fluorescent experimental particles were co-infused with a control liposome. Thus all fluorescent observations were normalized to the distribution of a standard control particle, delivered by an osmotic pump at  $0.14 \mu\text{L} / \text{min}$  for 24 hrs.

#### *3.4.1 Liposome co-infusion into the rat brain*

To determine the spatial distribution of liposomes, our approach was to co-infuse fluorescent particles with different emission spectra (different colors). This experimental design is helpful for overcoming variability between animals. The arrangement for pump implantation and infusion is pictured in Fig. 3-1A. Following co-infusions, we imaged sections of the brain macroscopically using a I fluorescence scanner (Fig. 3-1[B-C]), and made more detailed inspections using fluorescence confocal microscopy. To determine the radius of particle distribution, we performed image analysis within regions of convective flow that were uninterrupted by white matter tracts. Thus, these studies are representative of how nanoparticulates perfuse through gray matter. All comparisons have been made against a standard liposome formulation, 80 nm neutral



DSPC:Chol:PEG-DSG [50:40:10] with either 0.1% DiO (green) or 0.1% DiD (red) as appropriate. While the analyzed direction of convective flow was subjective, each particle was compared with an internal control liposome that allowed us to make definitive statements about particle location as a function of particle characteristics.



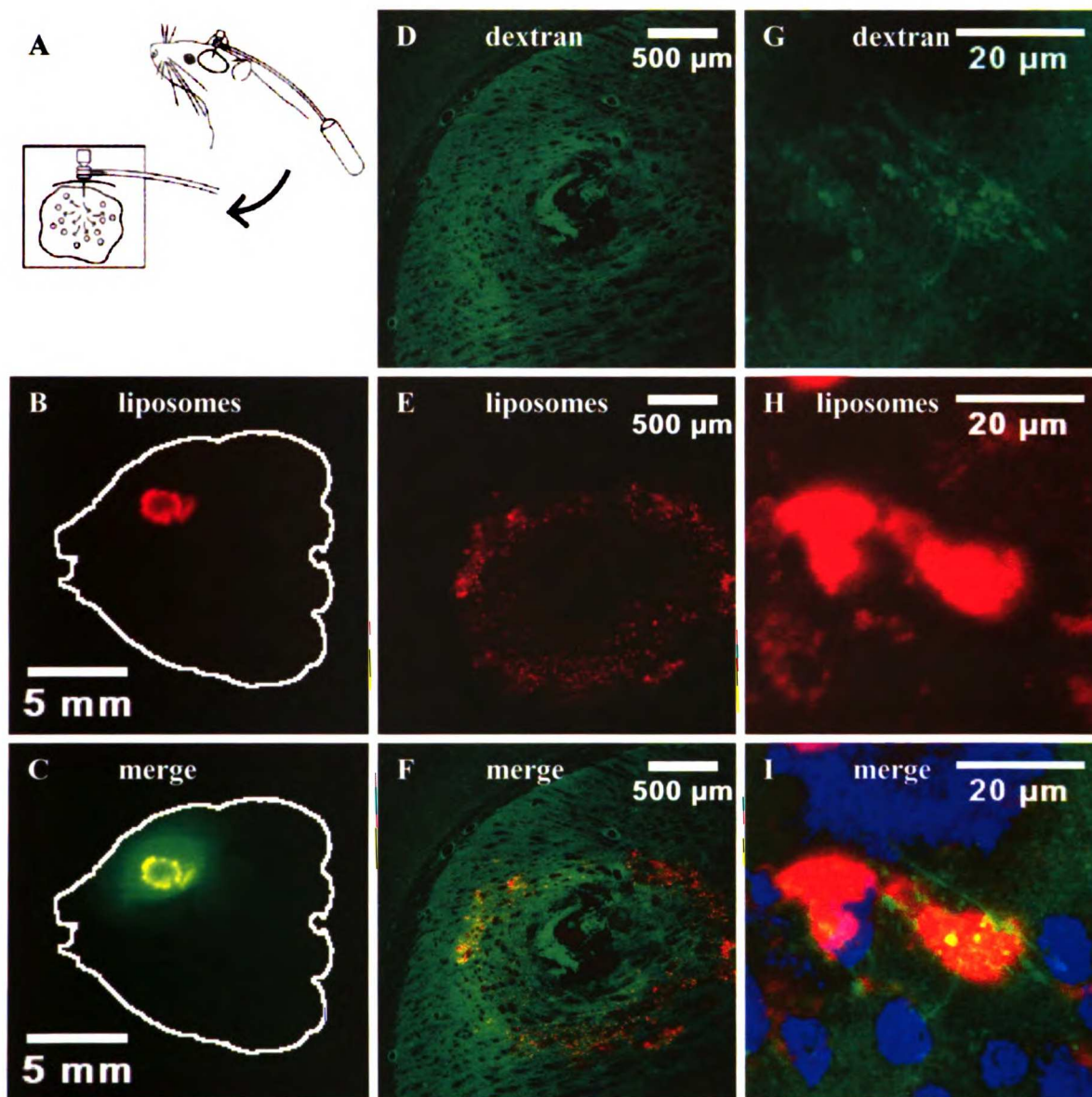


**Figure 3-1. Comparison of the distribution of fluorescent liposomes to fluorescent 10 kD dextran after co-infusion using CED.** All images are taken from axial brain sections with either neutral 80 nm PEG liposomes (red) or 10 kD dextran (green). [A] Animals are implanted with a brain infusion cannula attached to a subcutaneous osmotic pump as delivered in [B-I]. [B-C] a macroscopic fluorescence image of the brain slice imaged in [D-I]. [B] fluorescent liposomes. [C] merged image of liposomes and dextran. [D-F] taken using confocal microscopy with a 4x objective. [D] centers on the defect left by the tip of the infusion cannula. [E] cells containing liposomes appear as small punctate objects surrounding the infusion site. [F] merged image of [D] and [E] confirming that dextran penetrated beyond liposomes. [G-I] a z-projection through confocal images taken with a 40x objective. [G] dextran primarily stained interstitial space; however, the center of this panel shows that dextran also stained a branching capillary. [H] two cells containing red liposomes. [I] a merged image of [G] and [H] showing that liposome-containing cells are perivascular. The blue color depicts cells that excluded dextran. Two perivascular cells (red) in panel [I] also show internalized dextran within vacuoles (yellow) suggesting active phagocytosis.

Francisco

RARY

LIBRARY

LIBRARY

LIBRARY

LIBRARY

LIBRARY

LIBRARY

LIBRARY

LIBRARY

LIBRARY

LIBRARY

LIBRARY

LIBRARY

LIBRARY

LIBRARY

LIBRARY

LIBRARY

LIBRARY

LIBRARY

LIBRARY

LIBRARY

LIBRARY

LIBRARY

LIBRARY

LIBRARY

LIBRARY

LIBRARY

LIBRARY

LIBRARY

LIBRARY

LIBRARY

LIBRARY

LIBRARY

LIBRARY

LIBRARY

LIBRARY

LIBRARY

LIBRARY

LIBRARY

LIBRARY

LIBRARY

LIBRARY

LIBRARY

LIBRARY

LIBRARY

LIBRARY

LIBRARY

LIBRARY

LIBRARY

LIBRARY

LIBRARY

LIBRARY

LIBRARY

the  
loc

Fig. 3-1 [B-C] were taken with the macroscopic fluorescence scanner, and the entire outer edge of the axial brain section was highlighted in white. All subsequent images in this chapter were taken by confocal microscopy centered on the tip of the infusion cannula within the region illuminated by particles in Fig. 3-1 [B-C]. Fig. 3-1B shows the liposomes (red), and Fig. 3-1C contrasts the distribution of these liposomes with dextran (green). Dextran (10 kD) approximates how a protein, such as albumin [Lieberman *et al.* 1995, Chen *et al.* 1999] or transferrin [Bobo *et al.* 1994], might distribute under CED and covers a larger area than the 80 nm liposomes (Fig. 3-1C). Fig. 3-1[D-F] are confocal images of this same section. The dextran (green) shows the defect left by the cannula tip in the center of Fig. 3-1D. The liposomes (red) halted abruptly about 1 mm away from the center of infusion and have a punctate distribution (Fig. 3-1E), suggesting that these liposomes have been concentrated within a subpopulation of cells. The merged confocal image confirms that the dextran distributed farther than the liposomes (Fig. 3-1F). Fig. 3-1[G-I] are stacked confocal images at high magnification that center upon two liposome-engulfing cells. Fig. 3-1G shows a branching capillary stained by dextran. Fig. 3-1H shows a close up of two cells that have engulfed liposomes, leaving only low-level fluorescence in the surrounding tissue. The merged image (Fig. 3-1I) shows that the cells stained by the liposomes (red) also have vacuoles stained with dextran (yellow). At high magnification, the dextran is excluded from most brain cell types and these regions (~10  $\mu\text{m}$  in diameter) have been pseudo-colored blue in Fig. 3-1I. Most of the cells in Fig. 3-1I have taken up neither the dextran nor the liposomes. Inspection of Fig. 3-1I reveals that these phagocytic cells (red) are perivascular. Presumably, these cells are the primary location of elimination/degradation of neutral liposomes within brain parenchyma.





### 3.4.2 *Elimination of liposomes from the brain*

To learn more about the activity of the liposome engulfing cells imaged in Fig. 3-11, we infused radiolabeled liposomes into the brain to quantitatively assess the rate of elimination (Table 3-2). To determine the rate of probe elimination, we performed acute infusion of liposomes at 0.8  $\mu\text{L}/\text{min}$  directly to the brain. Animals were sacrificed at 1, 6, 24, and 48 hrs after the start of infusion and biodistribution was assessed. The  $^3\text{H}$ -Chol labeled liposomes showed no significant elimination from the brain parenchyma, with an average of  $49 \pm 13\%$  ( $n=3$ ) of the infused dose remaining in the brain at 48 hrs (Table 3-2). A variable percent of liposomes were found in the cerebrospinal fluid (CSF) immediately following the infusion at 1 hr, but the CSF at later time points contained virtually no radiolabel (Table 3-2).  $^{125}\text{I}$ -BPE labeled liposomes were eliminated from the brain with a more rapid  $9.9 \pm 2.0$  hr half-life with  $64 \pm 12\%$  remaining at 1 hr,  $49 \pm 8\%$  at 6 hrs, and  $10.9 \pm 2.4\%$  at 24 hrs. Thus, the bulk of the lipid components resided in the brain for long periods of time as shown by the tritium labeled liposomes; however, the liposomes were rapidly removed from extracellular space and subject to degradation by the perivascular cells.



**Table 3-2. Disposition of radiolabeled liposomes following convection enhanced delivery\***

Time After Infusion Start**	Lipid Radiolabel	Percent in Brain (%)	Percent in CSF***	Percent in Blood****	Percent in Liver (%)	Percent in Spleen (%)	Percent in Intestines (%)	Percent in Urine (%)	Percent in Feces (%)
1 hr	<sup>3</sup> H-Chol	63±17	19±19	1.0±1.0	1.1±1.4	0.02±0.01	nd*****	nd	nd
24 hrs	<sup>3</sup> H-Chol	39±7	0.02±0.01	4.1±1.0	7.6±1.2	1.0±0.4	nd	0.07±0.03	1.3±1.2
48 hrs	<sup>3</sup> H-Chol	49±13	0.01±0.01	1.0±0.1	12.0±4.1	1.0±0.4	nd	0.41±0.07	21.4±2.5
1 hr	<sup>125</sup> I-BPE	64±12	nd	0.3±0.4	0.1±0.1	0.01±0.01	0.08±0.05	nd	nd
6 hrs	<sup>125</sup> I-BPE	49±8	nd	16.5±4.0	2.5±0.4	0.6±0.1	1.9±0.3	1.5±0.5	0.02±0.01
24 hrs	<sup>125</sup> I-BPE	11±2	nd	16.0±0.8	3.5±0.3	0.9±0.1	11.8±8.3	21±14	8.7±5.6

\* ± indicates standard deviation of 3-4 animals

\*\* delivered at maximum flowrate of 0.8 µL per min for a total of 28 µL

\*\*\* assuming total volume of CSF is 0.3 mL

\*\*\*\* assuming blood total volume is 6.4% body weight

\*\*\*\*\* not determined



At 24 hrs, both probes showed a sizable percentage (4.1% to 16.0%) of label circulating within the blood. The level of label in the blood was higher for the  $^{125}\text{I}$ -BPE labeled liposomes (16.0%) probably because degradation in the brain released more label into the bloodstream. The  $^3\text{H}$ -Chol labeled liposomes were partially cleared from the blood at 48 hrs to only 1.0%, down from 4.1% at 24 hrs (Table 3-2). At 48 hrs  $12.0 \pm 4.1\%$  of the infused dose was found in the liver, indicating that the liposomes underwent slow elimination from the blood. At 24 hrs,  $21 \pm 4\%$  of the  $^{125}\text{I}$  label was in the urine, indicating degradation of the  $^{125}\text{I}$  from the lipid anchor, possibly within the brain. Lipids strongly bind into membranes and liposomes, forming large structures too large to be filtered into the urine by the kidney. In contrast, The  $^3\text{H}$ -Chol label cannot be degraded, and only small amounts were found in the urine. For both labels, only low levels of dose were found in the spleen; however, the  $^{125}\text{I}$  label was found to eliminate to the intestines at 24 hrs, and both labels were then found in the feces at 24 - 48 hrs after infusion. High levels of radioactivity of either label not were found in the thyroid, the stomach, the kidneys, the gall bladder, the lungs, or the heart (data not shown).

#### 3.4.3 *Validation of co-infusion measurements*

The radius of distribution for each curve was determined from a box of pixels extending away from the tip of the cannula along the flow of convection. Fig. 3-2 [A-B] shows a box of pixels that is 0.5 mm in height and 2 mm in length. Fig. 3-2A was derived from a macroscopic scanner image. Fig. 3-2B was derived from a confocal microscopy image of the same region. The profile of the image is plotted from left to right and indicated as red fluorescence (Fig. 3-2[A-B]). The percentage AUC was calculated from the raw data and

San Francisco

LIBRARY



See

Li

LIBRARY

San Francisco

112



112

San Francisco

LIBRARY



See

Li

LIBRARY

San Francisco

112



112

112

112

112

112

112

112

112

112

112

LIBRARY

plotted on Fig. 3-2[A-B]. Inspection of the curves shows that the fluorescence falls off dramatically at about 1 mm radius, which corresponds to the number determined by the half maximal radius,  $r_{50\% \max}$ . Importantly, the percentage AUC gives essentially the same profile for data taken either macroscopically (Fig. 3-2A) or by confocal microscopy (Fig. 3-2B).

We further validated our co-infusion measurements by determining if either the instrument of measurement or the color of measurement had a significant effect upon the radius of distribution. To verify that the instrument of measurement (macroscopic scanner vs. confocal microscopy) does not make a difference in the radius of distribution, we compared two groups of measurements on 80 nm PEG shielded liposomes. Animals in group 1 were measured on the macroscopic scanner and had an average distribution ( $r_{50\% \text{ AUC}}$ ) of  $0.95 \pm 0.56$  mm (n=7). Animals in group 2 were measured by confocal microscopy and had an average distribution ( $r_{50\% \text{ AUC}}$ ) of  $0.73 \pm 0.25$  mm (n=19). The difference between the means of these two groups was very slight and not statistically significant.





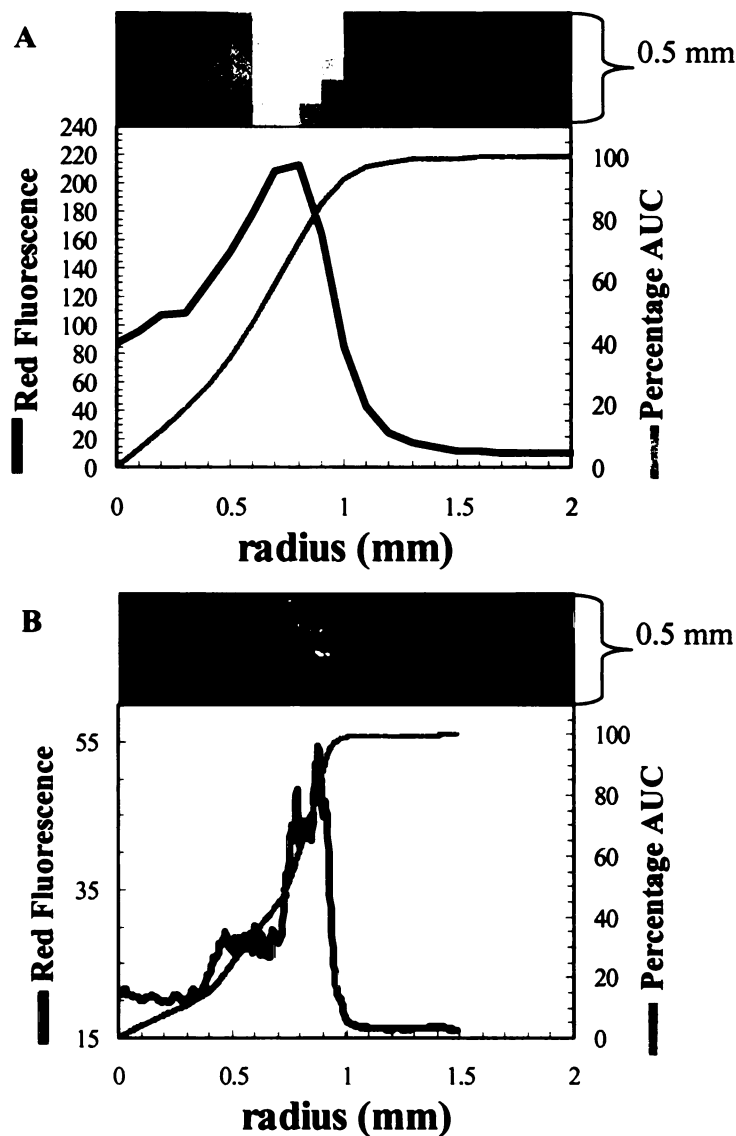


**Figure 3-2. Illustration of data analysis of fluorescence distribution in brain sections.** Panels [A] and [B] are 0.5 mm by 2 mm images of brain infused with 80 nm liposomes (DiD stained). Both images are from the same section and radial direction away from the cannula tip ( $r=0$ ). An average intensity profile across the section is plotted (black line). From the intensity profile, the percentage area under the curve (AUC) was calculated and is plotted (gray line). The percentage AUC can be interpreted as the radius where a given percentage of the signal has deposited. [A] was taken using a macroscopic fluorescence scanner at a resolution of 10 pixels per mm. [B] was taken using confocal microscopy at a resolution of 400 pixels per mm. The similarity between [A] and [B] illustrates that on either instrument (Storm<sup>TM</sup> or confocal microscope), image analysis gives similar radial distribution profiles for fluorescent liposomes following CED.



We also validated that the color of the fluorophore (green vs. red) did not affect the measured distribution ( $r_{50\% AUC}$ ) by comparing two groups of images. Group 1 consisted of animals given the DiO labeled (green) 80 nm liposomes and had an average distribution ( $r_{50\% AUC}$ ) of  $0.82 \pm 0.41$  mm (n=17). Group 2 animals were infused with DiD labeled (red) 80 nm liposomes with an average distribution ( $r_{50\% AUC}$ ) of  $0.73 \pm 0.23$  mm (n=9). Again, the difference between these means is small, and a t test between these groups showed no significant difference. These tests demonstrate that the observed radius of distribution is independent of the detection instrument, the chemical structure of the fluorescent probe, and detection color used to gather distribution data.

#### *3.4.4 Comparing co-infused particle radii of distribution*

To overcome animal variability within groups, direct comparison between particles was made by co-infusion with a control liposome. The resulting distributions,  $r_{50\% AUC}$ , for these compositions were compared to the control liposome (Table 3-3). For statistical comparison, the Log ( $r_{50\% AUC}$ ) was defined as the dependent variable to make standard deviations independent of radius. A two-way ANOVA model significantly explained variation in the data ( $R^2=0.980$ , n=42, p <0.0005). The particle variable was a significant component of the model (p<0.0005). Following ANOVA, multiple comparisons were performed using Dunnett's t test against the control liposomes and the associated p values are indicated (Table 3-3).

FRANCIS

RAY

LIBRARY  
UNIVERSITY OF  
MICHIGAN

1957

1957

FRANCIS

RAY

LIBRARY  
UNIVERSITY OF  
MICHIGAN

1957

1957

1957

1957

1957

1957

1957

1957

1957

LIBRARY

**Table 3-3. Summary of radii of distribution by fluorescent markers**

<b>Particle</b>	<b>n*</b>	<b>Radius** <math>r_{50\% AUC}</math> (mm)</b>	<b>Radius <math>r_{50\% max}</math> (mm)</b>	<b>Comparison to control</b>
10% positive	4	0.19±0.05	0.27±0.06	p<0.0005****
no PEG liposome	3	0.49±0.05	0.67±0.12	p=0.014
40 nm liposome	5	0.70±0.33	0.92±0.33	p=0.732
80 nm liposome	26	0.79±0.36	1.12±0.52	control
200 nm liposome	3	0.64±0.18	1.04±0.09	p=0.791
10% negative	4	0.74±0.42	0.96±0.41	p=0.978
10 kD dextran	7	0.97±0.11	1.63±0.27	p=0.010
dextran + 100 mM Excess Liposomes	3	1.27±0.21	2.00±0.62	p=0.057
80 nm liposome + 100 mM Excess Liposomes	3	1.37±0.45	2.30±1.00	p=0.037

\* n indicates number of times this particle was co-infused

\*\* ± indicates standard deviation

\*\*\*\* based on LOG( $r_{50\% AUC}$ ) two-way ANOVA ( $R^2=0.980$ ,  $n=42$ ,  $p<0.0005$ ) followed by two tailed Dunnett's t-test against 80 nm liposomes

\*\*\*\*\* based on LOG( $r_{50\% AUC}$ ) one-way ANOVA ( $R^2=0.264$ ,  $n=32$ ,  $p=0.012$ ) with excess liposomes followed by two tailed Dunnett's t-test against 80 nm liposomes without excess liposomes

10000

10000

10000

10000

10000

10000

10000

10000

10000

10000

10000

10000

10000

10000

10000

10000

10000

10000

10000

10000

10000

10000

10000

10000

10000

10000

10000

10000

10000

10000

10000

10000

10000

### 3.4.5 *Positive surface charge restricts particle distribution by CED*

DNA containing NLP were infused into an intracranial U251 human glioblastoma xenograft (Fig. 3-3[A-D]). Fig. 3-3D shows a lower magnification view of the defect left by the infusion cannula, a hole ~0.4 mm across. At the edge of the defect, particles can be seen penetrating into tissue (Fig. 3-3D). The particles appear to transfect cells immediately next to the defect left by the infusion cannula (green); however, the 50% positively charged NLP (red) in Fig. 3-3A or transfection in Fig. 3-3B were unable to penetrate more than 200  $\mu\text{m}$  into either tumor or brain tissue (Fig. 3-3[C-D]). These NLP were formulated with cationic lipid, DNA, and a pH sensitive PEG lipid; however, the PEG shielding proved insufficient to permit extensive particle distribution into the tissue.





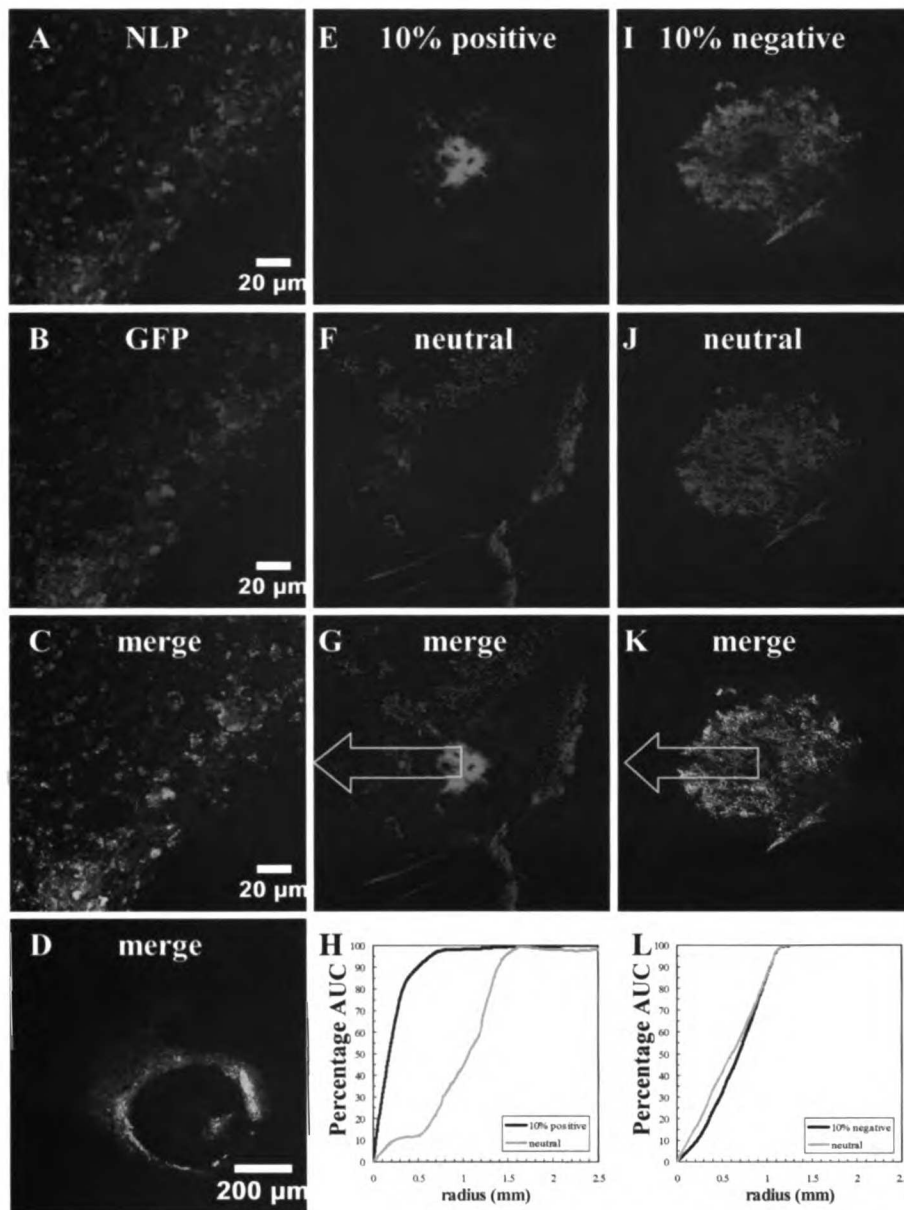


**Figure 3-3. Effect of surface charge on liposome distribution after CED.** All images are axial brain sections taken by confocal microscopy. [A-D] a pH sensitive NLP containing GFP plasmid infused into a U251 (day 26) intra-cranial tumor following sacrifice (day 28). [A] DiI labeled NLP (red). [B] GFP transfected cells (green) [C] merged high resolution image of [A] and [B] showing transfected cells (yellow) and untransfected cells with NLP entrapped in vacuoles (red). [D] low resolution merged image showing that NLP traveled only a short distance from the cannula tip; furthermore, extensive transfection was limited by poor particle penetration. [E-L] 4 mm by 4 mm images centered upon the tip of the infusion cannula. [E-H] co-infusion of positive (red) and neutral (green) liposomes. [E] liposomes with 10% positive surface charge under a 10% PEG coat. [F] neutral liposomes. [G] merged image of [E] and [F]. [H] the AUC as a function of radius, calculated along the arrow in [G], shows that positive charge restricts liposome penetration. [I-L] co-infusion of negative (red) and neutral (green) liposomes. [I] liposomes with 10% negative surface charge under a 10% PEG coat. [J] neutral liposomes. [K] merged image of [I] and [J]. [L] the AUC as a function of radius, along the arrow in [K], shows no major difference between the liposomes.

LIBRARY

LIBRARY

LIBRARY



LIBRARY

LIBRARY

LIBRARY

LIBRARY

LIBRARY

LIBRARY

LIBRARY

LIBRARY

LIBRARY

LIBRARY



To determine how moderate amounts of positive charge affect CED distribution, we prepared liposomes with 10% positive surface charge and shielded the charge with 10% of a neutral PEG-DSG (Table 3-1). These particles were co-infused with a neutral liposome, as summarized in Table 3-3. On average, positively charged particles penetrated ( $r_{50\% AUC}$ )  $0.19 \pm 0.05$  mm, neutral liposomes penetrated ( $r_{50\% AUC}$ )  $0.79 \pm 0.36$  mm, and this difference was significant with  $p < 0.0005$  (Table 3-3). Fig. 3-3[E-H] shows a representative co-infusion, where positive charged liposomes (red) remained directly at the site of infusion (Fig. 3-3E), but neutral liposomes (green) perfused outward easily (Fig. 3-3F). A box extending radially outward from the cannula tip of the merged image (Fig. 3-3G) was analyzed for the percentage AUC (Fig. 3-3H). At all points along the curve the positive liposomes, were deposited more readily than the neutral liposomes (Fig. 3-3H). We conclude that modest amounts (>10%) of positive charge severely restrict distribution even when sterically shielded by PEG.

We also prepared liposomes with 10% negative charge buried under a 10% PEG-DSG coat (Table 3-1) and co-infused these with neutral liposomes, as summarized in Table 3-3. On average, negatively charged particles penetrated ( $r_{50\% AUC}$ )  $0.74 \pm 0.42$  mm. Fig. 3-3[I-L] show a representative image of this condition. The negative liposomes (red) in Fig. 3-3I appear identical in distribution to neutral liposomes (green) in Fig. 3-3J. Again, a radial profile of the merged image was taken in the direction indicated on Fig. 3-3K and the percentage AUC was plotted. Fig. 3-3L shows that the neutral and negative charged liposomes percentage AUC curves overlay very closely (Fig. 3-3L). We conclude that modest amounts (10%) of negative charge did not reduce distribution by CED.

1940

1941  
1942  
1943  
1944  
1945  
1946  
1947  
1948  
1949  
1950



1951  
1952  
1953  
1954  
1955  
1956  
1957  
1958  
1959  
1960  
1961  
1962  
1963  
1964  
1965  
1966  
1967  
1968  
1969  
1970  
1971  
1972  
1973  
1974  
1975  
1976  
1977  
1978  
1979  
1980  
1981  
1982  
1983  
1984  
1985  
1986  
1987  
1988  
1989  
1990  
1991  
1992  
1993  
1994  
1995  
1996  
1997  
1998  
1999  
2000

1940  
1941  
1942  
1943  
1944  
1945  
1946  
1947  
1948  
1949  
1950



### 3.4.6 Particle size restricts distribution by CED

Four sizes of particles were compared to determine their relative distribution. From smallest to largest the particles were dextran (10 kD), 40 nm liposomes, 80 nm liposomes, and 200 nm liposomes (Table 3-1). Dextran penetrated to an average radius ( $r_{50\% AUC}$ ) of  $0.97 \pm 0.11$  mm, significantly ( $p=0.01$ ) greater than the 80 nm liposomes (Table 3-3). The 40 nm particles traveled an average radius ( $r_{50\% AUC}$ ) of  $0.70 \pm 0.33$  mm (Table 3-3). We conclude that in brain tissue, liposome distribution by CED is slightly hindered compared to dextran, but liposome diameter was not a factor between 40 and 80 nm.

We also investigated larger particle diameters and compared 200 nm liposomes (red) and 80 nm liposomes (green) (Fig. 3-4[A-D]). On average, the 200 nm liposomes penetrated ( $r_{50\% AUC}$ )  $0.64 \pm 0.18$  mm, a number slightly less than that for the 80 nm liposomes (Table 3-3). Fig. 3-4C is a merged image of the 80 nm and the 200 nm liposomes, showing that the 200 nm liposomes deposit slightly closer to the infusion cannula. Whereas the 80 nm liposomes have high concentrations out at one full mm, the 200 nm liposomes appear to have more staining near the cannula than at the periphery. We conclude that nanoparticles over a range of sizes can travel by convection through normal brain; however, a threshold exists near a diameter of 200 nm where retention near the site of infusion becomes more pronounced.

LIBRARY

LIBRARY

LIBRARY

LIBRARY

LIBRARY

LIBRARY

LIBRARY

LIBRARY

LIBRARY

LIBRARY

LIBRARY

LIBRARY

LIBRARY

LIBRARY

LIBRARY

LIBRARY

LIBRARY

LIBRARY

LIBRARY

LIBRARY

LIBRARY

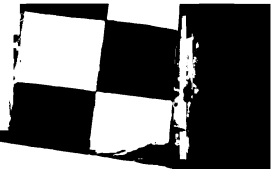
LIBRARY

LIBRARY

LIBRARY

LIBRARY

LIBRARY



LIBRARY

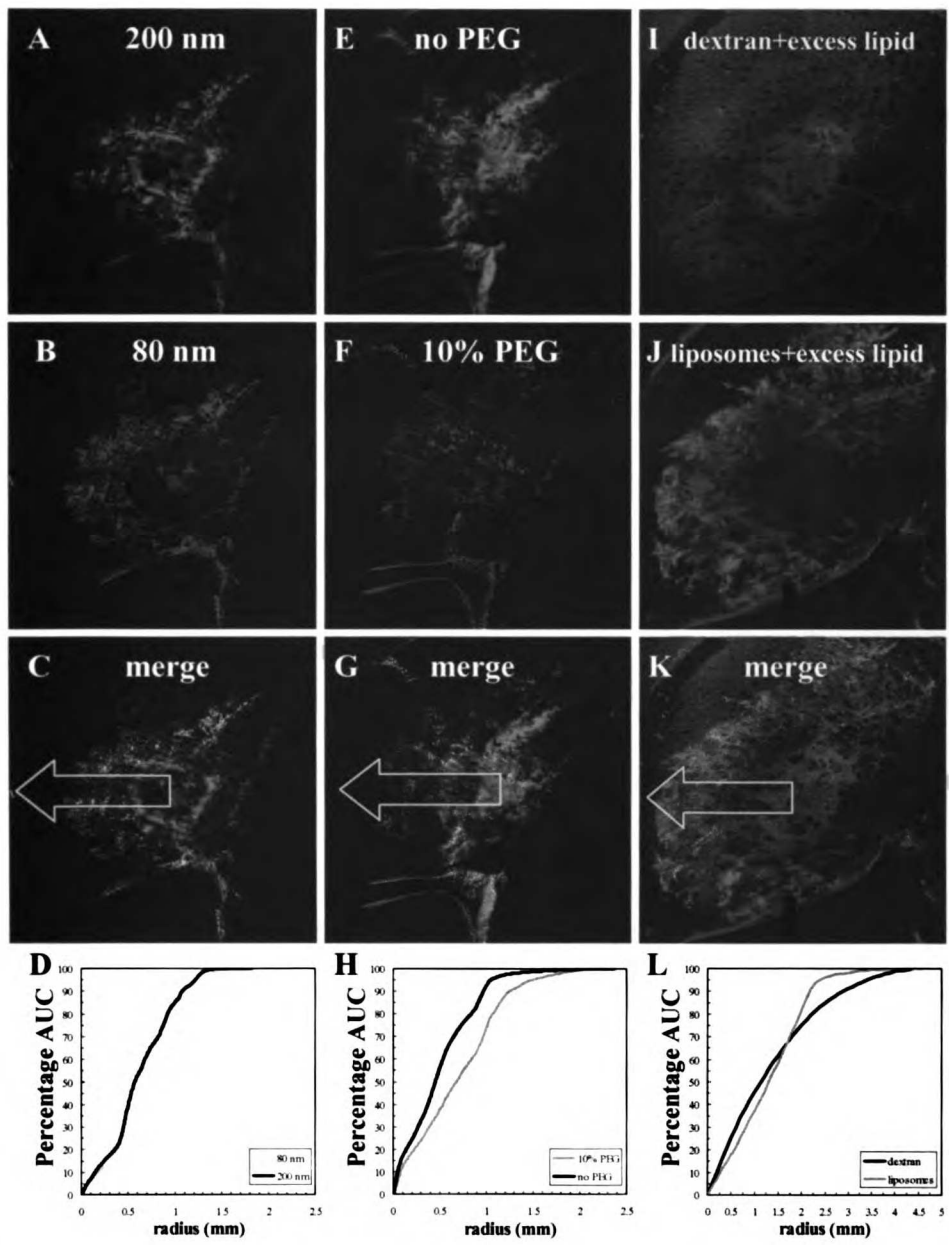


**Figure 3-4. Influence of particle diameter, PEG lipids, and excess lipid on liposome distribution after CED.** Images are axial brain sections taken by confocal microscopy using a 4x objective. Regions shown are 4 mm by 4 mm centered upon the tip of the infusion cannula. [A-D] co-infusion of 200 nm (red) and 80 nm (green) diameter liposomes. [A] 200 nm liposomes. [B] 80 nm liposomes. [C] merged image of [A] and [B]. [D] the AUC as a function of radius, along the arrow in [C], shows that 80 nm liposomes penetrate farther than 200 nm liposomes. [E-H] co-infusion of liposomes without PEG (red) and with a PEG coat (green). [E] liposomes without PEG. [F] 10% PEG shielded liposomes. [G] merged image of [E] and [F]. [H] the AUC as a function of radius, calculated along the arrow in [G], showing that liposomes with PEG penetrate farther than without PEG. [I-L] co-infusion of dextran (green) and liposomes (red) in the presence of 100 mM excess liposomes (DSPG:DSPC:Chol:mPEGDSG [10:40:40:10]). [I] 10 kD dextran. [J] neutral PEG shielded liposomes. [K] merged image of [I] and [J]. [L] the AUC as a function of radius, along the arrow in [K]. Note that the presence of excess liposomes increases the penetration radius ( $r_{50\% AUC}$ ) of the liposomes to a distance similar to that of dextran.





### 3.4.7 *Effect of polyethylene glycol steric shielding*

Polyethylene glycol (PEG) is used to sterically shield both drug-loaded and DNA-loaded liposomes. In Fig. 3-4[E-H] we directly compared sterically shielded liposomes to liposomes without PEG (Table 3-1). On average, the liposomes without PEG distributed ( $r_{50\% AUC}$ )  $0.49 \pm 0.05$  mm (Table 3-3), significantly less than the distribution for the control PEG shielded liposomes ( $p=0.014$ ). Fig. 3-4E shows a liposome with no PEG (red) and Fig. 3-4F shows the co-infused 10% PEG liposomes (green). The merger of these images (Fig. 3-4G) confirms that the PEG increased tissue penetration. A radial directed profile was taken from the center of the infusion (Fig. 3-4G) and analyzed for the percentage AUC (Fig. 3-4H). The presence of PEG significantly increased distribution by CED.

### 3.4.8 *Effect of excess liposomes*

We hypothesized that liposome engulfing cells (Fig. 3-1H) could be responsible for reducing the penetration of liposomes into the brain. This process would require particle adsorption, and it should be possible to reduce this source of elimination by competing for binding sites using excess unlabeled liposomes. We prepared concentrated unstained 10% negative PEG shielded liposomes using high-pressure extrusion through 80 nm membranes, obtaining particles with a diameter of  $108.3 \pm 0.8$  nm (Table 3-1). These liposomes (100 mM infusion concentration) were mixed into a co-infusion of dextran (green) 1 mg / mL and control liposomes (red) at 1 mM lipid concentration, as depicted in Fig. 3-4[I-L]. In the presence of excess liposomes, the dextran penetration ( $r_{50\% AUC}$ ) was  $1.27 \pm 0.21$  mm, which was similar to the dextran penetration ( $r_{50\% AUC}$ ) of  $0.97 \pm$

10000

10000  
10000  
10000  
10000  
10000  
10000



10000  
10000  
10000  
10000  
10000  
10000  
10000

10000  
10000  
10000  
10000  
10000  
10000  
10000  
10000

10000  
10000  
10000  
10000  
10000  
10000  
10000  
10000

10000  
10000  
10000  
10000  
10000  
10000  
10000  
10000

0.11 mm in animals lacking the excess liposomes (Table 3-3). Most interesting, the control liposomes in the presence of 100-fold excess liposomes had an average penetration ( $r_{50\% AUC}$ ) of  $1.37 \pm 0.45$  mm, significantly greater than without excess lipids ( $p=0.037$ ). The merged image in the presence of excess liposomes (Fig. 3-4K) was analyzed for percentage AUC within the box shown in Fig. 3-4L. Fig. 3-4L shows that the deposition line for the dextran (green) and the liposomes (red) actually cross over. For comparison, Fig. 3-4[E-H] used the same infusion conditions of liposomes (red) and dextran (green) without the excess liposomes. Excess liposomes increased liposome penetration, possibly by preventing the adsorption of liposomes along the convection pathway.

### **3.5 Discussion**

Convection enhanced delivery (CED) relies upon neither diffusion nor active transport by the circulatory system to carry drugs into the brain; it is suitable to deliver drugs with short blood half-lives, proteins, DNA, viruses, and nanoparticles directly to their site of action. The fate of nanoparticles infused into the brain is particularly important to the field of gene therapy since DNA vectors are large compared to typical small molecule drugs. Both viral and non-viral DNA particles span the range of sizes from 25 to 250 nm in diameter and have various binding affinities, both specific and nonspecific. To better understand the nanoparticle properties beneficial for CED, we have investigated liposomes in the rat brain. This is a small animal model of CED, used under the assumption that these effects will scale to larger infusion volumes required for human therapies. By manipulating the physical-chemical properties of these liposomes, we have

LIBRARY

LIBRARY

LIBRARY

LIBRARY

LIBRARY

LIBRARY

LIBRARY

LIBRARY

LIBRARY

LIBRARY

LIBRARY

LIBRARY

LIBRARY

LIBRARY

LIBRARY

LIBRARY

LIBRARY

LIBRARY

LIBRARY

LIBRARY

LIBRARY

LIBRARY

LIBRARY

LIBRARY

LIBRARY

LIBRARY

LIBRARY

LIBRARY

LIBRARY

LIBRARY

LIBRARY

LIBRARY

LIBRARY

LIBRARY

LIBRARY

LIBRARY

LIBRARY

LIBRARY

LIBRARY

LIBRARY

LIBRARY

LIBRARY

LIBRARY

LIBRARY

LIBRARY

LIBRARY

LIBRARY

LIBRARY

LIBRARY

LIBRARY

LIBRARY

LIBRARY

LIBRARY

LIBRARY

LIBRARY

LIBRARY

LIBRARY

LIBRARY

uncovered key factors including size, charge, and steric shielding that have strong effects on particle distribution.

### *3.5.1 Effects of particle composition on CED*

The effects of particle size, steric shielding, and charge on delivery by CED are compared in Fig. 3-5. Liposomes readily penetrate through brain tissue, 1 mm for this infusion model, up to about 200 nm diameter, at which point particles begin to be retained near the site of infusion. This observation suggests that large viral particles, such as Herpesvirus or Baculovirus, will be restricted in their mobility when delivered by CED. Likewise, stem cells are too large to be distributed by CED.

Steric shielding using polyethylene glycol lipids extends liposome systemic circulation half-life from hours to days by reducing binding to the reticuloendothelial system and clearance in the liver and spleen. Likewise, the liposomes used in these brain infusions were sterically shielded by 10 mole percent (of total lipid) 2 kD PEG. When delivered by CED, sterically shielded liposomes traveled for longer distances than non-shielded liposomes, suggesting that steric shielding reduces the rate of liposome binding to cells in the brain during CED.

11/11/50

11/11/50

11/11/50

11/11/50

11/11/50

11/11/50

11/11/50

11/11/50

11/11/50

11/11/50

11/11/50

11/11/50

11/11/50

11/11/50

11/11/50

11/11/50

11/11/50

11/11/50

11/11/50

11/11/50

11/11/50

11/11/50

11/11/50

11/11/50

11/11/50

11/11/50

11/11/50

11/11/50

11/11/50

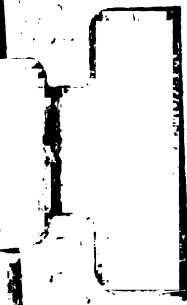
11/11/50

11/11/50

11/11/50

11/11/50

11/11/50



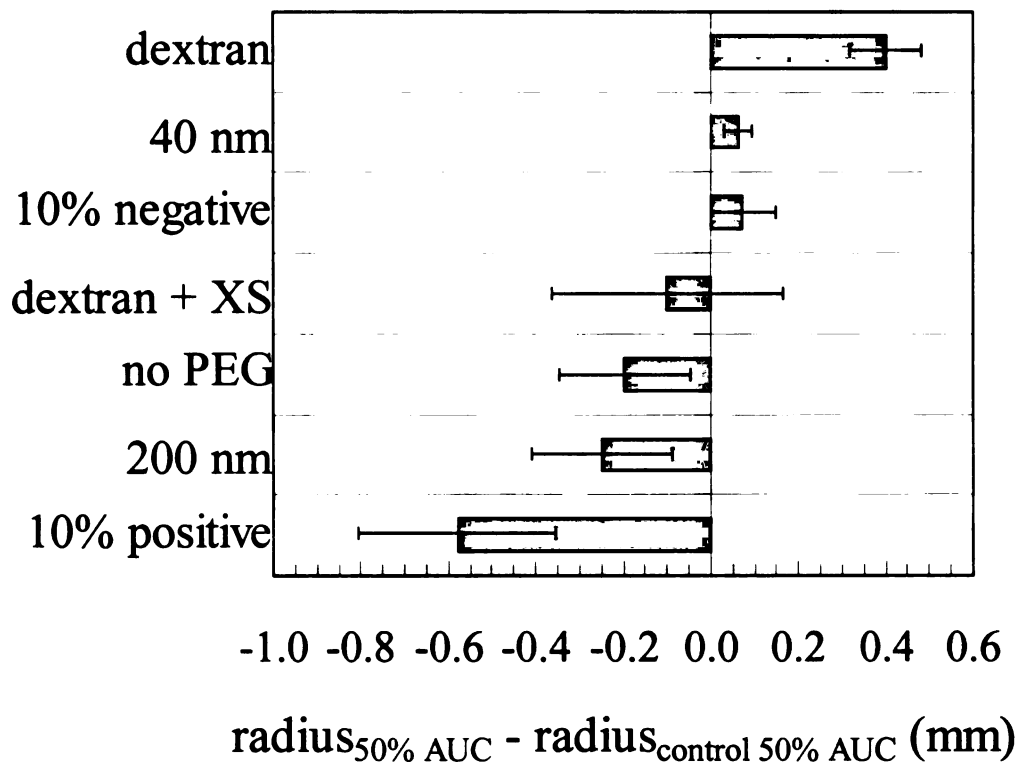


**Figure 3-5. Comparison of particles co-infused by CED.** The within animal difference in penetration radius,  $r_{50\% AUC}$ , between the infused particle and the control neutral liposomes are presented. Labels indicate the following: 'dextran' is a 10 kD dextran (n=4); '40 nm' diameter liposomes (n=3); '10% negative' charged liposomes (n=4), 'dextran + XS' include 100 mM excess (XS) liposomes (n=3); 'no PEG' are liposomes lacking steric shielding (n=3); '200 nm' diameter liposomes (n=3); and '10% positive' charged liposomes (n=4). Error bars indicate the standard deviation.

THURSDAY

FRIDAY

1917

1918

1919

1920

1921

1922

1923

1924

1925

1926

1927

1928

1929

1930

1931

1932

1933

1934

1935

1936

1937

1938

1939

1940

1941

1942

1943

1944

1917



Cationic DNA lipoplexes, a common non-viral particle, are around 200 nm in diameter [Xu *et al.* 1999], and hence less suitable for CED. Moreover, the highest transfection efficiency for cationic lipoplexes *in vitro* is obtained when particles are formed with high positive to negative charge ratios (+ / - above 2). Following i.v. administration, cationic lipoplexes bind rapidly to negatively charged proteoglycans in the lung [Uyechi *et al.* 2001] and are rapidly eliminated from circulation into the lung and liver.

In the brain, nonspecific binding also limits CED distribution of positively charged particles, even when the charge is moderate (10% by mole lipid) and shielded by PEG. Recognizing this possibility, investigators have infused negatively charged DNA lipoplexes by CED (+ / - = 0.5) in clinical studies [Voges *et al.* 2002, Voges *et al.* 2003]; however, these particles are larger than 200 nm in diameter [Xu *et al.* 1999] and will display size-limited penetration. Indeed, Voges and coworkers [2003] found it difficult to obtain uniform clinical distribution and transfection using these particles. To reduce nonspecific binding, cationic lipoplexes have been assembled with a PEG polymer coat [Wheeler *et al.* 1999, Harvie *et al.* 2000, Fenske *et al.* 2001, Choi *et al.* 2003]; however, we found that liposomes with 10% cationic charge and 10% PEG shielded DNA lipoplexes (NLP) bind at the tip of the infusion cannula. Thus cationic lipoplexes, even if shielded by a steric stabilizer such as PEG, are inadequate to allow large volumes of distribution by CED.

Neutral PEG coated liposomes target to a subpopulation of perivascular brain cells (Fig. 3-11). Liposome targeting to a subset of cells in the brain has been previously observed

770000

RARY

LIBRARY

LIBR

1917

11

LIBRARY

1917

RARY

LIBR

1917

11

LIBR

1917

11

LIBR

1917

11

LIBR

1917

11

LIBR

1917

11

LIBR

1917

11

LIBR

[Polfliet *et al.* 2001]. Polfliet and coworkers infused mannosylated liposomes containing clodronate directly to the fourth ventricle of the rat brain [2001]. In the brain, clodronate containing liposomes selectively depleted ED2 positive perivascular macrophages without impacting OX42 positive microglia [Polfliet *et al.* 2001]. Liposomes examined here may also target perivascular macrophages even though they lack the mannosylated targeting ligand (Fig. 3-11).

We have also shown that the addition of large excess of lipid increases the distribution of liposomes by CED (Table 3-3). Presumably, this effect comes from saturating the binding and uptake process responsible for liposome elimination; furthermore, we ruled out the possibility that this lipid concentration creates a high osmotic pressure. Other investigators [Sandberg *et al.* 2002, Mamot *et al.* 2004] have infused the brain with 25% mannitol solutions (measured  $1,900 \pm 36$  mOsm) by CED and shown an increase in penetration distance. The measured osmolality of the concentrated liposome solution infused here was only  $337 \pm 3$  mOsm (TBS buffer alone measured  $300 \pm 2$  mOsm). Because the osmolality of the liposome infusion was so far below that for a 25% mannitol solution, the possibility that excess liposome increased the penetration radius by an osmotic effect can be ruled out. So we conclude that the increased penetration distance for liposomes in the presence of excess lipid is due to saturation of the mechanism of elimination from interstitial space.

7/10/10

REPLY

10/10/10

11/10/10

12/10/10

1/11/11

2/11/11

3/11/11

4/11/11

5/11/11

6/11/11

7/11/11

8/11/11

9/11/11

10/11/11

11/11/11

12/11/11

1/12/12

2/12/12

3/12/12

4/12/12

5/12/12

6/12/12

7/12/12

8/12/12

9/12/12

10/12/12

11/12/12

12/12/12

13/12/12

### 3.5.2 Long duration CED in small animal models

In these studies, it was possible to draw definitive conclusions about the relative distribution of liposomes because these particles were co-infused with a control liposome. While this method enabled these scientific studies, the fact remains that delivery using a Alzet™ Brain Infusion Kit with a flowrate of 0.14 mL/min is only about 3.1% efficient at delivering a dose of a radiolabeled liposome into the rat brain. This surprising fact was unanticipated from observing fluorescent microscopy images. For the purpose of performing therapeutic and survival studies, this may not be an acceptable efficiency for the following reasons: 1. Cytotoxic compounds that are not delivered to the brain may cause peripheral toxicity; 2. The apparent dose *tolerated* by the brain may be on the order of 10-fold higher than the actual dose *delivered* to the brain; and 3. A decrease in flowrate into the brain will decrease the particle penetration distance and give poor coverage of brain and tumor treatment areas. All three of these factors will complicate the process of scaling up small animal results into successful human clinical trials.

Despite the poor performance of the Alzet™ Brain Infusion Cannula, there remains an urgent need for long duration CED using small animal models. We verified that leakback occurs with the 200  $\mu$ L osmotic pump, at 0.14  $\mu$ L/min. It is possible that at lower flowrates the efficiency of delivery is much higher. In 1999, Chen and coworkers discovered that significant leakback was caused by cannula diameters of 0.36 mm and larger, the same diameter used for the commercially available Brain Infusion Cannula. One obvious remedy would be to reduce the diameter of the cannula to the 0.16 mm fused silica cannula. In this study, a 0.16 mm diameter cannula was used successfully to

TRUSTED

RAKY

LIBR

1/2

[Redacted]

TRUSTED

RAKY

LIBR

1/2

deliver (efficiency of 63%) acute infusions at 0.8  $\mu\text{L}$  / min (Table 3-2). A final possibility is that animal movement promotes leakage by slightly moving the cannula back and forth. This could be improved by the use of alternatives to the cranioplastic (dental) cement, such as the Loctite Prism<sup>TM</sup> adhesive. To successfully complete future small animal studies using the Alzet<sup>TM</sup> system we recommend first optimizing the efficiency of delivery using radiolabels or quantitative dyes.

### *3.5.3 Fate of nanoparticles infused into the human brain*

Nanoparticles delivered by CED within the human brain will behave much differently than small molecules or even proteins because of their intrinsic clearance to perivascular cells, possibly perivascular macrophages. These cells sequester neutral liposomes with a brain half-life of about 9.9 hrs (Table 3-2), and this will restrict the distribution of liposome encapsulated drug. Based upon magnetic resonance imaging, shown by Saito and coworkers, we estimated that aqueous contents entrapped within liposomes eliminate with a half-life of about 60 hrs [Saito *et al.* 2004]. In the studies shown here, the lipid components of 80 nm liposomes also remained within the brain for extended periods (Table 3-2). Liposomes loaded with drug will tend to release that drug following cellular internalization, presumably inside perivascular macrophages. This may cause toxicity to perivascular macrophages, as previously observed with the clodronate containing liposomes; furthermore, only a small percent of the drug may reach its intended target. Neutral nonviral gene delivery systems may accumulate in these cells, thus invalidating approaches to gene therapy directed towards other normal or malignant cell types in the brain.

THURSDAY

RAVEY

87

LIBR

5/12

LIBRARY

LIBRARY



These studies primarily characterize nanoparticle movement through normal brain. It is equally important to examine the fate of nanoparticle CED in tumors where the hydraulic conductivity and the extracellular fraction may change radically compared to normal brain. Solid tumors partially exclude convective flow, as suggested by images of Mamot and coworkers [Mamot *et al.* 2004, Saito *et al.* 2004]. Within tumors, penetration by 40 nm and 90 nm diameter liposomes differed dramatically [Mamot *et al.* 2004]. In contrast, our findings show that 40 nm and 80 nm diameter particles distribute similarly in normal brain (Fig. 3-5). Due to dramatic variation between tumors in the clinic, we agree with previous assessments [Voges *et al.* 2003, Saito *et al.* 2004] that it will be invaluable to track these particles by magnetic resonance imaging or other suitable non-invasive techniques following administration. Additionally, it will be important to directly label the particles. Small molecule surrogate contrast agents used for MRI may not be eliminated at the same rate as the therapeutic nanoparticle, and may give misleading volumes of distribution.

This study suggests that liposome delivery by CED is a promising avenue for treating human diseases of the brain. Similar to proteins and small molecules, CED can deliver nanoparticulates to large volumes of brain with the following caveats: 1. the particle must be on the order of 100 nm in diameter or smaller, 2. the particle must be neutral or negatively charged, 3. the penetration distance may vary substantially between formulations, 4. particles infused for longer than their elimination half-life will cease to distribute to ever greater volumes, and 5. the source of elimination for particles with short

1947  
1948  
1949  
1950  
1951  
1952  
1953  
1954  
1955  
1956  
1957  
1958  
1959  
1960  
1961  
1962  
1963  
1964  
1965  
1966  
1967  
1968  
1969  
1970  
1971  
1972  
1973  
1974  
1975  
1976  
1977  
1978  
1979  
1980  
1981  
1982  
1983  
1984  
1985  
1986  
1987  
1988  
1989  
1990  
1991  
1992  
1993  
1994  
1995  
1996  
1997  
1998  
1999  
2000  
2001  
2002  
2003  
2004  
2005  
2006  
2007  
2008  
2009  
2010  
2011  
2012  
2013  
2014  
2015  
2016  
2017  
2018  
2019  
2020  
2021  
2022  
2023  
2024  
2025  
2026  
2027  
2028  
2029  
2030  
2031  
2032  
2033  
2034  
2035  
2036  
2037  
2038  
2039  
2040  
2041  
2042  
2043  
2044  
2045  
2046  
2047  
2048  
2049  
2050  
2051  
2052  
2053  
2054  
2055  
2056  
2057  
2058  
2059  
2060  
2061  
2062  
2063  
2064  
2065  
2066  
2067  
2068  
2069  
2070  
2071  
2072  
2073  
2074  
2075  
2076  
2077  
2078  
2079  
2080  
2081  
2082  
2083  
2084  
2085  
2086  
2087  
2088  
2089  
2090  
2091  
2092  
2093  
2094  
2095  
2096  
2097  
2098  
2099  
2100

1947  
1948  
1949  
1950  
1951  
1952  
1953  
1954  
1955  
1956  
1957  
1958  
1959  
1960  
1961  
1962  
1963  
1964  
1965  
1966  
1967  
1968  
1969  
1970  
1971  
1972  
1973  
1974  
1975  
1976  
1977  
1978  
1979  
1980  
1981  
1982  
1983  
1984  
1985  
1986  
1987  
1988  
1989  
1990  
1991  
1992  
1993  
1994  
1995  
1996  
1997  
1998  
1999  
2000  
2001  
2002  
2003  
2004  
2005  
2006  
2007  
2008  
2009  
2010  
2011  
2012  
2013  
2014  
2015  
2016  
2017  
2018  
2019  
2020  
2021  
2022  
2023  
2024  
2025  
2026  
2027  
2028  
2029  
2030  
2031  
2032  
2033  
2034  
2035  
2036  
2037  
2038  
2039  
2040  
2041  
2042  
2043  
2044  
2045  
2046  
2047  
2048  
2049  
2050  
2051  
2052  
2053  
2054  
2055  
2056  
2057  
2058  
2059  
2060  
2061  
2062  
2063  
2064  
2065  
2066  
2067  
2068  
2069  
2070  
2071  
2072  
2073  
2074  
2075  
2076  
2077  
2078  
2079  
2080  
2081  
2082  
2083  
2084  
2085  
2086  
2087  
2088  
2089  
2090  
2091  
2092  
2093  
2094  
2095  
2096  
2097  
2098  
2099  
2100

interstitial half-lives must be blocked. In this study we have increased the apparent penetration of particles both by shielding the particles with polyethylene glycol and by adding excess liposomes to saturate binding sites. Both of these approaches increase the apparent penetration distance, implying a decrease in the rate of particle removal from the interstitial space. With reduced particle binding kinetics, particles can be infused to greater volumes of distribution as required for clinical applications.

### **3.6 Conclusion**

We have investigated convection enhanced delivery (CED) as a means to deliver nanoparticulates through the brain by co-infusing differently labeled fluorescent and radiolabeled liposomes in the rat brain. Implantable osmotic pumps showed only 3.1% efficiency at delivering the dose of radiolabeled liposomes to the brain; however, this limitation was overcome by the co-infusion of control liposomes. Neutral liposomes target to perivascular cells with an elimination half-life of 9.9 hrs, and lipids from these particles stay within the cell for an extended period. The penetration distance for liposomes is less than that seen for 10 kD dextran. Liposomes with 10% positive charge under a PEG steric coat were retained at the site of infusion. Particles without PEG or larger than 200 nm in diameter did not penetrate as far as 80 nm liposomes. Based upon these findings, the ideal nanoparticle for CED will be less than 100 nm in diameter, shielded by PEG, have neutral or negative surface charge, and will need a targeting ligand to adhere the particle to the target cell. It will also have to be infused at a high total lipid concentration to minimize the fraction of the dose that is scavenged by perivascular cells in the brain.

## CHAPTER 4:

### Convection Enhanced Delivery: A Mathematical Model with First Order Binding

#### 4.1 Abstract

In Chapter 3, I investigated the role of diameter, charge, and steric shielding on the brain distribution of liposomes infused by convection enhanced delivery (CED) using both radiolabeled and fluorescent-labeled particles. Here, data are interpreted using a mathematical model of CED including a first order irreversible binding constant,  $k$ . Neutral liposomes had a binding constant of  $k = 0.0010 \pm 0.0002 \text{ min}^{-1}$ , whereas for positive charged liposomes  $k$  increased 50-fold. The binding constant was independently verified using a degradable lipid radiolabel that eliminated from the brain with a  $9.9 \pm 2.0$  hr half-life, equivalent to a first order elimination constant  $k = 0.0012 \pm 0.0002 \text{ min}^{-1}$ . A non-degradable lipid radiolabel showed that lipid components remained within these perivascular brain cells for at least 2 days. To reduce uptake, a 100-fold molar excess of non-labeled liposomes were co-infused with labeled liposomes, which reduced the binding constant to that measured using 10 kD fluorescein dextran. This analysis further supports the claim that optimization of therapeutic CED using nanoparticles will require a strategy to overcome particle binding and clearance by cells within the CNS.

#### 4.2 Introduction

As shown in Chapter 3, liposomes bind to a subpopulation of brain cells. These cells presumably have a high rate of phagocytosis as they also ingested some quantities of dextran; however, most of the dextran remains extracellular 24 hrs following infusion

into the brain. This is in stark contrast to the nearly complete internalization of liposomes. (Figure 3-11). In this chapter, I investigate the ramifications of this rate of uptake and consider one method for reducing the impact of the internalization rate. I use a mathematical model of convection with a term for first order irreversible binding. This model allows one to take fluorescent images of distribution and estimate a binding constant. Additionally, the simplicity of a first order binding constant allows us to evaluate uptake in terms of a half-life that we can compare to the half-life of elimination for an enzymatically degradable radiolabel attached to a liposomes.

The first paper describing convection enhanced delivery includes a rigorous mathematical model of the process [Morrison *et al.* 1994]. Contained within this paper are most of the details needed to model almost any compound perfused through living brain tissue; however, this requires the determination or assumption of a number of different parameters. This model included terms both for the diffusive spread and convective spread of compound. Additional terms were included for both reversible and irreversible binding to tissue, as well as pressure driven losses to the brain vasculature. Unfortunately, the complexity of the model makes it intractable for determining parameters from experimental data.

For the purposes of this analysis, a simplification of the model was used that neglects diffusion. The model is based upon convection from the tip of the infusion cannula modeled in spherical coordinates [Morrison *et al.* 1994]. The radius of the convected solvent wave,  $r_{wave}$ , spreads outward by the following equation:

$$r_{wave} = [3 q t / (4 \pi \phi)]^{1/3} \quad \text{Eq. 4-1}$$

Where  $q$  is the volumetric flowrate into the tissue,  $t$  is the time after the start of infusion, and  $\phi$  is the extracellular fraction volume. At the edge of the outward moving  $r_{wave}$ , liposomes are eliminated from solution to the tissue at a rate characterized by a first order irreversible rate constant,  $k$ , given by :

$$C_{(r,t)} / C_{infusion} \begin{cases} = \text{EXP} [-k r^3 4 \pi / (3 q)] & \text{for } 0 \leq r \leq r_{wave} \\ = 0 & \text{for } r > r_{wave} \end{cases} \quad \text{Eq. 4-2}$$

Where  $C_{infusion}$  is the free liposome concentration at the start of infusion.  $C_{(r,t)}$  is the free liposome concentration after infusion begins. In addition to the assumptions of Morrison and coworkers [1994], this simplification assumes that compounds do not undergo reversible binding to tissue, that no pressure driven elimination occurs through pores into the vasculature, and that the tip of the cannula is infinitely small. As  $r_{wave}$  moves outward, it traces the steady state solution of compound being eliminated by a first order rate constant in radial coordinates.

For the purpose interpreting CED data in the brain, a further simplification is often made whereby the tissue binding constant,  $k$ , is dropped from Eq. 4-2. Without tissue binding, the concentration is either zero before  $r_{wave}$  has arrived or  $C_{infusion}$  after  $r_{wave}$  has passed. A simplified equation can be derived by defining infusion volume,  $V_{infusion}$ , and measured volume of distribution ( $V_{distribution}$ ) as follows:

$$r_{wave} = [3 V_{distribution} / (4 \pi)]^{1/3} \quad \text{Eq. 4-3}$$

$$q t = V_{infusion} \quad \text{Eq. 4-4}$$

Then substitute Eq. 4-3 and 4-4 into Eq. 4-1 and obtain:

$$[3 V_{\text{distribution}} / (4 \pi)]^{1/3} = [3 V_{\text{infusion}} / (4 \pi \phi)]^{1/3} \quad \text{Eq. 4-5}$$

Solving for  $V_{\text{distribution}}$ :

$$V_{\text{distribution}} = V_{\text{infusion}} / \phi \quad \text{Eq. 4-6}$$

To obtain the equation typically used by investigators to describe CED data [Bobo *et al.* 1994, Kroll *et al.* 1996, Hamilton *et al.* 2000, Lonser *et al.* 2002, Saito *et al.* 2004], a constant,  $c$ , has been defined such that:

$$c = 1 / \phi \quad \text{Eq. 4-7}$$

Giving the a line with the constant,  $c$ , as the slope:

$$V_{\text{distribution}} = c V_{\text{infusion}} \quad \text{Eq. 4-8}$$

All but one parameter,  $c$ , are dropped from the model in Eq-4-8. The extracellular fraction of the brain volume,  $\phi$ , is typically between 0.2 and 0.4 [Morrison *et al.* 1994]. Thus, under this simplification, investigators should find  $c$  in the range of 5 to 2.5, respectively. In practice this constant ranges about 3 to 10 [Jain 2001]. Eq. 4-8 is now based on three main assumptions: 1. the compound does not bind tissue while moving through brain, 2. the compound is not lost to the vasculature, and 3. the compound has negligible diffusion.

Many CED experiments are done in small animals, with small infusion volumes; the assumption is that the data can be scaled up to human volumes by applying Eq. 4-8. In the absence of binding or diffusion, convection should be able to cover large volumes of distribution in humans. However, complications arise when the assumptions for Eq. 4-8 are not met. If the drug or particle undergoes rapid binding to tissue then  $c$  will fall near

or below a value of 1, indicating that the compound is unsuitable for scaling up to large volumes required for humans. Alternatively, if the drug has a high diffusion constant, then the experimentally determined  $c$  could be higher than 5 for small infusion volumes. A compound may even have both high diffusion and tissue binding, giving an apparent  $c$  between 5 and 2.5, in the range expected for successful convection. These values may deceptively suggest that the compound will scale well to larger volumes of human brain or tumor; however, in large volumes diffusion can only be expected to drive most drugs, macromolecules, or nanoparticles several millimeters through tissue [Saltzman *et al.* 1999].

For the purpose of modeling the convection of liposomes, diffusion is unlikely to play a role in distribution because the diffusion coefficient is more than an order of magnitude smaller than for a small molecule. Additionally, liposomes cannot diffuse through membranes and are too large to pass through the tight junctions of the blood brain barrier. This leaves tissue binding as the major factor that can affect the distribution of nanoparticles. In Chapter 3, I showed that liposomes are bound and mostly internalized to a subpopulation of brain cells at 24 hrs. Here I determine the rate of binding and internalization of liposomes by fluorescence microscopy and compare this to the loss of  $^{125}\text{I}$ -BPE radiolabel from the brain (Table 3-2).



## 4.3 Methods

### 4.3.1 Calculation of the Peclet number

The Peclet number is a ratio of the convective flux divided by the diffusive flux. This number is a common engineering tool used to determine the relative importance of diffusion vs. convection. For a Peclet number greater than 1, the flux of material will be governed by convection and diffusion terms may be dropped. Calculation of the radial Peclet number was performed as previously reported by Morrison and coworkers [1994].

The Peclet number is given by the following equation in radial coordinates:

$$Pe = [q / (3 D r)]^{0.5} \quad \text{Eq. 4-9}$$

Where  $q$  is the volumetric flowrate into the brain (0.0043  $\mu\text{L} / \text{min}$  for Alzet<sup>TM</sup> infusions) and  $r$  is the radius.  $D$  is the diffusion coefficient for a liposome ( $10^{-8} \text{ cm}^2 / \text{sec}$ ) in brain, which is much slower than for a protein. No distribution radii were observed greater than 3 mm, where  $Pe = 2.8$ . This means that the convective driving force for slow-diffusing liposomes is 2.8 times greater than diffusion and thus, we may neglect diffusion in a simplified model of liposome CED.

### 4.3.2 Mathematical model of CED with first order elimination

The model is based upon convection from the tip of the infusion cannula, modeled in spherical coordinates [Morrison *et al.* 1994]. The concentration of liposomes as a function of radius and time is given by Eq. 4-2. We assumed an extracellular fraction for brain,  $\phi$ , of 0.2, as reported elsewhere [Morrison *et al.* 1994]. As discussed in Chapter 3, the percent dose delivered by the Alzet<sup>TM</sup> Brain Infusion Cannula was low, and a significant portion of the dose flowed up the cannula track. To estimate the actual

fraction of dose delivered to the brain, the non-exchangeable  $^3\text{H}$ -Chol labeled liposomes were infused using the 24 hr Alzet<sup>TM</sup> pump, giving  $3.07 \pm 1.04\%$  ( $n=3$ ) of the infused dose in the brain. To correct for flow leakage outside of the brain,  $q$  was determined from the Alzet<sup>TM</sup> pump rate ( $0.14 \mu\text{L} / \text{min}$ ) multiplied by the fraction of dose in the brain at the end of the infusion. Thus, the flowrate,  $q$ , assumed for these calculations was  $0.14 \mu\text{L} / \text{min} * 0.0307 = 0.0043 \mu\text{L} / \text{min}$ .

#### 4.3.3 Estimation of binding constant from fluorescence microscopy

If the length of time of the infusion is longer than one binding half-life, then the following simplification of Eq. 4-2 can be derived as the radius of half maximum intensity,  $r_{50\% \text{ max}}$ , by letting

$$C(r_{50\% \text{ max}}) / C_{(0)} = 0.5 = \text{EXP} [-k r_{50\% \text{ max}}^3 4 \pi / (3 q)] \quad \text{Eq. 4-10}$$

then solving for  $k$  :

$$k = [\ln(2) 3 q] / [4 \pi r_{50\% \text{ max}}^3] \quad \text{Eq. 4-11}$$

So for every animal infused with particles for 24 hrs, an estimate of the magnitude of  $k$  can be determined from the radii of distribution,  $r_{50\% \text{ max}}$ , given in Table 3-3. These radii were obtained using a 24-hr continuous infusion; therefore, this assay can only determine half-lives below 24 hrs.

#### 4.3.4 Estimation of elimination constant from radiolabel half-life

The  $^{125}\text{I}$ -BPE degradable lipid was used to track elimination of label from the brain. The half-life,  $t_{1/2}$ , of this elimination can be translated into a first order elimination constant,  $k$ , using the following equation:

$$k = \ln(2) / t_{1/2}$$

Eq. 4-12

Operating on the assumption that the cellular degradation and release of this probe is rate limited by binding and internalization, this analysis should give a  $k$  on the same order of magnitude as the  $k$  derived from Eq. 4-11.

## 4.4 Results

### 4.4.1 Determination of a binding constant for neutral liposomes

To understand the rate of liposome elimination by the perivascular cells in the brain, I utilized two methods to estimate an irreversible elimination constant,  $k$ , from the interstitial space. The first elimination rate was obtained from the decay constant of the  $^{125}\text{I}$ -BPE labeled liposomes after acute infusion (Table 3-2). From the data gathered using  $^3\text{H}$ -Chol labeled liposomes, all of the lipid components remained in the brain (half-life of elimination > 48 hrs) (Table 3-2), so any removal of the  $^{125}\text{I}$ -BPE must be due to degradation of the label by cells within the brain. The half-life of  $^{125}\text{I}$ -BPE elimination ( $t_{1/2} = 9.9 \pm 2.0$  hrs) depends on one of two possible rate-limiting steps, either the rate of binding/endocytosis from interstitial space or the rate of enzymatic processing. If this half-life is interpreted as a first order elimination rate using Eq. 4-12 then  $k = 0.0012 \pm 0.0002 \text{ min}^{-1}$ . To determine if this  $k$  represents binding/endocytosis or enzymatic processing, a second method was used to estimate  $k$  based upon a less readily metabolized, fluorescent reporter group.

The second method for estimating the elimination of liposomes,  $k$ , is based upon the distribution radius,  $r_{50\% \text{ max}}$ , of particles obtained from fluorescent imaging (Table 3-3).

Data were analyzed using a simplification of the model proposed by Morrison and coworkers [1994]. Following this model, an illustration of the expected concentration profile at the end of these CED experiments is provided in Fig. 4-1 at the flowrate ( $q = 0.0043 \mu\text{L} / \text{min}$ ) and length of infusion (24 hrs) for the Alzet™ pump. Decreasing values of  $k$  from 0.1 to  $0.00001 \text{ min}^{-1}$  are shown (Fig. 4-1). The 80 nm control liposomes tend to have a  $r_{50\% \text{ max}}$  around 1 mm, visually corresponding to the curve labeled  $k = 0.001 \text{ min}^{-1}$ .

If the CED infusion has run for greater than one elimination half-life for a given particle, then the radius,  $r_{50\% \text{ max}}$ , obtained from microscopy can be determined using Eq. 4-11 and the data in Table 3-3 to estimate a value for  $k$ . The radius of distribution was determined for the 80 nm liposomes because their penetration was employed as a control in many of the animals. Eq. 4-11 was used to estimate a binding/endocytosis elimination constant  $k$  for each animal; the average was  $0.0010 \pm 0.0002 \text{ min}^{-1}$  ( $n=26$ ), closely agreeing with the  $k$ ,  $0.0012 \pm 0.0002 \text{ min}^{-1}$ , determined from the degradable radiolabel, and suggesting that the brain half-life of  $^{125}\text{I}$ -BPE radiolabel was rate-limited by binding/endocytosis, and not dependent upon the rate of enzymatic degradation. If enzymatic degradation were rate limiting, then the elimination of radiolabel would give a much slower estimate of  $k$  than the fluorescent binding constant.

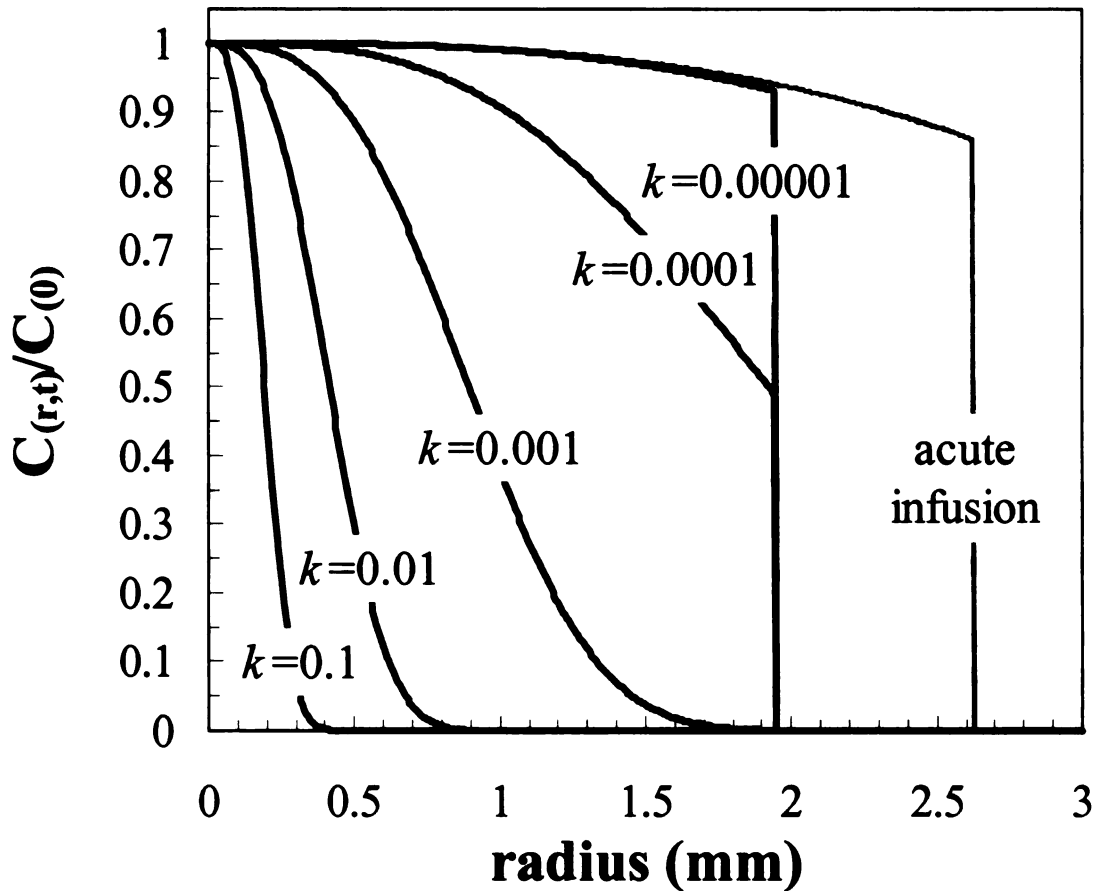


**Figure 4-1. Prediction of liposome concentration profile.** (black curves) Mathematical model of the distribution profiles expected for particles delivered with osmotic pump over 24 hours with  $q = 0.0043 \mu\text{L} / \text{min}$  and  $\phi = 0.2$ . Values of the elimination constant  $k$  from 0.1 to 0.00001 ( $\text{min}^{-1}$ ) are indicated. At low values of  $k$ , the relative concentration is not significantly affected until the wave of the solvent front is reached at a radius of  $\sim 2$  mm. (gray curve) Distribution profile predicted for particles delivered by acute infusion (Table 3-2) over a period of 30 min with  $q = 0.50 \mu\text{L} / \text{min}$ ,  $\phi = 0.2$ , and  $k = 0.001 \text{ min}^{-1}$ . To correct for flow leakage outside the brain, the flowrate,  $q$ , was calculated by multiplying the pump flowrate ( $0.8 \mu\text{L} / \text{min}$ ) by the fraction (0.63) of non-exchangeable  $^3\text{H}$ -Chol radiolabel in the brain immediately following infusion.

#### 4.4.2 *Positive charge increases the binding constant of liposomes*

It was shown in Chapter 3 that positive charge greatly restricts the penetration of liposomes under CED. So it was expected that this would give a significantly higher estimate of the rate constant,  $k$ . Analysis using Eq. 4-11 was applied to the images taken with other types of particles and the resulting elimination constants,  $k$ , are summarized in Fig. 4-2. The typical liposome has a  $k$  near  $0.001 \text{ min}^{-1}$ . Indeed, the highest value of  $k$  observed in this analysis is for positively charged liposomes. The constant  $k = 0.046 \pm 0.020 \text{ min}^{-1}$  for positive liposomes is approximately 50-fold higher than that of neutral liposomes. This increase in  $k$  was significant ( $p < 0.001$ ), as determined with a two tailed t-test used to compare the  $\text{Log}(k)$  obtained from animals given positive ( $n=4$ ) and neutral liposomes ( $n=26$ ).

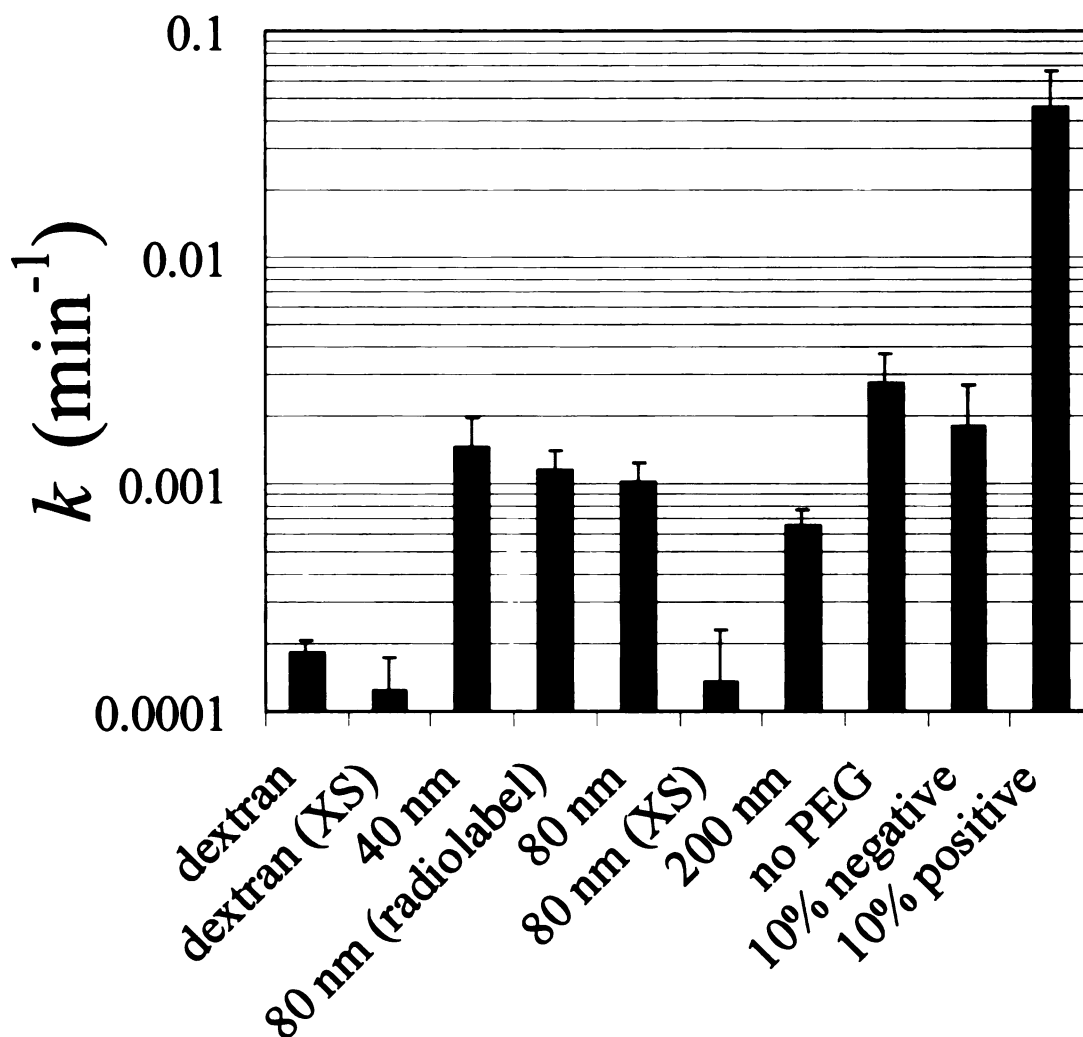


**Figure 4-2. Calculated elimination rate constants for different liposomes.** Calculated elimination rate constants  $k$ , based upon Table 5-2 and Table 5-3. Labels indicate the following: 'dextran' is a 10 kD dextran (n=7); 'dextran (XS)' includes 100 mM excess liposomes (n=3); '40 nm' diameter liposomes (n=5); '80 nm (radiolabel)' diameter liposomes determined from  $^{125}\text{I}$ -BPE elimination (n=9); '80 nm' diameter liposomes (n=26); '80 nm (XS)' diameter liposomes with 100 mM excess liposomes (n=3); '200 nm' diameter liposomes (n=3); 'no PEG' are liposomes lacking steric shielding (n=3); '10% negative' charged liposomes (n=4); '10% positive' charged liposomes (n=4). Error bars indicate the standard error.

#### 4.4.3 *Enhancement of distribution by adding excess liposomes*

I have shown that PEG shielded liposomes are rapidly entrapped into perivascular brain cells with an interstitial brain half-life of 9.9 hrs. I attempted to increase the radius of distribution for these particles by dramatically increasing the dose of liposomes from 1 mM to 100 mM total lipid by adding 100-fold excess unlabeled liposomes (Fig. 3-4[I-L]). This significantly increased the penetration distance (Table 3-3) and caused a 7.6-fold decrease in the apparent elimination constant to  $k = 0.00013 \pm 0.00010 \text{ min}^{-1}$  (Fig. 4-2). This reduction in  $k$  was significant ( $p=0.001$ ) using a t-test to compare the  $\text{Log}(k)$  obtained for animals with ( $n=3$ ) and without ( $n=26$ ) excess liposomes. In terms of an elimination half-life, the excess liposomes lengthened the elimination of liposomes to at least  $t_{1/2} = 24$  hrs, a major improvement over the 9.9 hr half-life for liposomes at low concentration. This suggests that the concentration of dose will play a major role in the penetration distance of nanoparticles delivered by CED.

The addition of excess liposomes reduced the liposome elimination constant to a value which is not significantly different than that observed for dextran. Without excess liposomes, dextran had a low apparent elimination constant in the brain of  $k = 0.00018 \pm 0.00002 \text{ min}^{-1}$  and the addition of excess liposomes did not alter this (Fig. 4-2). Because these infusions lasted only 24 hrs, we are unable to use this method to accurately estimate  $k$  less than about  $0.00048 \text{ min}^{-1}$ . Thus all reported values of  $k$  below  $0.0005 \text{ min}^{-1}$  are only apparent values (Fig. 4-2) and fall below the true limit of detection.



#### 4.5 Discussion

In considering the use of CED for nanoparticles in human clinical trials, it is prudent to assess the penetration distance for new nanoparticles within an animal model system to assure that the elimination constant for the particle is not too rapid. As a useful rule of thumb, nanoparticle penetration will never exceed the distance that it can travel during its first half-life since diffusion cannot appreciably contribute to the movement of the particle over the duration of time that CED is used. Thus, if a particle has an elimination half-life of 15 min ( $k = 0.046 \text{ min}^{-1}$ ), such as the positively charged liposomes in this study, then infusing for longer than 15 min will not increase the penetration distance unless the elimination mechanism is saturated or otherwise circumvented. After 15 min, a steady state 'standing wave' solution is obtained (Fig. 4-1,  $k = 0.01$ ). This situation is akin to a standing salt gradient established within the filtrate of the kidney (Vander *et al.* 1994).

For small animals, CED can be performed in less than a half an hour to reach sizable regions of brain; however, in humans, to reach large volumes, it is necessary to infuse for longer periods of time, from hours to days. As the length of the infusion time surpasses the half-life of nanoparticle elimination (9.9 hrs for a neutral liposome at low concentration), it will become impossible to deliver the particle farther through tissue using CED without addressing this source of the elimination.

We have shown that the tissue binding of neutral liposomes can be reduced by adding excess liposomes. For slowly eliminated compounds such as dextran and sucrose, the

concentration of the infusion should not significantly affect the penetration of particle by CED. In contrast, the concentration of infused liposomes has a large effect on the penetration distance. A related observation has been reported by Kroll *et al.* [1996] where the penetration distance of magnetic nanoparticles was increased by increasing the concentration of the infusion. The authors were unable to explain this effect; however, it is possible that all neutral nanoparticles suffer from binding and internalization by cells active in phagocytosis within the brain. Thus, the concentration of the infusion can be adjusted to saturate this binding and extend the penetration distance of the particle. For particles with high toxicity, we would propose blocking uptake using non-toxic liposomes that are easily tolerated in the brain at 100 mM lipid concentrations.

#### **4.6 Conclusion**

Through analysis of fluorescent images, I have successfully used a mathematical model to determine a first order irreversible rate constant that partially limits the distribution of uncharged liposomes. The higher the rate constant, the shorter the penetration distance for a particle infused by CED. The rate constant for uncharged liposomes was independently validated using a radiolabel that degrades and eliminates from the brain following cell internalization. The addition of 100-fold excess liposomes was then able to decrease this rate constant 7.6-fold for neutral liposomes. When this analysis was applied to liposomes with modest positive charge (10%), the rate constant rose 50-fold compared to a neutral liposome. I conclude that in order to scale up the distribution of liposomes, virus, and DNA lipoplex for human therapy, it will be critical to overcome tissue binding mediated by even modest amounts of positive charge.

## CHAPTER 5:

### **HIV TAT protein transduction domain mediates cell binding and intracellular delivery of liposomes and DNA nanolipoparticles**

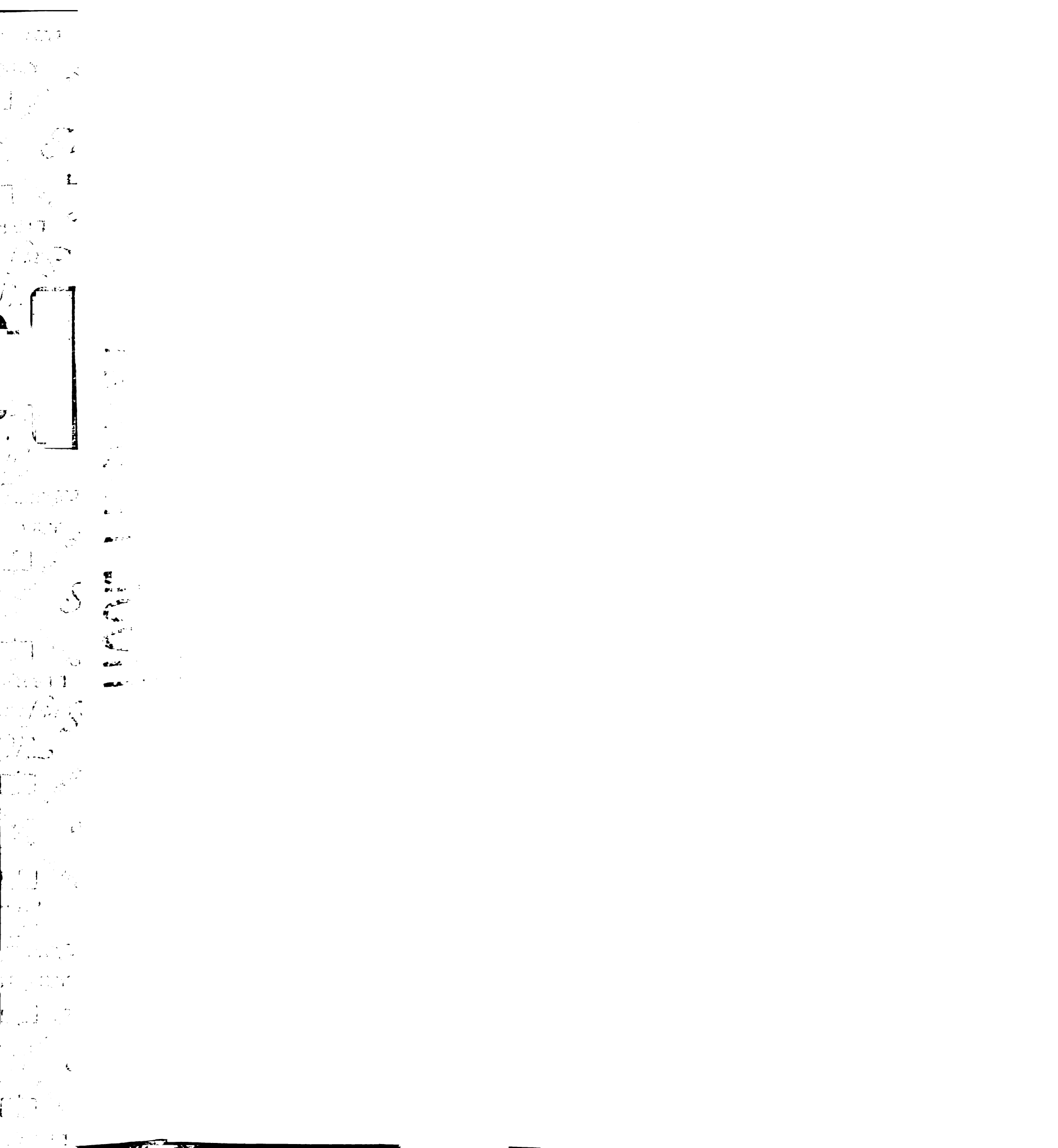
#### **5.1 Abstract**

A major barrier to effective non-viral transfection is that DNA has limited access to the cytosol. pH sensitive PEG shielded nanolipoparticles (NLP) have proven useful for stimulating content release upon particle internalization. Unfortunately, PEG shielding also reduces the probability of cellular interactions. For this reason, it is beneficial to incorporate a ligand into the vector that facilitates cell binding and internalization. The HIV TAT peptide is a short cationic sequence that allows TAT protein to traffic between the cytoplasm of adjacent cells. When the TAT sequence is attached to small molecules, proteins, phages, liposomes, and nanoparticles, this peptide promotes cell binding and internalization. I attached the TATp to the surface of a liposome, both at the phospholipid-aqueous interface and separated by a PEG linker. I characterized the kinetics of liposome binding. TATp attached directly to the liposome surface shows saturable binding, but TATp attached by a PEG linker does not. The TATp PEG lipid was incorporated into nanolipoparticles containing DNA using a micelle transfer method. The TATp modified NLP had substantially increased binding to and transfection of tumor cells following convection enhanced delivery to an intracranial tumor model. When incorporated into a bioresponsive PEG shielded nanolipoparticle, the TATp substantially increases transfection.

## 5.2 Introduction

Gene therapy has been hampered by a lack of safe and efficient gene delivery vectors. Nonviral cationic particles are effective but toxic; neutral particles are much better tolerated but exhibit low levels of transfection in the absence of a ligand. Neutral lipids, phosphatidylcholine and phosphatidylethanolamine, similar to those in the body are relatively non-toxic and non-immunogenic; however, uncharged liposomes show poor transfection efficiency [Huang *et al.* 1999], especially when compared with viral vectors. Recent efforts to boost transfection have been driven by the view that fundamental viral behaviors can be imitated in a liposome [Kaneda 2000]. By mimicking viral activities, such as cell surface binding, endosomal escape, and nuclear transport of DNA, it may be possible to create a safe and efficient liposome vector.

The cytoplasmic delivery of liposome contents, or any PEG shielded nanoparticle, depends upon the ability of the particle to interact with cells, which may require the use of a cell binding ligand. A number of ligands have been proposed [Eliaz and Szoka 2001, Torchilin *et al.* 2001, Hood *et al.* 2002]. This study discusses the characterization of a peptide ligand based upon a human immunodeficiency virus (HIV) peptide that induces strong nonspecific binding and internalization of liposomes [Torchilin *et al.* 2001, Tseng *et al.* 2002] to low pH compartments [Fretz *et al.* 2004]. The HIV genome contains a protein called trans-acting transcriptional activator (TAT). This protein can rapidly enter and exit the cytosol of cells. A short, arginine rich sequence on TAT is necessary and sufficient for cell binding (TATp). We have synthesized and characterized the properties of TATp(GRKKRRQRRRGYG) and attached it directly to a lipid anchor and indirectly



via a PEG (MW=2000) anchor. We propose to use this TATp lipid conjugate to promote particle cell binding and internalization for the purpose of drug and gene delivery.

The goal of this project is to use this ligand to deliver DNA directly to a rat brain tumor model by convection enhanced delivery. To do so, we needed a platform for encapsulating DNA into small, PEG shielded, bioresponsive particles. A detergent dialysis technique has been introduced to form PEG lipid stabilized DNA-containing particles (SPLP) [Mok *et al.* 1999, Tam *et al.* 2000]. The PEG lipid shields the positive surface charge (cationic lipids) used to form a complex with DNA and provides a steric hindrance to particle binding by the reticuloendothelial system. This nanoparticle evokes a minimal immune response and circulates for a prolonged period in the body [Tam *et al.* 2000]; however, these properties also prevent binding and efficient transfection of target cells. More recently this technique has been optimized within our group to formulate both pH sensitive nanolipoparticles (NLP) [Choi *et al.* 2003, Li *et al.* 2005] and reduction sensitive NLP [Huang *et al.* 2005]. Here, we focus upon improving the uptake of bioresponsive NLP using rationally designed lipids that achieve both strong cell binding, internalization, and transfection.

## **5.3 Methods**

### *5.3.1 Materials*

1-palmitoyl, 2-oleoyl-sn-glycero-3-phosphocholine (POPC), 1,2-dioleoyl-sn-glycero-3-phosphoethanolamine (DOPE), 1,2-dipalmitoyl-3-trimethylammonium-propane (DPTAP), 1,2-dioleoyl-3-trimethylammonium-propane (DOTAP), 1,2-distearoyl-sn-

LIBRARY

LIBRARY

LIBRARY

LIBRARY

LIBRARY

LIBRARY

LIBRARY

LIBRARY

LIBRARY

LIBRARY

LIBRARY

LIBRARY

LIBRARY

LIBRARY

LIBRARY

LIBRARY

LIBRARY

LIBRARY

LIBRARY

LIBRARY

LIBRARY

LIBRARY

LIBRARY

LIBRARY

LIBRARY

LIBRARY

LIBRARY

LIBRARY

LIBRARY

LIBRARY

LIBRARY

LIBRARY

LIBRARY

LIBRARY

LIBRARY

LIBRARY

LIBRARY

LIBRARY

LIBRARY

LIBRARY

LIBRARY

LIBRARY

LIBRARY

glycero-3-phosphoglycerol-N-(polyethyleneglycol)2000 (PEG-DSPE), cholesterol, and fluorescent tracers 1,2-dioleoyl-sn-glycero-3-phosphoethanolamine-N-(lissamine rhodamine b sulfonyl) (Rh-PE), and 1,2-dioleoyl-sn-glycero-3-phosphoethanolamine-n-(carboxyfluorescein) (CF-PE) were obtained from Avanti Polar Lipids (Alabaster, AL). Fluorescent lipid tracers DiO (D-275), DiI (D-282), and DiD (D-307) were purchased from Molecular Probes (Eugene, OR). The pH sensitive PEG-lipid (POD) was synthesized in our lab as described elsewhere [Guo *et al.* 2003]. A reduction sensitive cationic cholesterol compound (317) was also synthesized in our lab as described elsewhere [Huang *et al.* 2005]. Green fluorescent protein (GFP) encoding plasmid was a generous gift from Valentis (Burlingame, CA).

### 5.3.2 *Synthesis and purification of TATp and TATp lipids*

The HIV TAT peptide (TATp), GRKKRRQRRRGYG, was synthesized by solid-phase Fmoc chemistry as described by Wyman *et al.* [1997]. ~300 mg of resin containing either the peptide or peptide conjugates were cleaved from the resin by stirring 4 hrs at room temperature in a 10 mL solution of 95% trifluoroacetic acid (TFA), 2.5% distilled dionized water, and 2.5% triisopropylsilane. Resin was removed by filtration through a bed of glass fibers, and deprotected material was precipitated into 80 mL of cold ether on ice. The precipitate was centrifuged and the supernatant was discarded. The pellet was dried and hydrated in 4 mL of distilled deionized water. The solution was frozen and water was removed under high vacuum. Samples were purified by a high pressure liquid chromatography (HPLC) (Dionex Sunnyvale, CA). The unmodified peptide was purified using a semi-preparative scale C18 column at 10 mL /min with a 100 min gradient from



Handwritten notes at the top left, including the word "MAY" and other illegible characters.



Vertical handwritten text on the left side, possibly a list or index.

Main body of handwritten text on the left side, including the word "MAY" and other illegible characters.

0% to 100% acetonitrile with 0.1% TFA. The unmodified peptide eluted at 13% acetonitrile (ACN) and the mass was confirmed by matrix assisted laser desorption ionization (MALDI) mass spectroscopy (expected:1,672.9 g/mol; observed:1,673.04 g/mol).

The TATp-lipid (Fig. 5-1A) conjugate was prepared using 1,2 dipalmitoyl-sn-glycero-3 succinate (Avanti; Alabaster, AL). 50  $\mu$ moles of lipid were dissolved in 4 mL dichloromethane (DCM): 7.5 mL n-methyl-2-pyrrolidone (NMP) in the presence of 400  $\mu$ moles of n-methyl-morpholine and 120  $\mu$ moles of 1-H-Benzotriazolium, 1-[bis(dimethylamino)methylene]-hexafluorophosphate(1-),3-oxide O-(Benzotriazol-1-yl)-N,N,N',N' tetramethyluronium hexafluorophosphate (HBTU). 60  $\mu$ moles of protected TATp on the resin were added to the reaction cocktail and stirred overnight at room temperature. The reaction was stopped by washing the resin with 20 mL of DCM over a bed of glass fibers. The resin was recovered, dried, and TATp-lipid was deprotected as described above. TATp-lipid was dissolved in water:ACN:TFA [33:66:0.1] and purified on a semipreparative C4 column at 4 mL/min using a 20 min gradient from 45 to 65% ACN in the presence of 0.1% TFA. The TATp-lipid peak eluted at about 50% ACN and was identified by MALDI (expected: 2,324.09g/mol; observed: 2,326.01g/mol).

The TATp-PEG-lipid (Fig. 5-1B) conjugate was prepared using 1,2, dipalmitoyl-sn-glycero-3-phosphoethanolamine -N- amino(polyethylene glycol)2000 (Avanti; Alabaster, AL) in a 2 step reaction. For reaction 1, in 4 mL of NMP, the unprotected amino-terminal end of the peptide (60  $\mu$ moles) was reacted for 4 hrs at room temperature under stirring

7/15/50

REAR

7/15/50

7/15/50

7/15/50

7/15/50

7/15/50

7/15/50

7/15/50

7/15/50

7/15/50

7/15/50

7/15/50

7/15/50

7/15/50

7/15/50

7/15/50

7/15/50

7/15/50

7/15/50

7/15/50

7/15/50

7/15/50

7/15/50

7/15/50

7/15/50

7/15/50

7/15/50

7/15/50

7/15/50

7/15/50

7/15/50

7/15/50

7/15/50

7/15/50

7/15/50

with excess 180  $\mu$ moles of disuccinimidyl suberate (Pierce, Rockford, IL, USA) in the presence of 160  $\mu$ moles of n-methyl morpholine. The reaction was stopped by washing with 20 mL of NMP over a bed of glass fibers. For reaction 2, the resin was stirred with 72  $\mu$ moles of lipid dissolved in 4 mL NMP in the presence of 360  $\mu$ moles of n-methyl morpholine. The reaction proceeded for 4 hrs at room temperature and was stopped by washing the resin with 20 mL of DCM over a bed of glass fibers. The resin was recovered, dried, and TATp-PEG-lipid was deprotected as described above. TATp-PEG-lipid was dissolved in water:ACN:TFA [50:50:0.1] and then purified on a semipreparative C4 column at 4 mL/min using a 10 min gradient from 50 to 70% ACN in the presence of 0.1% TFA. The TATp-PEG-lipid peak eluted at about 60% ACN and was identified by MALDI (expected: 4,500 g/mole +44 PEG series; observed: 4,391g/mol). Obtaining a successful MALDI spectra from the PEG lipid series was enabled by first dissolving the TATp-PEG-lipid in water:ACN:TFA [50:50:0.1] and then mixing this 1:1 with ACN saturated with sinapinic acid.

Handwritten notes on the left margin, including the word "SOUTH" and other illegible text.

Vertical handwritten text, possibly a date or reference number.



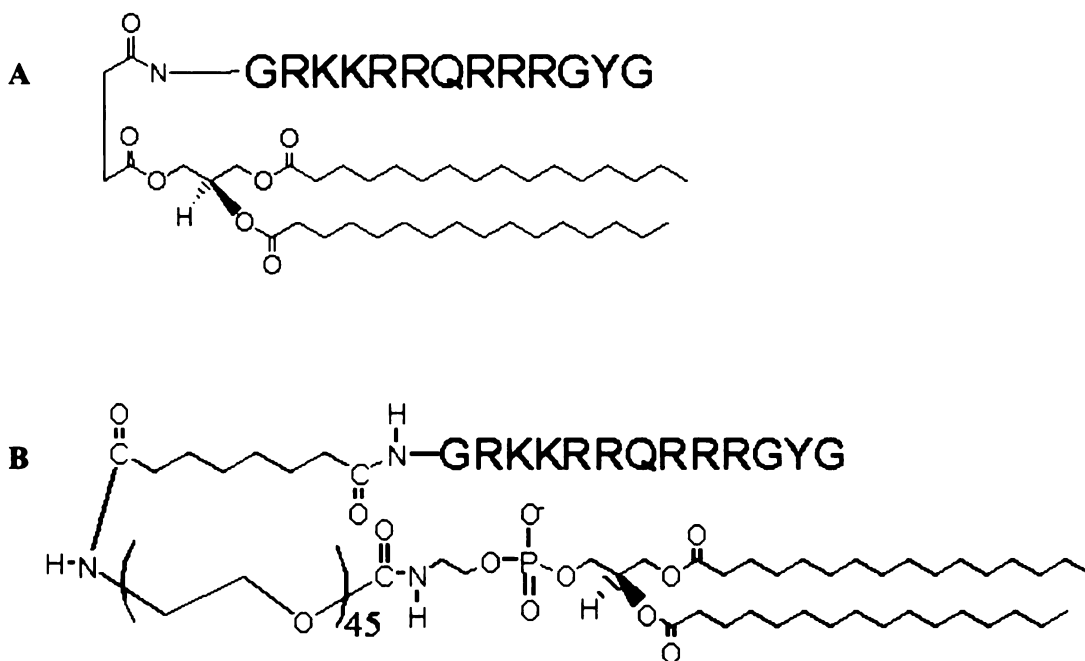


**Figure 5-1. Structures of TATp ligands.** [A] TATp-lipid: TATp is linked directly to the surface of the liposome. [B] TATp-PEG-lipid: TATp is linked to a phosphatidylethanolamine via a 2000 Da PEG polymer.

Handwritten text at the top left of the page.

Handwritten text below the first line.

Handwritten text with a small square symbol below it.

Handwritten text with a small square symbol below it.

Handwritten text with a small square symbol below it.

Handwritten text with a small square symbol below it.

Handwritten text with a small square symbol below it.

Handwritten text with a small square symbol below it.

Handwritten text with a small square symbol below it.

Handwritten text with a small square symbol below it.

Handwritten text with a small square symbol below it.

Handwritten text with a small square symbol below it.

Handwritten text with a small square symbol below it.

Handwritten text with a small square symbol below it.

Handwritten text with a small square symbol below it.

Handwritten text with a small square symbol below it.

Handwritten text with a small square symbol below it.

Handwritten text with a small square symbol below it.

Handwritten text with a small square symbol below it.

Handwritten text with a small square symbol below it.

Handwritten text at the bottom left of the page.

### *5.3.3 Preparation of liposomes*

For the preparation of liposomes, 5-10  $\mu$ moles of total lipid was mixed in chloroform and dried in a glass test tube by rotary evaporation under reduced pressure. The lipid film was placed under high vacuum for 4 hrs to remove residual solvent. Liposomes were formed either in pH 7.5 Hepes buffered saline (145 mM NaCl, 5 mM Hepes) or pH 8.5 Tris buffered saline (150 mM NaCl, 5 mM Tris). The lipid (10 mM) was hydrated at 20°C with intermittent vortexing. ~200 nm liposomes were formed by extrusion (41x) through 200 nm pores in polycarbonate membranes. ~100 nm liposomes were then formed through extrusion through 80 nm pores (11x). ~50 nm liposomes were then extruded (11x) through 50 nm pores. Particle size and zeta potential were determined using a Malvern (Southborough, MA) Zeta3000 Dynamic Light Scattering Instrument and are presented in Table 5-1.



LIBRARY

LIBRARY

LIBRARY

LIBRARY

LIBRARY

LIBRARY

LIBRARY

LIBRARY

LIBRARY

LIBRARY

LIBRARY

LIBRARY

LIBRARY

LIBRARY

LIBRARY

LIBRARY

LIBRARY

LIBRARY

LIBRARY

LIBRARY

LIBRARY

LIBRARY

LIBRARY

LIBRARY

LIBRARY

LIBRARY

LIBRARY

LIBRARY

LIBRARY

LIBRARY

LIBRARY

LIBRARY

**Table 5-1-1. Compositions and characteristics of polymers and particles used in TATp binding experiments**

Particle	Label	Composition	Formation	Size (nm)*	Zeta Potential (mV)**
Neutral control	<sup>125</sup> I	POPC:Chol: <sup>125</sup> I-BPE [60:40:<0.01]	200 nm extruded	223.8 ± 3.4	nd***
DPTAP control	<sup>125</sup> I	DPTAP:POPC:Chol: <sup>125</sup> I-BPE [2.4:60:40:<0.01]	200 nm extruded	298.7 ± 22.9	nd
0.03% TATp-lipid	<sup>125</sup> I	TATp-lipid:POPC:Chol: <sup>125</sup> I-BPE [0.03:60:40:<0.01]	200 nm extruded	249.5 ± 3.2	nd
0.1% TATp-lipid	<sup>125</sup> I	TATp-lipid:POPC:Chol: <sup>125</sup> I-BPE [0.1:60:40:<0.01]	200 nm extruded	328.4 ± 27.4	nd
0.3% TATp-lipid	<sup>125</sup> I	TATp-lipid:POPC:Chol: <sup>125</sup> I-BPE [0.3:60:40:<0.01]	200 nm extruded	203.5 ± 0.5	nd
1.0% TATp-lipid	<sup>125</sup> I	TATp-lipid:POPC:Chol: <sup>125</sup> I-BPE [1:60:40:<0.01]	200 nm extruded	312.3 ± 19.1	nd
0.3% TATp-PEG-lipid	<sup>125</sup> I	TATp-PEG-lipid:POPC:Chol: <sup>125</sup> I-BPE [0.3:60:40:<0.01]	50 nm extruded	76.5 ± 4.6	nd
0.3% TATp-PEG-lipid	<sup>125</sup> I	TATp-PEG-lipid:POPC:Chol: <sup>125</sup> I-BPE [0.3:60:40:<0.01]	80 nm extruded	117.1 ± 2.2	nd
0.3% TATp-PEG-lipid	<sup>125</sup> I	TATp-PEG-lipid:POPC:Chol: <sup>125</sup> I-BPE [0.3:60:40:<0.01]	200 nm extruded	161.6 ± 0.9	nd
0.3% TATp-lipid	<sup>125</sup> I	PEG2000-DSPE:TATp-lipid:POPC:Chol: <sup>125</sup> I-BPE [5:0.3:60:40:<0.01]	200 nm extruded	154.9 ± 1.4	nd
Zeta control	none	POPC	200 nm extruded	Nd	-5.7 ± 0.6
Zeta control	none	DOTAP:POPC[10:90]	200 nm extruded	Nd	31.9 ± 0.8
DPTAP control	none	DPTAP:POPC:Chol [2.4:60:40]	100 nm extruded	187.9 ± 8.0	2.2 ± 0.4
0.3% TATp-lipid	none	TATp-lipid:POPC:Chol [0.3:60:40]	100 nm extruded	135.7 ± 2.1	1.9 ± 0.8

\* particle diameter measured by light scattering zeta average size, ± indicates standard deviation

\*\* zeta potentials all at low salt 10 mM NaCl, 0.1 mM MOPS, pH 7.5, ± indicates standard deviation

\*\*\* not determined

1942  
1943  
1944  
1945  
1946  
1947  
1948  
1949  
1950  
1951  
1952  
1953  
1954  
1955  
1956  
1957  
1958  
1959  
1960  
1961  
1962  
1963  
1964  
1965  
1966  
1967  
1968  
1969  
1970  
1971  
1972  
1973  
1974  
1975  
1976  
1977  
1978  
1979  
1980  
1981  
1982  
1983  
1984  
1985  
1986  
1987  
1988  
1989  
1990  
1991  
1992  
1993  
1994  
1995  
1996  
1997  
1998  
1999  
2000  
2001  
2002  
2003  
2004  
2005  
2006  
2007  
2008  
2009  
2010  
2011  
2012  
2013  
2014  
2015  
2016  
2017  
2018  
2019  
2020  
2021  
2022  
2023  
2024  
2025



1942  
1943  
1944  
1945  
1946  
1947  
1948  
1949  
1950  
1951  
1952  
1953  
1954  
1955  
1956  
1957  
1958  
1959  
1960  
1961  
1962  
1963  
1964  
1965  
1966  
1967  
1968  
1969  
1970  
1971  
1972  
1973  
1974  
1975  
1976  
1977  
1978  
1979  
1980  
1981  
1982  
1983  
1984  
1985  
1986  
1987  
1988  
1989  
1990  
1991  
1992  
1993  
1994  
1995  
1996  
1997  
1998  
1999  
2000  
2001  
2002  
2003  
2004  
2005  
2006  
2007  
2008  
2009  
2010  
2011  
2012  
2013  
2014  
2015  
2016  
2017  
2018  
2019  
2020  
2021  
2022  
2023  
2024  
2025

#### 5.3.4 *In vitro uptake of TATp modified radiolabeled liposomes*

To quantitatively determine the kinetic uptake of TATp modified liposomes in cell culture, we labeled liposomes with a headgroup iodinated benzamidine phospholipid ( $^{125}\text{I}$ -BPE), as described previously [Abra *et al.* 1982]. Radiolabeled lipid (less than 0.01% mole percent of the total lipid) were deposited as a film with other lipid components from a chloroform solution before hydration. Gamma radiation activity was determined using a Perkin Elmer Wizard Gamma Counter (Boston, MA). These experiments were performed with B16F10 cells in a 96 well based assay as follows. Cells were trypsinized and seeded into plates at  $0.5 - 1 * 10^4$  cells per well per 100  $\mu\text{L}$  Modified Eagle Media (UCSF Cell Culture Facility) supplemented with 10% Fetal Bovine Serum (FBS) (UCSF Cell Culture Facility). Cells were allowed to grow for 24 hrs prior to the assay. At the time of assay, 3 wells were trypsinized into 50  $\mu\text{L}$  and the cell number per well was counted, typically containing  $2 * 10^4$  cells per well at the time of assay.

During the assay, liquid manipulations were made gently using a multichannel pipettor. At the start of each assay ( $t=0$ ), the cells were washed once with 100  $\mu\text{L}$  of media. During the course of the assay, this wash was removed and replaced with 100  $\mu\text{L}$  of media containing radiolabeled liposomes ( $t=0, 60, 90, 105, 120$  min). The media used for the washing and binding assay was FBS free MEM supplemented with 10 mM Hepes buffer, to maintain pH at neutral. All cells were incubated with liposomes either in a  $4^\circ\text{C}$  cold room or in a  $37^\circ\text{C}$  incubator for 2 hrs under gentle orbital shaking. At the end of the 120 min, all cell incubations ( $t=0,15,30,60,120$  min) were washed simultaneously to recover

LIBRARY  
UNIVERSITY OF  
MICHIGAN  
ANN ARBOR  
MICHIGAN  
48106-1000  
SERIALS ACQUISITION  
300 N ZEEB RD  
ANN ARBOR MI 48106-1000  
TEL: 734 763 1000  
FAX: 734 763 1001  
WWW: WWW.LIBRARY.MICHIGAN.EDU

radioactive counts. For every well, 3 fractions were obtained. Fraction 1 included the supernatant and unbound liposomes that washed off with 2 changes of PBS. Fraction 2 included surface bound liposomes that were washed off by 3 changes of 1.6M NaCl PBS. Fraction 3 included cell-internalized liposomes obtained by solubilizing the cells in 0.5M NaOH. All 3 fractions were measured on a gamma counter. Each data point was performed in triplicate and the average recovery of radioactivity was typically 85%.

### 5.3.5 Formation of bioresponsive NLP

pH sensitive NLP (Fig. 5-5) were prepared as described by Choi *et al.* [2003]. Briefly, the lipid components (POD:DOTAP:DOPE:Rh-Pe [20:12:68:0.2]) were dissolved in chloroform, mixed, and dried in a glass vial. 10  $\mu$ moles of total lipid were dissolved into 1.5 mL (5 mM Tris, 200 mM OGP, 145 mM NaCl, pH8.5) into micelles composed of a detergent, n-octyl glucoside (OGP), and mixed with 200  $\mu$ g DNA in 1.5 mL (5 mM Tris, 200 mM OGP, 145 mM NaCl, pH 8.5). Only 12% of the lipid components were positively charged, and these associate with the negatively charged phosphate DNA backbone at a charge ratio of 2:1 (+:-). Detergent was dialyzed away at 20°C through a 10,000 MWCO membrane, allowing formation of lipid bilayers around the DNA. Particle formation was confirmed by photon correlation spectroscopy. The resulting particles were about 60 nm in diameter.

Reduction sensitive NLP (Fig. 5-6) were prepared as described by Huang *et al.* [2005]. Briefly, the lipid components (PEG-DSPE:317:DOPE:DiD [10:50:40:0.1]) were dissolved in chloroform, mixed, and dried in a glass vial. Compound 317 is a reducible

San Francisco

Library

1

2

3

4

5

6

7

8

9

10

11

12

13

14

15

16

17

18

19

20

21

22

23

24

25

26

27

28

29

30

100

101

102

103

104

105

106

107

108

109

110

111

112

113

114

115

116

117

118

119

120

121

122

LIBRARY

cationic lipid that can release DNA following internalization into a cell. 20  $\mu$ moles of total lipid were dissolved into 1.5 mL (5 mM Tris, pH8.5) and mixed with 1 mg DNA in 1.5mL ethanol:water [1:1] (5 mM Tris, pH8.5). 50% of the lipid components were positively charged (Compound 317), and these associate with the negatively charged phosphate DNA backbone at a charge ratio of 3:1 (+:-). Ethanol was dialyzed away at 20°C through a 10,000 MWCO membrane, allowing formation of lipid bilayers around the DNA. Particle formation is confirmed by Photon correlation spectroscopy where a diameter of 76 nm was observed. The salt concentration was adjusted to 150 mM NaCl immediately before use.

#### *5.3.6 Incorporation of TATp into NLP.*

TATp linked to a lipid anchor via a PEG (2000 Da) can easily be incorporated into liposomes or NLP after particle formation using a micelle transfer method [Tseng *et al.* 2002]. 0.3% by mole TATp-PEG-lipid was dried in a glass tube under high vacuum and an appropriate amount of NLP were added to the tube, vortexed, and incubated for either 1 hr (60°C) or 5 hrs (20°C). Under these conditions, the TATp-PEG-lipid micelles spontaneously insert into fluid bilayers. TATp incorporation was monitored by particle binding to a cation exchange column. For this assay, NLP were washed through a CM-25 Sephadex bed (5 cm \* 1 cm) in 150 mM NaCl Tris buffer pH 8.5. Unmodified NLP flow through the column in the void volume. TATp-PEG-lipid modified NLP bind to the column and can be eluted with the addition of 1M NaCl Tris buffer. Liposome concentration was observed using the lipid label (Rh-PE) and observing the rhodamine fluorescence (arbitrary units).



LIBRARY

LIBRARY

LIBRARY

LIBRARY

LIBRARY

LIBRARY

LIBRARY

LIBRARY

LIBRARY

LIBRARY

LIBRARY

LIBRARY

LIBRARY

LIBRARY

LIBRARY

LIBRARY

LIBRARY

LIBRARY

LIBRARY

LIBRARY

LIBRARY

LIBRARY

LIBRARY

LIBRARY

LIBRARY

LIBRARY

LIBRARY

LIBRARY

LIBRARY

LIBRARY

### *5.3.7 Implantation of U87-MG tumors in athymic rat brains*

Athymic rats were purchased from the National Cancer Institute and cared for at the UCSF Laboratory Animal Resource Center. We adhered to strict protocols as recommended by the National Institute of Health Guide for the Care and Use of Laboratory Animals and as approved by the UCSF Institutional Animal Care and Use Committee. To minimize pain and discomfort, animals were sedated with an intra peritoneal injection of Ketamine (60 mg / kg body weight) and Xylazine (7.5 mg / kg body weight). After anesthesia was attained, an incision was made in the scalp above the bregma and the animal was mounted in a stereotactic frame (Stoelting, Wood Dale IL). A hole was drilled in the skull 3 mm right of the bregma and a guide screw was installed. Subconfluent U87-MG cells were trypsinized on the day of implantation, washed once in Hanks Balanced Salt Solution (UCSF Cell Culture Facility), stored on ice, and centrifuged to obtain a cell pellet, which was then injected into the brain. Through the guide screw, at a depth of 5 mm, a Hamilton syringe was used to inject 10  $\mu$ L of  $\chi\omicron\nu\chi\epsilon\nu\tau\rho\alpha\tau\epsilon\delta$  cells over a 1 min period of a U87-MG cell pellet. The stereotactic coordinates of injection were centered within the caudate putamen [Paxinos and Watson 1982]. To relieve pain following surgery, animals were given a subcutaneous injection of Buprenorphine (0.05 mg / kg body weight).

### *5.3.8 Convection enhanced delivery by acute stereotactic infusion*

Convection enhanced delivery (peak flowrate of 0.8  $\mu$ L / min) of liposomes and NLP were performed into both normal rat brains and U87-MG intracranial tumors respectively. NLP infusions were performed at day 19-21 post implantation when the

San Francisco

RAINY

11

11/11

11

11/17

11/17

11/17

11/17

11/17

11/17

11/17

11/17

11/17

11/17

11/17

11/17

11/17

11/17

11/17

11/17

11/17

11/17

11/17

11/17

11/17

11/17

11/17

11/17

11/17

11/17

11/17

11/17

11/17

11/17

11/17

11/17

11/17

tumor was approximately 100-300 mg. Prior to infusion, liposomes were diluted to a concentration of 1 mM lipid in TBS and NLP were diluted to a concentration of 4 mM lipid. Animals were sedated and mounted on a stereotactic frame. To prevent backflow at this flowrate, [Chen *et al.* 1999] a narrow cannula was prepared from fused silica tubing with an outer diameter of 0.16 mm (Polymicro Technologies, Phoenix, AZ), extending 3 mm from the tip of a 24 gauge needle used for support. This cannula was inserted into the same stereotactic coordinates used for tumor implantation except the cannula was inserted only 4 mm rather than 5 mm. This was done to insure that the cannula was positioned within the tumor mass rather than at the edge of or below the tumor. A syringe pump was used to infuse solutions into the brain at an increasing flowrate as follows: 0.1  $\mu\text{L}$  /min for 5 min, 0.2  $\mu\text{L}$  /min for 5 min, 0.5  $\mu\text{L}$  /min for 5 min, and 0.8  $\mu\text{L}$  /min for 30 min for a total volume of 28  $\mu\text{L}$  infused over 45 min [Mamot *et al.* 2004, Saito *et al.* 2004]. The infusion cannula was withdrawn over a 5 min period following cessation of infusion. Post infusion, animals were sacrificed at 1, 6, 24, or 48 hrs. After sedation, animals were prepared by perfusion fixation with 200 mL of phosphate buffered saline PBS (100 mM phosphate, 150 mM NaCl, pH 7.4) and 200 mL of 4% paraformaldehyde in PBS. Brains were removed and post-fixed overnight in 4% paraformaldehyde at 4°C.

### 5.3.9 *Macroscopic imaging*

The entire brain was sliced into 1 mm axial sections and imaged macroscopically at a resolution of 10 pixels per mm using a macroscopic fluorescence scanner, the Molecular Dynamics Storm<sup>TM</sup> (Amersham Biosciences; Piscataway, NJ) for DiD far red fluorescence (excitation = 640 nm; emission > 650 nm). 16 bit images were saved as



TIFF files for analysis. For illustrative purposes, the images have been processed to show 3 edges. Edges were created using the threshold function and edge-detect function in Image J version 1.34i (<http://rsb.info.nih.gov/ij/>). To define the brain background, a 1 mm by 1 mm control box was drawn on the caudate putamen of the un-infused left side of the brain. The average and standard deviation of the control box were calculated, and this average was defined as the background intensity. The outermost edge (black) was thresholded to show the outer edge of the brain slice. The middle edge (red) was thresholded at a pixel intensity equal to the brain background plus 5 times the standard deviation, defined as the outer limit of detection. The inner edge (yellow) was thresholded at the half maximal intensity between the background and the maximum pixel intensity for the section. Thus, the red edge gives the farthest detectable signal from particles, and the yellow edge illustrates the area where half of the fluorescence intensity had dissipated. The sections with the highest fluorescence intensity occur near the tip of the infusion cannula, and these sections were used for confocal laser scanning microscopy.

#### *5.3.10 Fluorescence microscopy*

Confocal images were obtained to observe the *in vitro* cellular distribution of liposome uptake and the *in vivo* distribution of liposomes in brain sections. All images were taken using LaserSharpe Software on a Biorad 1024 Confocal Scanning Laser Microscope (Hercules, CA) mounted on a Nikon Diaphot 200 microscope. The Rh-PE or DiI signal was acquired in photomultiplier 1 with excitation from the 568 nm line of a krypton-argon laser. The CF-PE signal was acquired in photomultiplier 2 with excitation from the

1917

1918

1919

1920

1921

1922

1923

1924

1925

1926

1927

1928

1929

1930

1931

1932

1933

1934

1935

1936

1937

1938

1939

1940

1941

1942

1943

1944

1945



488 nm line of a krypton-argon laser. DiD signals were acquired in photomultiplier 3 with excitation from the 633 nm line of a helium-neon laser. Cells were viewed using a 60x objective at a resolution of 3 pixels per  $\mu\text{m}$ . Cell images were acquired as a stack of 10, separated by 2  $\mu\text{m}$  per image. Images were processed and given scale bars using Image J, and a z-projection was taken through the stacks using the maximum intensity (Fig. 5-2). Brain sections were imaged using a 4x objective lens at a resolution of 2.5  $\mu\text{m}$  per pixel. Within the figures, GFP is depicted in green color, DiI or Rh-PE are depicted in red color, and DiD is depicted in blue color.

In Figure 5-5 only, cells were viewed with epifluorescence microscopy performed on a Nikon Eclipse TS1000 fluorescence microscope and images were taken using a SPOT version 3.5 (Diagnostic Instruments Inc.; Kanagawa, Japan). Rh-PE signal was imaged using a 532-587 nm excitation filter, a 608-683 nm emission filter, and a 30 msec exposure. GFP signal was imaged using a 460-500 nm excitation filter, a 510-560 nm emission filter, and a 1.4 sec exposure. Images were merged using Image J.

#### **5.4 Results**

Two TATp ligands (Fig. 5-1) were successfully synthesized and mediated liposome uptake into both B16F10 and MDA-MB-435 (Fig. 5-2). Using confocal microscopy we observed that TATp modified liposomes do indeed internalize into cells; however, it is difficult to quantitatively distinguish between surface bound and internalized liposomes. For this reason, we developed a radiolabel assay that separated surface bound and internalized liposomes using washes of high salt concentration. It was confirmed by



THURSDAY

RAINY

11/11/11

11/11/11

11/11/11

11/11/11

11/11/11

11/11/11

11/11/11

11/11/11

11/11/11

11/11/11

11/11/11

11/11/11

11/11/11

11/11/11

11/11/11

11/11/11

11/11/11

11/11/11

11/11/11

11/11/11

11/11/11

11/11/11

11/11/11

11/11/11

11/11/11

11/11/11

11/11/11

11/11/11

11/11/11

11/11/11

11/11/11

11/11/11

fluorescence microscopy that high salt removes cell-surface associated fluorescence, but leaves punctate signals that appear to be liposomes entrapped in endosomal compartments. Encouraged by these results, I then modified DNA containing NLP with the TATp ligand and observed an increase for *in vitro* particle binding and transfection. Lastly, I tested TATp modified liposomes and NLP *in vivo*, utilizing a convection enhanced delivery model to normal and tumored rat brains. In the brain, the TATp ligand has strong binding capabilities, which successfully increased transfection of NLP within the tumor.

#### 5.4.1 *Properties of liposomes for radiolabel assays*

Liposomes were prepared with and without the TATp ligands by extrusion to a size of about 200 nm (Table 5-1). Because TATp has a slight amount of positive charge (8 per peptide) it was important to include a control liposome with a conventional cationic lipid, DPTAP. Most of the TATp liposomes were prepared at a mole percent ligand of 0.3% and thus have a 2.4% by mole positive charge, so 2.4% by mole DPTAP liposome were prepared as a control for charge induced liposome uptake. Both liposomes with 2.4% DPTAP and 0.3% TATp ligand were confirmed to have a similar amount of positive surface charge using zeta potential measurements (Table 5-1). Both the DSTAP control ( $2.2 \pm 0.4$  mV) and the TATp-lipid liposomes ( $1.9 \pm 0.8$  mV) had detectably higher surface charge than did neutral POPC liposomes ( $-5.7 \pm 0.6$  mV), but neither formulation was as high as a 10% DOTAP liposome ( $31.9 \pm 0.8$  mV). I concluded that the 2.4% DPTAP liposomes have a similar surface charge to the 0.3% TATp-lipid liposomes and proceeded to use these as controls for the kinetic uptake of radiolabeled liposomes.

#### 5.4.2 Validation of high salt washing

TATp-lipid successfully induced cell surface binding and internalization to MDA-MB-435 cells after a 1-hr incubation (Fig. 5-2A). Using confocal microscopy, the difference between the cell inside and outside is difficult to determine quantitatively; however, cross-sections through the cell suggested that most of the signal in Fig. 5-2A is surface bound. To investigate this further, high salt washes were used to displace the electrostatically bound TATp from cell surface proteoglycans [Tyagi *et al.* 2001]. 1M NaCl in PBS was sufficient to displace much, but not the all, of the cell associated fluorescence (Fig. 5-2B); this removable fraction is defined as “surface bound” liposomes. There was also a good amount of internalized fluorescence that could not be removed by high salt washes. This amount (Fig. 5-2B) of fluorescence is significantly higher than unmodified liposomes also washed with high salt (Fig. 5-2C). We conclude that TATp-lipid enhances liposome internalization, and we decided to develop a more quantitative method for determining the kinetics of internalization.

This high salt wash method was used to quantify the kinetics of TATp liposome uptake in conjunction with radiolabeled liposomes (Table 5-1). Before proceeding with the assay, the number of washes needed to remove all surface bound liposomes was validated (Fig. 5-2G). A 96 well plate assay was performed on B16F10 cells incubated for 1 hr with 0.3% TATp-lipid or 2.4% DPTAP liposomes. At the end of the incubation period, radioactive liposomes and media were removed. Wells were washed 0 to 4 times with 1.6 M NaCl PBS, dissolved, and counted for radioactivity. The percent of counts per well

Francisco

Ruby

1917

1918

1919

1920

1921

1922

1923

1924

1925

1926

1927

1928

1929

1930

1931

1932

1933

1934

1935

1936

1937

1938

1939

1940

1941

1942

1943

1917

that remained in the cells is plotted (Fig. 5-2G), showing that 10% of the TATp modified liposomes have bound to the cells, but only 1% of the dose was actually internalized. The amount of liposomes remaining in the cells stabilized after 3 washes for both DPTAP and TATp liposomes. It was observed that after 3 high salt washes, no additional radiolabel from either formulation was removed from the cell bound material. Thus, 3 high salt washes are sufficient to distinguish between surface bound and internalized liposomes.

Using this validated assay, a number of liposomes were prepared (Table 5-1) and assayed for their binding kinetics to a model tumor cell line, B16F10. TATp ligands appear to bind to a variety of cell types via cell surface proteoglycans, and binding is not thought to be cell type dependent (for more information see Appendix A). B16F10 cells are of mouse melanoma origin; however, due to the non-specificity of TATp ligands, trends in binding kinetics are assumed to be representative of many cell lines, including human brain tumor cells.



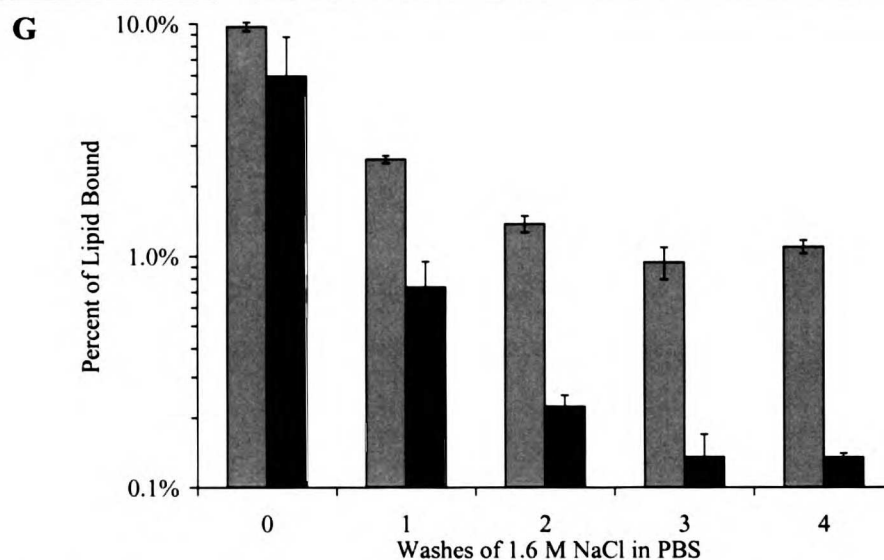
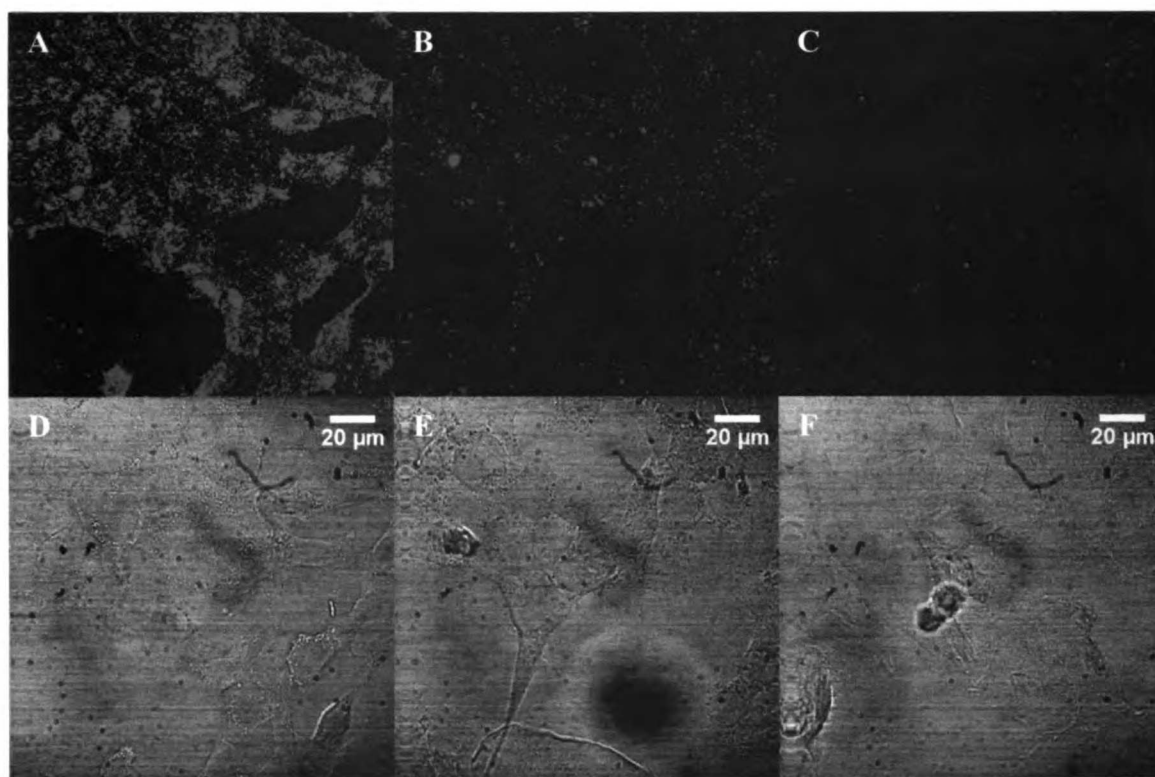


**Figure 5-2. High salt washes remove surface bound TATp liposomes.** [A-F] MDA-MB-435 cells incubated with 50  $\mu$ M lipid (0.1% CF-PE) 1 hour 37°C. (green) stained liposomes on cells, stack of 10 confocal images taken using identical settings. (gray) transmitted light image of corresponding cells. [A,D] TATp liposomes TATp-lipid:POPC:Chol:CF-PE [0.5:70:30:0.1] washed twice with PBS. [B,E] TATp liposomes TATp-lipid:POPC:Chol:CF-PE [0.5:70:30:0.1] washed twice with 1M NaCl in PBS. [C,F] control liposomes POPC:Chol:CF-PE [70:30:0.1] washed twice with 1M NaCl in PBS. [G] Fraction of liposomes remaining bound as a function of the number of high salt (1.6 M NaCl) PBS washes. 96 well assay with B16F10 cells incubated at 50  $\mu$ M lipid of  $^{125}$ I-BPE labeled liposomes for 1 hr. (gray bars) TATp liposomes TATp-lipid:POPC:Chol [0.3:60:40]. (black bars) DPTAP liposomes DPTAP:POPC:Chol [2.4:60:40]. Error bars indicate the standard error (n=3).

1945

1946

1947

1948

1949

1950

1951

1952

1953

1954

1955

1956

1957

1958

1959

1960

1961

1962

1963

1964

1965

1966

1967

1968

1969

1970

1971

1972

1973

1974

1975

1976

1977

1978

1979

1980

1981

1982

1983

1984

1985

1986

1987

1988

1989

1990

1991

1992

1993

1945 1946 1947 1948 1949 1950 1951 1952 1953 1954 1955 1956 1957 1958 1959 1960 1961 1962 1963 1964 1965 1966 1967 1968 1969 1970 1971 1972 1973 1974 1975 1976 1977 1978 1979 1980 1981 1982 1983 1984 1985 1986 1987 1988 1989 1990 1991 1992 1993

1994



#### *5.4.3 Liposome binding is dependent upon method of chemical attachment*

Two TATp lipid conjugates were prepared. One ligand consisted of a TATp directly linked to a lipid anchor on the surface of the liposome, TATp-lipid (Fig. 5-1A). The second ligand was prepared by linking the TATp peptide to the end of a flexible 2000 Da PEG linked to a phospholipid anchor. At 37 °C, both these ligands showed strong evidence of rapid binding kinetics followed by a quick internalization (Fig. 5-3A) and the amount of cell surface lipid quickly reached a steady state (Fig. 5-3B). At a density of 0.3% by mole, surface density is  $0.005 \text{ ligands} / \text{nm}^2$ , the TATp-PEG-lipid performed the best, with  $24 \pm 1\%$  of liposomes internalized after only a 120 min incubation. This uptake was steady and did not level off. The 0.3% TATp-lipid liposomes internalized only  $6 \pm 1\%$  of the liposomes in the cells. Additionally, this internalization reached a plateau at 60 min, suggesting that TATp-lipid uptake saturated the cellular capacity for uptake, which did not regenerate in this period. Both the neutral control liposome and the 2.4% DPTAP control liposome showed less than 0.5% uptake over the course of this assay. We conclude that the TATp-PEG-lipid is the most attractive ligand for sustainable rapid uptake.

Tranche

SAUCY

1/2

1/2

1/2

1/2

1/2

1/2

1/2

1/2

1/2

1/2

1/2

1/2

1/2

1/2

1/2

1/2

1/2

1/2

1/2

1/2

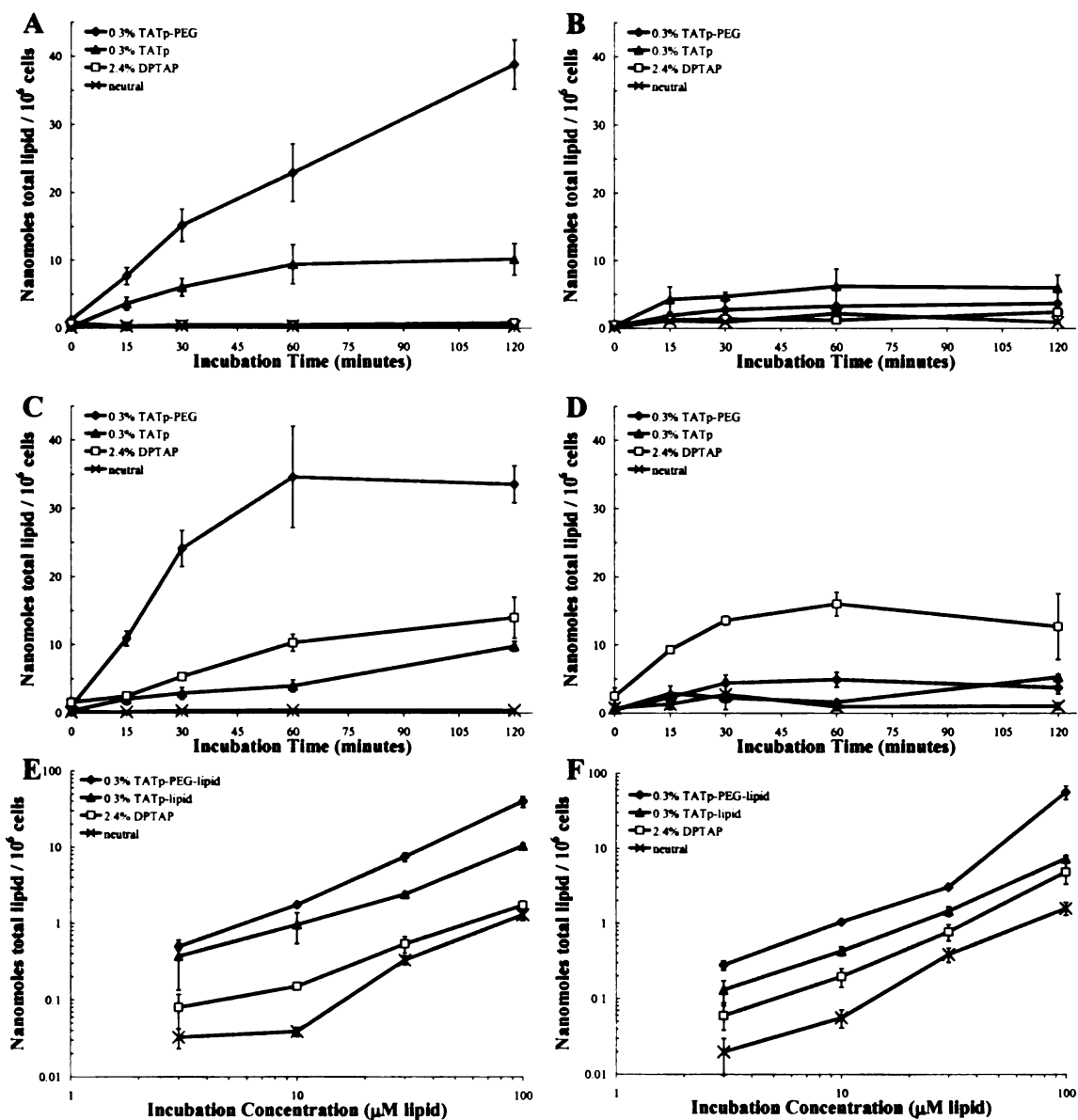


**Figure 5-3. Effect of temperature and concentration on the binding kinetics of TATp liposomes.** TATp-lipid, TATp-PEG-lipid, DPTAP, and neutral control liposomes POPC:Chol [6:4] interaction with B16F10 cells. [A-D] 30  $\mu\text{M}$  lipid concentration. [A] 37°C, internalized liposomes. [B] 37°C, surface bound liposomes. [C] 4°C, internalized liposomes. [D] 4°C, surface bound liposomes. [E-F] 60 min incubation of liposomes as a function of concentration [E] 37°C, internalized liposomes. [F] 37°C, surface bound liposomes. Data are plotted as nanomoles total lipid per  $10^6$  cells for clarity. Average recovery per well was  $85 \pm 10\%$ . Errors bars indicate the standard error of the mean ( $n=3$ ).

San Francisco

Library

1881

1882

1883

1884

1885

1886

1887

1888

1889

1890

1891

1892

1893

1894

1895

1896

1897

1898

1899

1900

1901

1902

1903

1904

1905

1906

1907

1908

1909

1910

LIBRARY

All of the kinetics experiments were performed at a 30  $\mu\text{M}$  lipid concentration. To verify that this concentration was acceptable for performing this assay, a range of concentrations were observed from 3 to 100  $\mu\text{M}$ . The results are shown in log scale to allow all of the data to be visualized simultaneously. At every concentration, all 4 liposome compositions maintain the same relationship for internalization (Fig. 5-3E) and surface binding (Fig. 5-3F). Interestingly, this range of concentration does not saturate the binding sites on the cell surface or the internalization process into the cell for the 0.3% TATp-PEG-lipid. In this range of concentrations, the amount of lipid bound to the cells is a concentration driven process that has not been saturated.

#### *5.4.4 TATp modified liposomes internalize at low temperature*

Reports in the literature conflict as to whether TATp uptake is ATP energy dependent or dependent upon some other undetermined property of the cell or both. To investigate the effect of temperature on cell association a similar kinetic experiments was performed at 4°C to determine if TATp can lead to internalization at this temperature. Figure 5-3C shows that 0.3% TATp-PEG-lipid internalizes at 4°C more rapidly than at 37°C; however, this binding attains a plateau, suggesting that the method of entry is saturated. Furthermore, uptake proceeded without causing an increase in surface binding by TATp-PEG-lipid (Fig. 5-3D). The 0.3% TATp-lipid particles have nearly the same internalization profile at 37°C and 4°C. The neutral control liposomes do not bind nor are they internalized into the cells; however, the 2.4% DPTAP liposomes *do* bind (Fig. 5-3D) and internalize (Fig. 5-3C) more significantly at 4°C than at 37°C. The fact that such a

San Francisco

Rocky

1871

1872

1873

1874

1875

1876

1877

1878

1879

1880

1881

1882

1883

1884

1885

1886

1887

1888

1889

1890

1891

1892

1893

1894

1895

1896

1897

1898

1899

1900

1871

1872

1873

1874

1875

1876

1877

1878

1879

1880

small amount of positive charge induces uptake at low temperatures is very interesting and the reason for this behavior is not known.

#### *5.4.5 Effect of TATp surface density on liposome binding*

Liposomes were prepared with surface densities of the TATp-lipid ranging from 0.03 to 1.0% (Table 5-1). As expected, the extent and rate of internalization (Fig. 5-4A) was dependent upon the surface density of ligand; however, there was very little difference in liposome binding to the cell surface (Fig. 5-4B). The 1% condition gave the most favorable binding kinetics seen for the TATp-lipid, with  $8.3 \pm 0.9\%$  of the liposomes bound after 2 hrs of incubation. The fact that surface binding was not substantially increased for the 1% TATp-lipid liposomes suggests that the increase in surface density has an effect only upon the transfer rate of liposomes from the surface to the cellular interior.

#### *5.4.6 2000 Da PEG can shield binding and uptake of TATp liposomes*

In contrast to the increased internalization rate of the 1% TATp-lipid, the presence of 5% PEG-DSPE caused a dramatic reduction in the rate of cell surface binding (Fig. 5-4D). This reduction in the surface binding of liposomes translated to less liposome internalization (Fig. 5-4C). We conclude that the presence of this particular PEG lipid can hinder the binding of TATp.

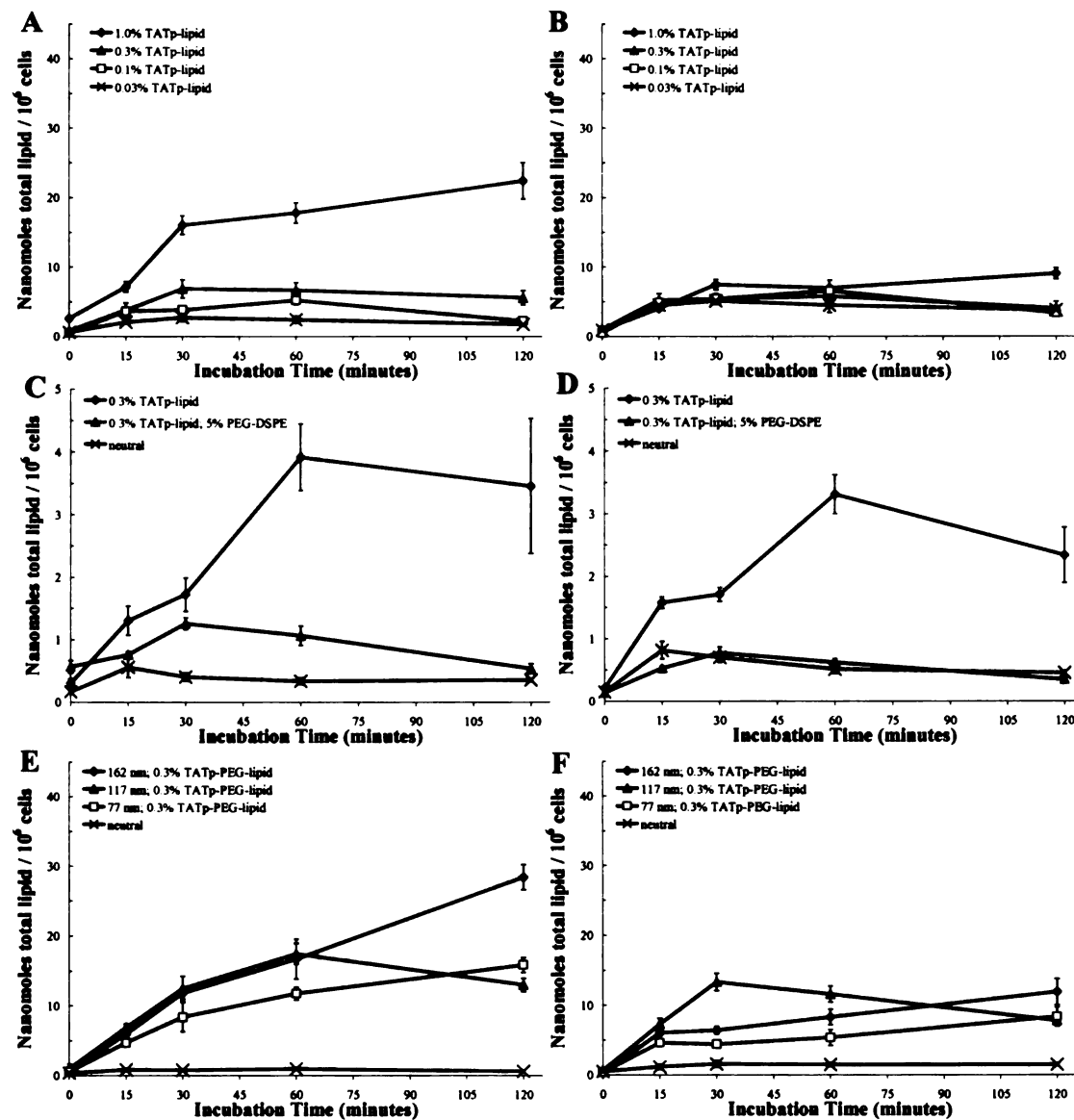


**Figure 5-4. Effect of TATp density, PEG shielding, and particle diameter on binding kinetics.** All liposomes were incubated, at 37°C, at a concentration of 30  $\mu$ M lipid on B16F10 cells. [A-B] effect of TATp density: 1.0, 0.3, 0.1, and 0.03% TATp-lipid liposomes [A] internalized liposomes. [B] surface bound liposomes. [C-D] effect of PEG shielding: 0.3% TATp-lipid with and without 5% PEG(2000)-DSPE and neutral control. [C] internalized liposomes. [D] surface bound liposomes. [E-F] effect of particle size: 77, 117, 162 nm diameter of 0.3% TATp-PEG-lipid liposomes and neutral control liposome (224 nm). [E] internalized liposomes. [F] surface bound liposomes. Errors bars indicate the standard error of the mean (n=3).



1970

1971

1972

1973

1974

1975

1976

1977

1978

1979

1980

1981

1982

1983

1984

1985

1986

1987

1988

1989

1990

1991

1992

1993

1994

1995

1996

1997

1998

1999

2000

2001

2002

2003

2004

2005

2006

2007

2008

2009

1970 1971 1972 1973 1974 1975 1976 1977 1978 1979 1980 1981 1982 1983 1984 1985 1986 1987 1988 1989 1990 1991 1992 1993 1994 1995 1996 1997 1998 1999 2000 2001 2002 2003 2004 2005 2006 2007 2008 2009

1970

#### *5.4.7 Liposome size does not affect kinetics of binding*

Liposomes with 0.3% TATp-PEG-lipid were prepared with diameters of 77 nm, 117 nm and 162 nm as measured in Table 5-1. All 3 sizes of liposomes showed similar internalization (Fig. 5-4E) and surface binding (Fig. 5-4F) to that seen previously for TATp-PEG-lipid; furthermore, there did not appear to be a relationship between particle size and binding kinetics. A larger particle has many more TATp ligands per particle and potential for higher avidity binding; however, this result suggests that only the by-mole-percent surface density of TATp ligand moderates the extent of cell internalization.

#### *5.4.8 DNA NLP bind and transfect more efficiently after TATp modification*

TATp-PEG-lipid was the strongest binding reagent of the 2 ligands synthesized. Additionally, the PEG-lipid portion of this ligand allows for the formation of micelles. PEG micelles can insert into lipid bilayers above their phase transition temperature. For these reasons, the TATp-PEG-lipid was pursued for the purposes of modifying bioresponsive DNA containing nanolipoparticles (NLP) to enhance transfection. In Figure 5-5, the micelle insertion method consisted of incubating 0.5% by mole lipid of the TATp-PEG-lipid in the presence of RH-PE labeled pH sensitive NLP for 5 hrs at 20°C. To confirm the presence of TATp ligand, I assayed the formulation by passing it down a cation exchange column, CM-25 Sephadex. Unmodified NLP elute in the void volume in the presence of 150 mM NaCl and 5 mM Tris, pH 8.5, and the addition of 1M NaCl did not elute additional fluorescence (Fig. 5-5A). In contrast, TATp modified NLP are primarily retained by the resin and do not wash until the addition of 1M NaCl.

Handwritten text at the top left of the page.

Handwritten text below the top left.

Handwritten text in the upper left section, possibly including a name or title.

Handwritten text in the middle left section.

Handwritten text in the lower middle left section.

Handwritten text in the lower middle left section.

Handwritten text in the lower middle left section.

Handwritten text in the lower middle left section.

Handwritten text in the lower middle left section.

Handwritten text in the lower middle left section.

Handwritten text in the lower middle left section.

Handwritten text in the lower middle left section.

Handwritten text in the lower middle left section.

Handwritten text in the lower middle left section.

Handwritten text in the lower middle left section.

Handwritten text in the lower middle left section.

Handwritten text in the lower middle left section.

Handwritten text in the lower middle left section.

Handwritten text in the lower middle left section.

Handwritten text in the lower middle left section.

Handwritten text in the lower middle left section.

Handwritten text in the lower middle left section.

Handwritten text in the lower middle left section.

Handwritten text in the lower middle left section.

Vertical handwritten text on the left side of the page.

Handwritten text at the bottom left corner.

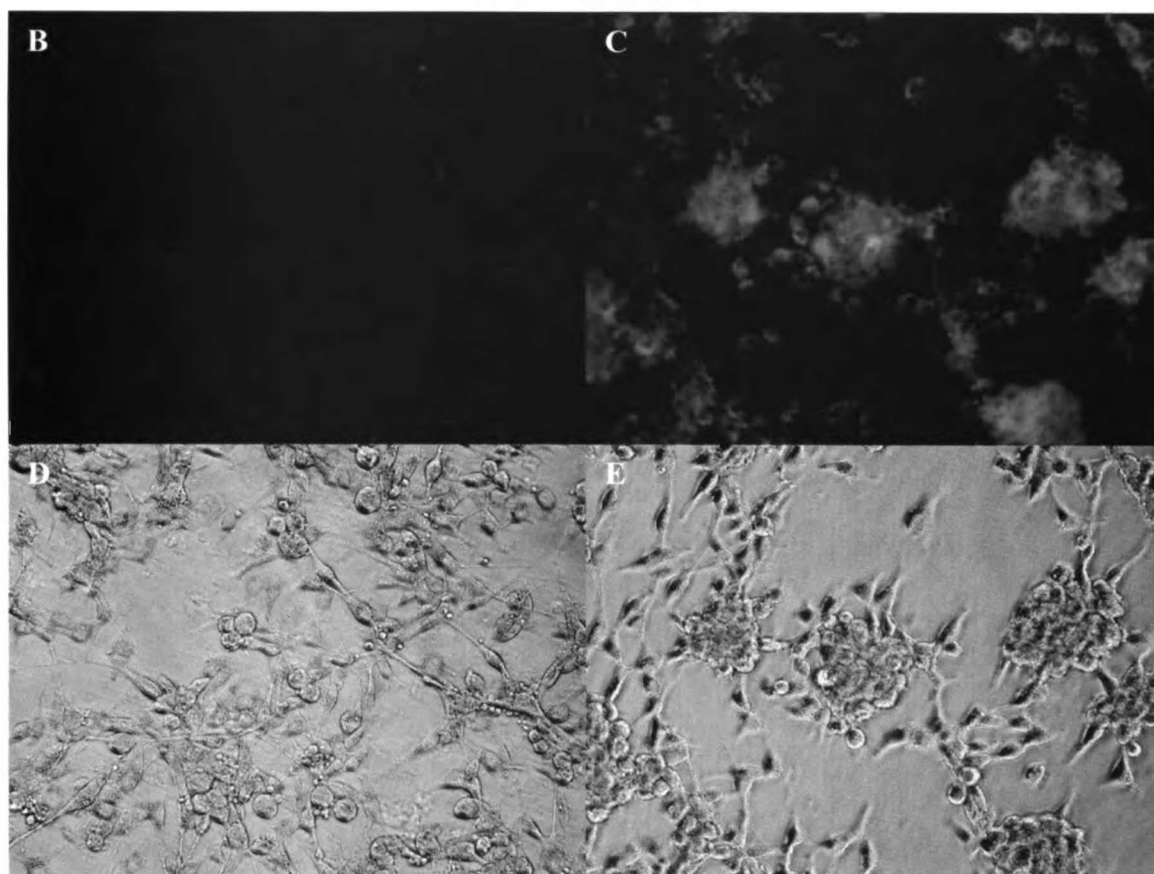
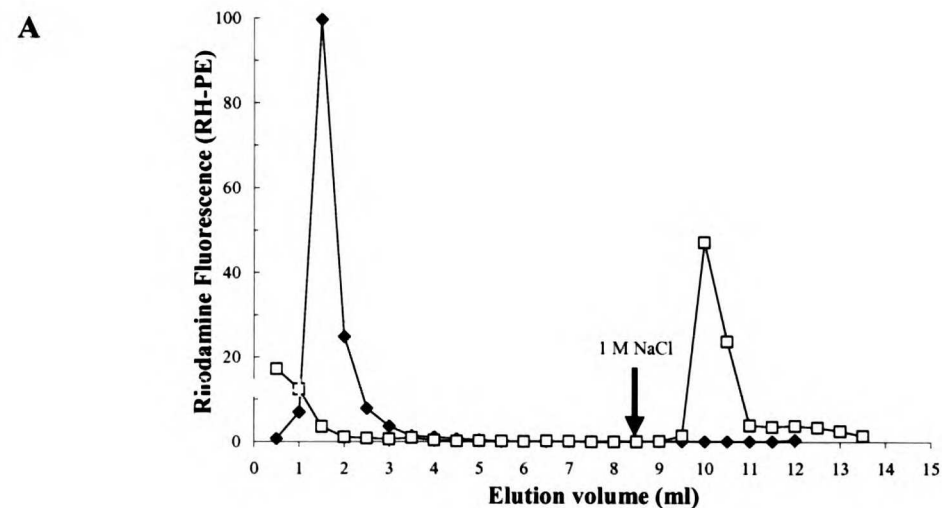


**Figure 5-5. TATp-PEG-lipid enhances particle binding and transfection.** pH sensitive DNA NLP (POD:DOTAP:DOPE:Rh-PE[20:12:68:0.1]) [A] 0.5% by mol lipid TATp-PEG-lipid was inserted by micelle transfer and confirmed by cation exchange chromatography. Unmodified NLP (diamonds) do not adhere to the resin. TATp NLP (squares) are retained on the column and can be washed out by 1M NaCl. [B-E] U87-MG cells incubated 24 hrs with 2  $\mu$ g DNA / 24 well plate. [B] Unmodified RH-PE labeled NLP (red) bound only slightly to cells, but showed no transfected cells (green). [C] Using the same exposure settings for Rh-PE and GFP, TATp NLP bind strongly to cells and show GFP transfection (green). [D,E] phase contrast images of [B,C] respectively.

1887  
LIBRARY  
ST. JOHN'S  
UNIVERSITY  
NEW YORK  
1887

NLP were prepared with a GFP reporter plasmid and incubated with human glioblastoma cells, U87-MG. Incubation was at 2  $\mu$ g DNA / 24 well for 24 hrs either with or without 0.5% TATp-PEG-lipid modification and imaged for Rh-PE (red) and GFP (green). These 2 colors have been merged in each of the images in Fig. 5-5A,B. The cells incubated with unmodified NLP showed dramatically less red staining (Fig. 5-5B) than cells with the TATp NLP (Fig. 5-5C). This is consistent with TATp studies of fluorescent and radiolabeled liposomes, already discussed. The concentration of DNA used was insufficient to observe strong GFP staining from the unmodified NLP; however, using the same GFP exposure settings, it was easy to observe brightly stained GFP cells (Fig. 5-5C). This result is likely because only a small fraction of the unmodified NLP associates with the cells, whereas the 0.5% TATp modified NLP may exceed 25% cell association.

#### 5.4.9 Convection enhanced delivery of TATp nanoparticles to the rat brain

Having shown that the TATp-PEG-lipid greatly enhances binding and transfection *in vitro*, we moved to an *in vivo* model to look for a biological effect using convection enhanced delivery. Empty liposomes were prepared and co-infused into normal rat brain (Fig. 5-6[A-D]). Fig. 5-6A shows a macroscopic image of the axial brain section illustrating the particle distribution for a 0.3% TATp-PEG-lipid liposome (TATp-PEG-lipid:POPC:Chol:DiD [0.3:60:40:0.1], blue,  $103.5 \pm 0.6$  nm) and this same particle distribution is imaged at higher magnification in Fig. 5-6B. For comparison, the 0.3% TATp-PEG-lipid was co-infused with a 0.3% TATp-lipid liposome (TATp-lipid:POPC:Chol:DiI [0.3:60:40:0.1], red,  $100.5 \pm 0.7$  nm). This observation was representative of 3 animals. The TATp ligand linked by the PEG linker exhibited strong

1850  
1851  
1852  
1853  
1854  
1855  
1856  
1857  
1858  
1859  
1860  
1861  
1862  
1863  
1864  
1865  
1866  
1867  
1868  
1869  
1870  
1871  
1872  
1873  
1874  
1875  
1876  
1877  
1878  
1879  
1880  
1881  
1882  
1883  
1884  
1885  
1886  
1887  
1888  
1889  
1890  
1891  
1892  
1893  
1894  
1895  
1896  
1897  
1898  
1899  
1900

binding and retained the particles near the infusion cannula, whereas the weak binding TATp-lipid particles perfused outward through the tissue, much like a neutral liposome (Fig. 5-6D). Similar to *in vitro* assays, the TATp-PEG-lipid appears to have much stronger binding affinity than the TATp-lipid *in vivo*.

Bioresponsive NLP, prepared with a reducible disulfide cationic lipid, were also modified with 0.3% TATp-PEG-lipid. The encapsulated DNA encoded for a GFP reporter gene. A fraction of these particles was modified with 0.3% by mole TATp-PEG-lipid using the micelle transfer method, 1 hr incubation at 60°C. NLP were infused at a DNA concentration of 0.22  $\mu\text{g}/\mu\text{L}$ . 24 hrs after the infusion, animals were sacrificed and brains were imaged for tumor distribution and GFP fluorescence. In Fig. 5-6[E-H], the unmodified NLP (flowed partially through the tumor and then traversed around the periphery of the tumor. Fluorescence imaging showed few particles were retained immediately at the site of infusion (Fig. 5-6F). GFP imaging showed the presence of some transfected cells within the tumor (Fig. 5-6G). These observations are representative of 3 animals where the NLP were in contact with tumor.

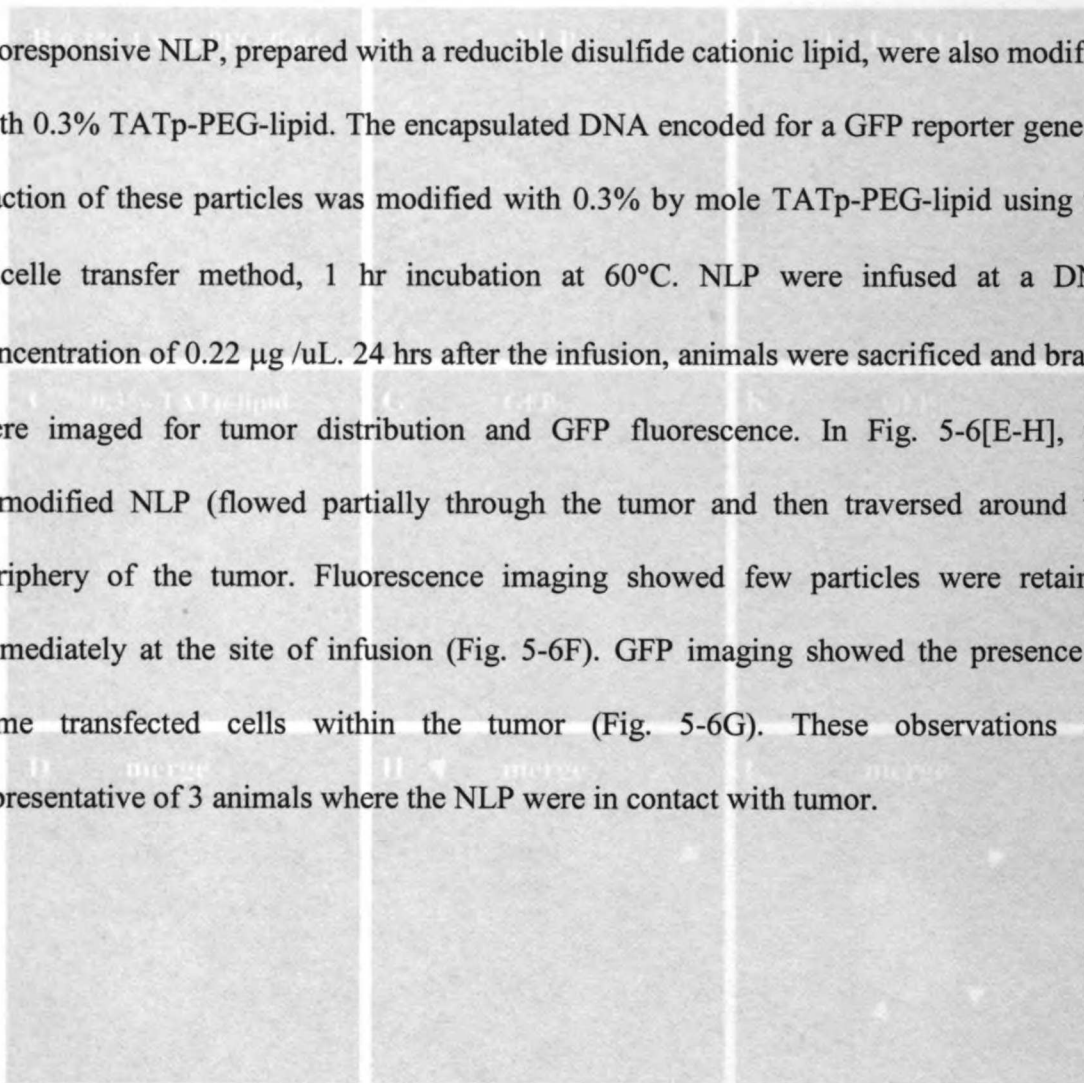
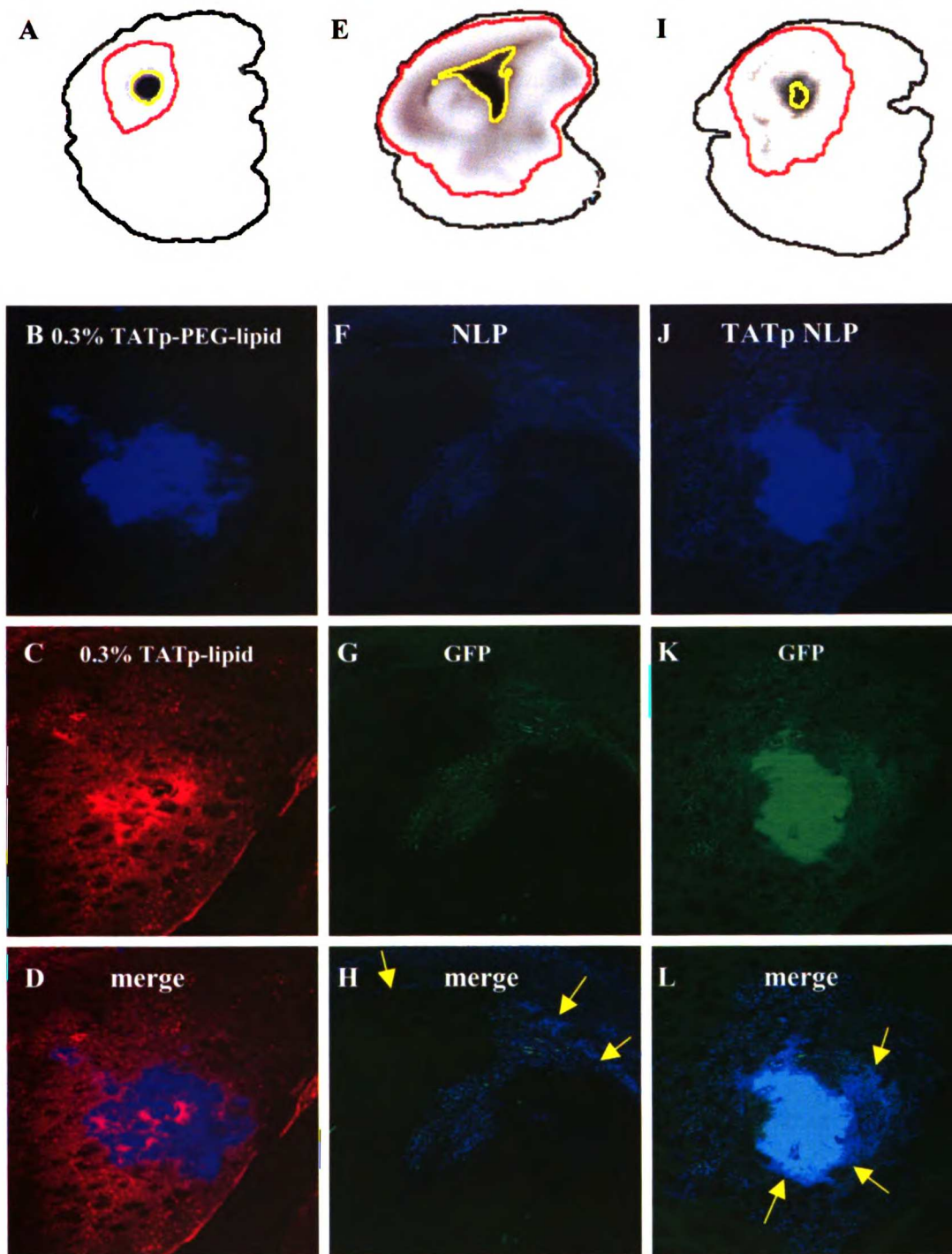


Figure 5-6. Convection enhanced delivery of TATp modified particles to the rat brain. [top row] 2x2 cm DiD (blue signal) image, outer limit of detection (red edge), half maximal intensity (yellow edge). [bottom three rows] 2.5x2.5 mm confocal images centered on the infusion. [A-D] Co-infusion of 0.3% TATp-PEG-lipid (blue) and 0.3% TATp-lipid (red) into rat brain. [E-H] infusion of NLP (blue) with 6  $\mu\text{g}$  GFP plasmid (green) into U87-MG tumor. [I-L] infusion of 0.3% TATp-PEG-lipid modified NLP (blue) with 6  $\mu\text{g}$  GFP plasmid (green) into U87-MG tumor. Yellow arrows indicate the tumor border. Images are representative of 3 animals.





**Figure 5-6. Convection enhanced delivery of TATp modified particles to the rat brain.** [top row] 2x2 cm DiD (blue signal) image, outer limit of detection (red edge), half maximal intensity (yellow edge). [bottom three rows] 2.5x2.5 mm confocal images centered on the infusion. [A-D] Co-infusion of 0.3% TATp-PEG-lipid (blue) and 0.3% TATp-lipid (red) into rat brain. [E-H] infusion of NLP (blue) with 6  $\mu$ g GFP plasmid (green) into U87-MG tumor. [I-L] infusion of 0.3% TATp-PEG-lipid modified NLP (blue) with 6  $\mu$ g GFP plasmid (green) into U87-MG tumor. Yellow arrows indicate the tumor border. Images are representative of 3 animals.



The TATp-PEG-lipid modified NLP behaved quite differently (Fig. 5-6[I-L]) than the unmodified NLP. The TATp ligand allowed the distribution of detectable levels of fluorescence throughout the tumor (Fig. 5-6I), but was also able to induce strong binding near the tip of the infusion cannula. When the cannula was placed in or next to the tumor, strong binding within a fraction of the tumor itself resulted (Fig. 5-6J). This binding is similar to that for TATp-PEG-lipid liposomes in Fig. 5-6B and in complete contrast with the lack of strong binding in Fig. 5-6F. This strong binding area is associated with a strong GFP signal (Fig. 5-6K), and this was observed in 4 of 4 animals. We conclude that TATp modification is beneficial for CED transfection and may aid in keeping the particles from distributing widely outside the tumor and into normal brain.

## 5.5 Discussion

Intracellular delivery of non-transported therapeutic agents has traditionally been thought possible only for low molecular weight (<500 Da) hydrophobic molecules. Higher molecular weight agents including oligonucleotides, proteins, DNA, liposomes and nanoparticles do not readily enter the cytoplasm. The human immunodeficiency virus (HIV) trans acting transcriptional activator (TAT) protein enters the cytosol by way of an 11 amino acid cationic peptide (TATp). When this cationic sequence is attached to a variety of small pharmacological agents including paramagnetic ions [Polyakov *et al.* 2000, Bhorade *et al.* 2000] and proteins [Stein *et al.* 1999, Schwarze *et al.* 1999, Mi *et al.* 2000, Xia *et al.* 2001], they are delivered into cells. The size limitations for cargo delivered by a single TATp are currently undetermined, but multiple TATp attached to polymers, nanoparticles, liposomes, and phage mediate cell internalization.

Torchilin and coworkers [2001] have shown that TATp (YGRKKRRQRRR) attached via a PEG (MW = 3.0 kDa) polymer to a 200 nm diameter liposome results in improved binding and internalization. These results have quantitatively demonstrated the claim that TATp-PEG-lipid is an excellent binding ligand; however, these data also show that TATp linked directly to the surface of a liposome significantly induces cellular uptake (Fig. 5-3A), in contrast to previous reports [Torchilin *et al.* 2001]. This may be due to the chemistry of attachment, which is an amide bond between the primary amines either at the nitrogen terminus or the lysine sidechains. This uncontrolled chemistry means that a significant fraction of their TATp ligand may be conjugated in the middle of the peptide; regardless, with 100 to 500 PEG-linked peptides per liposome, these particles were internalized into cytoplasmic vesicles within an hour [Torchilin *et al.* 2001].

Torchilin and coworkers [2001] also claim that PEG lipids can be used to shield TATp binding, and this was confirmed in the above kinetics studies (Fig. 5-4C). 5% PEG-DSPE was successfully able to shield the binding of 0.3% TATp-lipid. There are 2 possible reasons for this effect: the PEG provides a steric hindrance that prevents binding or the negatively charged (5% by mol) phospholipid anchor for the PEG is binding the 2.4% positive charge on the TATp ligand. We are unable to distinguish between these possibilities; however, the ability to shield the effect of TATp ligands by either method could prove useful. In the case that PEG provides steric shielding, a pH sensitive PEG lipid (POD) could be employed to preferentially shield the TATp binding activity until the liposome is in position near a target cell.

UNCLASSIFIED  
CONFIDENTIAL  
SECRET



CONFIDENTIAL

CONFIDENTIAL  
SECRET  
UNCLASSIFIED



Tseng and coworkers [2002] have studied the kinetics of TATp modified liposomes with various numbers of peptides on the particle surface. They conjugated the TATp sequence (CYGRKKRRQRRRPPQ) to a PEG (MW = 3.4 kD) phosphatidylethanolamine. The chemistry of attachment was to the nitrogen terminal cysteine via a stable thio ether bond. The TATp-PEG-lipid was inserted into preformed phosphatidylcholine: cholesterol (6:4) 100 nm liposomes using a micelle insertion method. Greater than 90% insertion of TATp-PEG-lipid occurred in all preparations. Liposomes containing a pH sensitive dye, 8-hydroxypyrene-1,3,6-trisulfonic acid, were incubated with cells, and fluorescence was assayed using FACS. Tseng and coworkers [2002] showed that increasing numbers of peptides per particle raised the fluorescence substantially. Internalization was evident with above 5 peptides per particle, surface density is 0.0002 ligands / nm<sup>2</sup>. This increase in fluorescence began to saturate by 100 peptides per particle, surface density is 0.003 ligands / nm<sup>2</sup>, for HTB-9 cells but continued to increase linearly for A431 cells. The fact that a pH sensitive dye greatly increases in fluorescence upon binding strongly suggests that TATp labeled liposomes are entrapped separate from the cytoplasm, in a low pH compartment.

The method of Tseng and coworkers [2002] for using micelle insertion of the ligand has been adopted in these studies for the ability to enhance cell binding of DNA containing NLP. Using a mild cation exchange column, it was possible to monitor the insertion of TATp-PEG-lipid into preformed NLP (Fig. 5-5A). The modification of NLP by TATp greatly increased the binding properties for the particle both *in vitro* (Fig. 5-5C) and *in*

*vivo* (Fig. 5-6J). In fact, the TATp ligand induced so much binding that the particles appear to be retained near the site of the cannula, similar to the effect of 10% positive charged liposomes in Chapter 3. As expected, an increase in binding also increases the level of transfection. Clearly, these CED studies show a trade-off between transfection and distribution. Future studies should attempt to solve this problem by using a cleavable PEG lipid shield. For example, during the distribution phase the TATp ligand could be blocked by POD, and after several hours, the POD would hydrolyze enough to expose the TATp ligands. This approach could enable both distribution and efficient transfection.

A point of contention in the literature is that TATp-PEG-lipids internalize liposomes even below 4°C; however, it has been suggested that this is an artifact of fixation [Fretz *et al.* 2004]. In this radiolabel binding study there is no use of fixative, and thus the data confirmed that TATp-PEG-lipids *do indeed* contribute to particle internalization at 4°C. The relevance of this finding is uncertain, because the control 2.4% DPTAP liposomes also dramatically increased their binding and internalization at 4°C. The possibility exists that both DPTAP and TATp lipids internalize at low temperatures by undergoing a phase change, or raft formation, that brings together many cationic moieties. This event, coupled with other cellular mechanisms, may enable particle uptake even at low temperatures where endosomal fusion is prevented. Indeed the apparent uptake by the TATp liposomes may not be mediated by the same forces at 37°C and 4°C.

This study has expanded on previous work in three ways: optimized a radiolabel assay that enables quantitative molar assessment of binding vs. internalization; characterized a

structure activity relationship between 2 peptide lipid conjugates covalently bound only at the N terminus; and as shown that this TATp can influence *in vivo* particle distribution and enhance transfection when administered by CED. These results suggest that TATp is an effective binding ligand and could have important therapeutic applications for the development of non-viral DNA delivery. Additionally, for the purposes of liposomal drug delivery, the presence of TATp lipids enables fine-tuning of the binding parameters required for CED to brain tumors.

## **5.6 Conclusions**

A peptide (TATp) that mediates strong binding and cell internalization was synthesized and conjugated directly to a lipid or to a PEG(2000 Da) lipid. TATp was confirmed to induce liposome binding and internalization using both fluorescence microscopy and a quantitative radiolabel assay. TATp internalization,  $24 \pm 1\%$  of the lipid dose over 2 hrs, was found to be greater than a control liposome with similar cationic charge. Uptake was enhanced by having a PEG linker between the peptide and lipid. Alternatively, binding was reduced by 5% of a PEG (2000 Da) phosphatidylethanolamine. TATp also enhanced binding and transfection of DNA containing particles *in vitro* and *in vivo*. Data also showed that TATp may provide an important method for modifying the cell binding properties of particles delivered by convection enhanced delivery for the purpose of treating brain tumors.



## APPENDIX A

### Review: HIV TAT Protein Transduction Domain Mediated Cell Binding and Intracellular Delivery of Nanoparticles

#### A.1 Abstract

Intracellular delivery of non-transported therapeutic agents has traditionally been thought possible only for low molecular weight (<500 Da) hydrophobic molecules. Higher molecular weight agents, including oligonucleotides, proteins, DNA, liposomes and nanoparticles do not readily enter the cytoplasm; however, the human immunodeficiency virus (HIV) trans acting transcriptional activator (TAT) protein enters the cytosol by way of an 11 amino acid cationic peptide (TATp). When this cationic sequence is attached to a variety of small pharmacological agents including paramagnetic ions [Polyakov *et al.* 2000, Bhorade *et al.* 2000] and proteins [Stein *et al.* 1999, Schwarze *et al.* 1999, Mi *et al.* 2000, Xia *et al.* 2001], they are delivered into cells. Further, TATp modification of large cargo, such as proteins, polymers, and nanoparticles, may enable them to internalize into cells as well. The size limitations for cargo delivered by a single TATp are currently undetermined, but multiple TATp attached to polymers, nanoparticles, liposomes, and phage mediate their internalization. This latter process appears to follow an endocytotic or potocytic pathway and does not directly transfer cargo into the cytoplasm of the cell. Here I review recent publications in which multiple TATp have been attached and resulted in successful intracellular delivery of nanoparticles.

## A.2 Introduction

Trans acting transcriptional activator (TAT) is a protein produced and secreted by HIV infected cells. TAT then enters the cytosol of adjacent cells, traffics to the nucleus, and directly participates in transcriptional regulation. The mechanism of TAT protein internalization was first investigated by Mann and Frankel [1991] over a decade ago. They concluded that a cationic peptide sequence (TATp) with 8 positively charged side chains (RKKRRQRRR) binds nonspecifically to greater than  $10^7$  binding sites per cell and is required for transactivation activity. The peptide is short and highly charged, suggesting that it functions through an electrostatic mechanism and not via a specific protein-protein interface. The researchers hypothesized that TATp fusion proteins could be tools for delivering active protein to the cytosol and nucleus. This discovery was not widely applied to enhance the uptake of other cargo until the late 1990's. The upsurge in activity in this field is reviewed in a number of recent articles written on TATp and TAT-like sequences and their putative uses [Schwarze *et al.* 2000, Morris *et al.* 2000]. I focus here on reports in which multiple TATp sequences are attached to a nanoparticle (Table A-1).

1887

RAILY

1887  
S

1887

1887

1887

1887

1887

1887

1887

1887

1887

1887

1887

1887

1887

1887

1887

1887

1887

1887

1887

1887

1887

1887

1887

1887

1887

1887

1887

1887

1887

1887

1887

1887

1887

1887

1887

1887

1887

1887

1887

**Table A-1: Comparison of multi-valent cationic peptide modifications of nanoparticles**

Peptide Sequence*	Particle	Attachment	Size	Peptides/ particle	Transfect	Reference
acetyl-KETW <sup>W</sup> ETW <sup>W</sup> TEW <sup>W</sup> SQPKKKRKV- cysteamine	Peptide-GFP	hydrophobic complex	25-30 (kD)	12-14	n.a.**	Morris <i>et al.</i> 2001
RKKRRQRRRK[biotin] <u>C</u> -amide	PEG-lysine co-polymer	disulfide	27 (kD)	8	n.a.	Huang <i>et al.</i> 1998
GRKKRRQRRRPPQC-amide	Peptide-DNA	electrostatic complex	n.r.***	n.a.	yes	Sandgren <i>et al.</i> 2002
<u>GGGGYGRKKRRQRRR</u>	SCK****	amide	13 (nm)	n.r.	n.a.	Liu <i>et al.</i> 2001
<u>GGCGRKKRRQRRR</u> GYK[FITC]-amide	CLIO*****	disulfide	41 (nm)	7	n.a.	Josephson <i>et al.</i> 1999
GRKKRRQRRRGYK[FITC] <u>C</u> -amide	CLIO	disulfide	45 (nm)	1-15	n.a.	Lewin <i>et al.</i> 2000, Zhao <i>et al.</i> 2002
GRKKRRQRRRGYK[FITC] <u>C</u> -amide	CLIO	thio ether	65 (nm)	10	n.a.	Dodd <i>et al.</i> 2001, Wunderbaldinger <i>et al.</i> 2002
<u>YGRKKRRQRRR</u>	liposome	amide PEG (MW=3.0 kDa)	200 (nm)	100-500	yes	Torchilin <i>et al.</i> 2001, Torchilin 2002
<u>CYGRKKRRQRRR</u> PPQ	liposome	thio ether PEG (MW=3.4 kDa)	100 (nm)	5-100	n.a.	Tseng <i>et al.</i> 2002
MLGISYGRKKRRQRRRPPPPQT-D protein	λ phage	fusion coat protein D	55 (nm)	420	yes	Eguchi <i>et al.</i> 2001

\* If applicable, residue of covalent linkage to nanoparticle is underlined

\*\* not applicable

\*\*\* not reported

\*\*\*\* shell cross linked

\*\*\*\*\* cross linked iron oxide

### **A.3 Other peptides with properties similar to TATp**

It is worth noting that the TAT peptide shares internalization characteristics with other short cationic polymers, including poly arginine, the antennapedia peptide penetratin, and the herpes virus peptide VP22. These peptides are all cationic, rich in arginine or lysine. In fact, poly arginine has been shown similarly effective at delivering cargo [Futaki *et al.* 2002, Wender *et al.* 2000, Suzuki *et al.* 2002]. These peptides still function if their sequence is reversed or if the d-isomer amino acids are used. Wender and coworkers [2000] report similar activity using a peptoid backbone instead of the natural peptide backbone. The peptides internalize by a common pathway that is reported to function at 4°C, where endosomal vesicles cannot fuse [Derossi *et al.* 1996, Vives *et al.* 1997]; however, this may be an artifact of fixation [Richard *et al.* 2003, Lundberg and Johansson 2001,2002, Leifert *et al.* 2002].

### **A.4 Promising aspects of TATp research**

Most importantly, these peptides can be used to ferry cargo across the membrane into the cell and possibly into the cytosol. Cell penetrating peptides potentially offer a mechanism to bind and internalize large molecules and nanoparticles rapidly into cells *in vivo*. This would greatly benefit the fields of protein and gene delivery by allowing passage to targets within the cytoplasm and nucleus [Schwarze *et al.* 2000, Morris *et al.* 2000]. These peptides may also divert the cargo to an alternative trafficking pathway and permit the particle to avoid the lysosomal route, hence exposure to degrading enzymes.

## A.5 Mechanism

Despite the proliferation of new applications for these peptides, the mechanism by which they cross cell membrane remains uncertain. TATp, antennapedia, poly arginine, VP22, and similar cationic peptides convey similar internalization properties when attached to cargo due to their high linear density of flexible, cationic side chains. The TAT protein interacts strongly with heparin oligosaccharides [Rusnati *et al.* 1997, 1999]. In fact heparan sulfated proteoglycans (HSPG) are critical for TATp internalization [Chang *et al.* 1997, Watson *et al.* 1999, Tyagi *et al.* 2001]. Negatively charged lipids [Derossi *et al.* 1996] and sialic acids are other possible cell-surface attachment sites for TATp. Thus, TATp binds its cargo nonspecifically to negatively charged cell-surface molecules via electrostatic forces. This interaction of TATp with negatively charged heparan is similar to what occurs when certain viruses bind to mammalian cells [Shukla *et al.* 2001]. Cationic polymers and cationic liposomes also interact with negatively charged glycosaminoglycans [Barron and Szoka 1999]. Thus, the mechanism of TATp internalization should be considered in the larger context of the biology of glycosaminoglycans.

Three modes of internalization have been proposed for cationic peptide mediated internalization: endocytosis [Mann and Frankel 1991], potocytosis [Eguchi *et al.* 2001], and direct membrane destabilization [Derossi *et al.* 1996]. Endocytosis and potocytosis are both mechanisms for entrapping surface bound particles within a cellular membrane, whereas membrane destabilization would allow direct access to the cytosol.

The initial mechanistic study of TAT protein internalization by Mann and Frankel [1991] suggested adsorptive endocytosis. That is, TAT binds to the cell-surface and is internalized into a clathrin-coated pit. Subsequent publications reported that TATp does not internalize by classical endocytotic mechanisms because it has the ability to internalize at 4°C or in the presence of inhibitors of endocytosis [Vives *et al.* 1997, Suzuki *et al.* 2002]. Recent reports indicate that data collected showing rapid uptake of TATp were obtained under fixation conditions that permeabilize the cell membrane sufficiently to allow nuclear localization of TATp and VP22 [Lundberg *et al.* 2001,2002 Leifert *et al.* 2002, Richard *et al.* 2003]. Thus, one cannot consider the rapid uptake of TATp at 4°C to be convincingly established.

In an effort to explain rapid TATp internalization at low temperatures, potocytosis was investigated [Eguchi *et al.* 2001]. Potocytosis is an alternative internalization method, similar to endocytosis. Unlike endocytosis, potocytosis internalizes surface bound cholesterol rich membrane into pits coated with caveolin proteins. Lending credibility to this hypothesis, the addition of molecular blockers of potocytosis reduced the internalization of TATp coated phage by about 50% [Eguchi *et al.* 2001].

Alternative explanations of the rapid antennapedia peptide internalization suggested that the antennapedia peptide interacts directly with negatively charged lipids on the outer surface of the cell to form inverted micelles [Derossi *et al.* 1996]. These inverted micelles then open inward and allow the cationic peptide and cargo direct access to the cytosol; however, this mechanism does not easily explain the observation that TATp mediated

internalization is saturable [Mi *et al.* 2000]. Additionally, evidence of contents leakage induced by TATp from model phospholipid vesicles has not been reported.

The size of the attached cargo has a very significant effect upon the mechanism of internalization. Silhol and coworkers [2002] showed that TATp carrying a low-molecular weight fluorescent molecule are not dependent upon HSPG for internalization and uptake is not blocked at low temperatures. Uptake of the low molecular weight peptides are however, easily saturated at about 1  $\mu$ M. When TATp is attached to the green fluorescent protein (GFP) the results are strikingly different; GFP-TATp uptake exhibits strong temperature dependence and strong HSPG dependence. Without HSPG or at low temperatures, internalization is essentially abolished. Clearly the mechanism of internalization for the peptide may be very different than for proteins and larger particles.

In light of recently reported fixation artifacts, it seems most likely that the mechanism of TATp mediated internalization of nanoparticulates is via adsorptive endocytosis. Individual TATp and similar cationic peptides have both the flexibility to penetrate into HSPG and a sufficient positive charge density to bind with moderate affinity. Multi-valent TATp particles will therefore exhibit an even higher avidity for the cell-surface. Surface binding becomes saturated as the HSPG are filled. Surface bound particles will then be internalized into a low pH compartment [Tseng *et al.* 2002]. At this point, some undetermined mechanism may allow for escape to the cytosol. Thus, the most recent evidence suggests that TATp modified particles bind to the cell-surface through negatively charged cell-surface molecules, principally heparan sulfate and possibly sialic



acid. Subsequent to binding they are internalized either through endocytosis, macropinocytosis, or via caveolae.

#### *A.6.1 Applications: Polymers*

Huang and coworkers [1998] synthesized a 12 repeat block copolymer of PEG and lysine (MW = 26.9 kDa, 2.198 kDa/repeat). Lysine residues were incorporated as attachment points for peptides. TATp (RKKRRQRRRK[Biotin]C-amide) were attached at the cysteine via a disulfide linkage to activated lysines on the PEG-lysine copolymer. The carboxy terminal lysine sidechain was conjugated to biotin. The disulfide linkage was designed to break upon exposure to the reducing cytoplasmic environment. The resulting macromolecules had 8 TATp branches per macromolecule. The macromolecule was stable under non-reducing conditions at physiological pH, but the addition of 3 mM glutathione released the TATp within minutes. Peptide delivery was assessed by inhibition of normal TAT transactivation as shown by the chloramphenicol acetyltransferase assay (CAT). In the CAT assay, cells are stably transfected with a CAT reporter gene under control of the HIV trans activator response element (TAR). Subsequently, the cells are transfected with a plasmid that expresses a functional TAT protein that up-regulates TAR elements. The peptide TATp binds the TAR element, but does not induce transcription. Thus, TATp competes with TAT protein and reduces CAT reporter expression. At similar peptide concentrations, both free TATp and the multi-valent TATp macromolecule significantly reduced CAT activity. This indicates that when initially bound to the polymer backbone, TATp successfully internalizes, traffics to the

nucleus, and reduces transactivation; however, it remains unclear whether TATp detaches from the PEG-lysine copolymer before or after internalization.

#### *A.6.2 Applications: Complexes*

Because TATp is highly cationic, it can condense anionic polymers, such as heparan sulfate and DNA, into electrostatic stabilized complexes. Sandgren and coworkers [2002] created such complexes by mixing poly-anion with TATp (GRKKRRQRRRPPQC-amide) poly-cation using a 1:1 w/w ratio. For heparan sulfate this corresponded to a 1.4 : 1 positive to negative charge ratio. Both TATp and poly-anion were labeled with fluorophores. The labeled complexes were incubated with cells and tracked by fluorescence microscopy. Both heparan sulfate-TATp and DNA-TATp complexes strongly bound on the cell-surface in a heparan sulfate dependent manner. Binding and internalization were abolished in a proteoglycan deficient cell line. Chlorate treatment to prevent sulfation also abolished uptake. Treatment with chondroitin ABC lyase or heparitinase enzymes significantly reduced, but did not eliminate binding and internalization. By fluorescence microscopy, the heparan sulfate – TATp complex internalized to the cells and at 24 hrs heparan sulfate could be seen in the nucleus; however, the fluorescence labeled TATp was retained in low pH vesicles that stained with lysotracker. At no time did the TATp escape from the low pH compartments and it was presumably degraded. Interestingly, this is in contrast to the observation that free TATp localizes to the nucleus. This suggests that free TATp and multivalent particulate TATp internalize by different mechanisms.



Morris and coworkers [2001] synthesized a carboxy terminal cationic peptide with a nitrogen terminal hydrophobic end (acetyl-KETWWETWWTEWSQPKKKRKV - Cysteamine). The cationic portion of this peptide was not derived from TAT, but instead from the cationic SV-40 nuclear localization sequence. The peptide has a hydrophobic sequence that associates with protein surfaces, presumably onto hydrophobic patches. The peptide was mixed with green fluorescent protein at a ratio of 30 to 1 and formed a complex consisting of 12-14 peptides per protein as assessed by gel filtration chromatography. The complexes delivered both fluorescence labeled peptide and GFP into up to 90% of the cells as indicated by fluorescence microscopy. Incubation in the presence of serum or at 4 °C only slightly reduced the number of fluorescent cells. While this was not a TAT derived particle, it may share a similar mechanism of entry into the cell. That is, the high multi-valency of positive charge can induce similar particulate binding to cell-surface proteoglycans and escape from endolysosomal degradation. The authors proposed formation of these hydrophobic complexes as a means to deliver otherwise unmodified proteins to the cell interior.

#### *A.6.3 Applications: Shell Cross-Linked Nanoparticles*

A stabilized micelle modified with TATp (GGGGYGRKKRRQRRR), attached by the nitrogen terminus, was prepared from shell cross-linked (SCK) nanoparticles [Liu *et al.* 2001]. These 13 nm particles are formed around a micelle that is cross-linked at its surface. The majority (68%) of particles were 13 nm in diameter as measured by dynamic light scattering; however, a significant fraction of large aggregates (329 nm) were formed (32%). It is not clear if the appearance of aggregates in the TATp modified nanoparticles

is due to an intrinsic feature of TATp or to the method used to attach the TATp to the particle surface. The fluorescent TATp nanoparticles were incubated with CHO cells and shown using confocal microscopy to bind to the cell, whereas the unmodified nanoparticles did not associate with cells; however, it was not determined if the 13 nm particle or the 329 nm particle was responsible for the cell association, so conclusions concerning the number of TATp per particle required for cell association or internalization can not be drawn from this study.

#### *A.6.4 Applications: Nanoparticles*

Magnetic resonance imaging (MRI) can be used to track the location of cells loaded with contrast enhancing agents. One such agent is a nanoparticle designated a cross-linked-iron-oxide (CLIO) nanoparticle [Josephson *et al.* 1999]. A CLIO particle has an iron oxide crystal core of about 5 nm in diameter. The iron core is covered with a biocompatible, cross-linked dextran coat. This forms a particle 41 nm in diameter that can be functionalized with different molecules and peptides at the surface. This type of cell label is of interest because *in vitro* labeled cells can be followed *in vivo* by magnetic resonance imaging. Josephson and coworkers [1999] first reported preparing TATp labeled CLIO particles by attaching TATp (GGCGRKKRRQRRRGYK[FITC]-amide) at the nitrogen terminal cysteine via a disulfide bond. These particles were determined to have about 7 peptides each. This enhanced the cellular internalization of iron by greater than 100-fold compared to non-modified particles. Over a concentration range of 1 to 100  $\mu\text{g}$  of iron per million cells, the TATp CLIO particles did not show saturation. Microscopy was employed to document that the particles had internalized. Additionally,

TATp CLIO labeled cells could be isolated by passage over a magnetic chromatography column [Josephson *et al.* 1999], permitting labeled cells to be recovered after injection into animals.

A different variation of the TATp modified CLIO particles was later prepared using a stable thio ether linkage to attach a slightly different peptide (GRKKRRQRRRGYK[FITC]C-amide) at a cysteine located at the carboxy terminus (35-36). These particles had 10 peptides each and were 65 nm in diameter. The direction of attachment had no effect upon cellular internalization. Dodd and coworkers [2001] showed that up to 30,000 particles per cell were internalized into 97% of lymphocytes treated with the 8 $\mu$ g/ml TATp CLIO nanoparticles for 18 hrs. TATp CLIO labeling of T cells also did not appear to affect cell behavior, including activation and activation-induced cell death [Dodd *et al.* 2001]. Important to the *in vivo* use of TATp modified nanoparticles, Wunderbaldinger and coworkers [2002] showed that addition of 10 TATp per particle decreased the clearance half-life in blood from 682 to 42 min compared to non-functionalized CLIO particles; however, biodistribution of the TATp functionalized particles did not differ significantly from the unmodified CLIO particles. This rapid elimination from the blood could be a troubling issue for the use of TATp modified nanoparticles to distribute to regions of the body with a small fraction of the blood flow. Most of the particles will be eliminated from the blood before a significant fraction of the dose circulates through a small target site such as a metastasis.

A third preparation of TATp modified CLIO particles was also examined [Lewin *et al.* 2000, Zhao *et al.* 2002] whereby the TATp sequence (GRKKRRQRRRGYK[FITC]C-amide) was linked to the cysteine at the carboxy terminus by a degradable disulfide bond. These particles were 45 nm in diameter. Again, the direction of attachment for the peptide did not prevent the TATp CLIO particles from binding and internalizing. The relationship between the number of TATp/particle and cell binding was examined by Zhao and coworkers [2002], who reported the effect of varying the number of TATp per particle between 1 and 15. The uptake of particles increased 100-fold when the number of TATp per particle was increased from 1.2 to 15 TATp. Again, this illustrates the cooperative nature of the binding observed with multivalent TATp particles.

#### *A.6.5 Applications: Liposomes*

Liposomes are synthetic vesicles consisting of bilayers of phospholipids similar to those found in mammalian cell membranes. Liposomes have been extensively investigated as platforms for drug, gene, and protein delivery. Neutrally charged liposomes interact poorly with cells, and these interactions are further reduced when a polyethylene glycol (PEG) polymer is attached to the surface. Such PEG shielded particles can circulate in the blood for several days. Recently, Torchilin and coworkers [2001] showed that TATp (YGRKKRRQRRR) attached via a PEG (MW = 3.0 kDa) polymer to a 200 nm diameter liposome results in improved binding and internalization. The chemistry of attachment formed an amide bond between the primary amines either at the nitrogen terminus or the lysine sidechains. With 100 to 500 peptides per liposome the particles were internalized into cytoplasmic vesicles within 1 hr. The attachment of 4.5% of 3000 Da PEG polymer

to the surface of the liposome had little effect on binding and internalization, whereas the addition of 4.5% 5000 Da PEG polymer to the liposome surface blocked binding and internalization. In contrast to the TATp modified CLIO, the direct attachment of TATp to the liposome surface did not mediate association with cells. Torchilin [2001] proposed a steric hindrance model to explain the lack of binding when TATp was attached directly to the liposome surface and to explain the ability of the 5000 Da PEG to interfere with cell association mediated by TATp coupled to the 3000 Da PEG.

In a short communication, Torchilin and colleagues reported that in addition to delivering the polyanion dextran [2002], these TATp liposomes also deliver and express DNA [2002]. Reportedly, TATp liposomes containing dextran show punctate staining within the cytoplasm within 1 hr of incubation. From 2 to 4 hrs, the staining appears near the nucleus. Between 9 and 24 hrs, released dextran becomes visible throughout the cell. Torchilin also reported the transfection of cells with TATp liposomes [Torchilin 2002]. TATp labeled liposomes were prepared with less than 10% of the positively charged lipid DOTAP, needed to form a complex with DNA. The liposomes and DNA were mixed together and placed on cells. Torchilin reports that TATp enabled this complex to transfect a high percentage of cells while TATp deficient complexes could not [2002]. No obvious signs of cytotoxicity were reported.

Tseng and coworkers [2002] have studied the kinetics of TATp modified liposomes with varied numbers of peptides on the particle surface. They conjugated the TATp sequence (CYGRKKRRQRRRPPQ) to a PEG (MW = 3.4 kDa) phosphatidylethanolamine. The



chemistry of attachment was to the nitrogen terminal cysteine via a stable thio ether bond. The TATp-PEG-lipid was inserted into preformed phosphatidylcholine: cholesterol (6:4) 100 nm liposomes using a micelle insertion method. Greater than 90% insertion of TATp-PEG-lipid occurred in all preparations. Liposomes containing a pH sensitive dye, 8-hydroxypyrene-1,3,6-trisulfonic acid, were incubated with cells, and fluorescence was assayed using FACS. Tseng and coworkers [2002] showed that increasing numbers of peptides per particle raised the fluorescence substantially. Internalization was evident with above 5 peptides per particle. This increase in fluorescence began to saturate by 50 to 100 peptides per particle for HTB-9 cells, but continued to increase linearly for A431 cells. The fact that a pH sensitive dye greatly increases in fluorescence upon binding strongly suggests that TATp labeled liposomes are entrapped separate from the cytoplasm, in a low pH compartment.

Additionally, Tseng and coworkers [2002] used Doxorubicin (Dox) loaded TATp modified liposomes and measured cell proliferation and tumor killing. *In vitro* cell assays showed that TATp modified Dox loaded liposomes delivered 12-fold more Dox than unmodified Dox loaded liposomes at 2 hrs incubation with 1  $\mu$ g Dox / ml. Still, the TATp modified Dox liposomes delivered about half as much Dox as that delivered by free drug. Cell proliferation assays revealed that TATp modified Dox loaded liposomes were only slightly more effective at reducing cell growth than were the unmodified liposomes. In summary, free Dox had the most antiproliferative activity, while liposomal entrapped Dox reduced cellular exposure, with or without TATp modification.

Having shown a 12-fold improvement in delivery of Dox by TATp modification of the liposomes, Tseng and coworkers [2002] presented data from an *in vivo* test. They monitored tumor size as a function of time after treatment in a BALB/c mouse C26 hind limb tumor model. Both liposomal Dox formulations reduced tumor growth rate better than treatment with free drug; however, for the Dox loaded liposomes, there was no significant difference between the groups treated with or without TATp modification. A likely explanation is that the presence of TATp on the liposome surface enhanced their elimination from circulation as was observed with the CLIO nanoparticles. This result illustrates a potential pitfall of TATp modified particles *in vivo*.

#### *A.6.6 Applications: Phage*

TATp has also been used to modify biological viral particles for improved transfection. Eguchi and coworkers [2001] created a variant of the lambda bacteriophage that expresses TATp on its capsid. They engineered a fusion protein of the TATp sequence (MLGISYGRKKRRRQRRRPPPPQT) connected at the carboxy terminal residue to the D coat protein. A single Lambda phage, 55 nm in diameter, would express 420 TATp - D fusion proteins. Interestingly, these bacteriophage were able to transfect mammalian cells. Eguchi and coworkers [2001] compared the TATp phage both with normal phage and phage modified with an integrin binding RGD sequence. The unmodified phage showed minimal cellular binding, while both the RGD and TATp modified phage showed strong cellular binding.

*In vitro*, the TATp modified phage showed the most significant transfection with 30% of

the cells transfected with  $10^6$  particles/cell [Eguchi *et al.* 2001]. Interestingly, the presence of serum in the media significantly accelerated the kinetics of transfection in COS-1 cells. Typically, serum proteins interfere with cationic transfection reagents, but this is not the case for TATp modified phage. The authors also investigated the possibility that potocytosis is involved with the uptake of TATp phage. COS-1 cells were incubated with TATp phage with or without the presence of filipin and nystatin, inhibitors of caveolae internalization. Both filipin and nystatin caused a 50% decrease in luciferase transfection compared to a control with no inhibitor. This result suggests that potocytosis may play a role in TATp mediated internalization of nanoparticles. *In vivo*, TATp phage mediated GFP transfection of mouse liver, as observed by microscopy. The authors concluded that the binding and internalization seen in the TAT phage were dependent upon a low affinity absorption process and that internalization may be partly due to potocytosis.

#### A.7 Conclusions

The HIV TAT peptide can effectively increase the binding and internalization to a wide array of cells both *in vivo* and *in vitro*. Nanoparticles between 13 and 200 nm in diameter with between 5 and 500 TAT peptides per particle show high avidity for poly-anions on the cell-surface such as heparan sulfate proteoglycans. As evidenced by pH sensitive dyes, TATp modified particles are targeted to low pH compartments, which may be independent from the classical lysosomal degradation pathway. This precludes the possibility that TATp nanoparticles have direct access to the cytosol, but instead must traffic through a vesicle, such as a caveolae or endosome. The true mechanism of

internalization has been difficult to determine, especially in light of recently described fixation artifacts; however, some of the internalized cargo must reach the cytoplasm and nucleus because of the expression of proteins from delivered DNA. Lastly, the presence of unshielded TATp on a nanoparticle surface may greatly hinder its usefulness for intravenous administration. Without blocking TATp activity, injected nanoparticles may be rapidly cleared from the bloodstream. Regardless, the use of TATp for delivering therapeutic cargo is not restricted to small molecules and proteins, but extends to a variety of large polymers and nanoparticles.

## REFERENCES

Abra RM, Schreier H, Szoka FC Jr. The use of a new radioactive-iodine labeled lipid marker to follow in vivo disposition of liposomes: comparison with an encapsulated aqueous space marker. *Res Commun Chem Pathol Pharmacol*. 1982 Aug;37(2): 199-213.

American Cancer Society. Cancer Facts and Figures 2002. [www.cancer.org](http://www.cancer.org).

Bankiewicz KS, Eberling JL, Kohutnicka M, Jagust W, Pivrotto P, Bringas J, Cunningham J, Budinger TF, Harvey-White J. Convection-enhanced delivery of AAV vector in parkinsonian monkeys; in vivo detection of gene expression and restoration of dopaminergic function using pro-drug approach. *Exp Neurol*. 2000 Jul;164(1): 2-14.

Barron LG, Szoka FC Jr. The Perplexing Delivery Mechanism of Lipoplexes. *Nonviral Vectors for Gene Therapy*. Huang L, Hung M, Wagner E, Eds. Academic Press: San Diego, 1999; 229-266.

Bartlett GR. Phosphorous assay in column chromatography. *J Bio Chem*. 1959; 234: 466-468.

Betz AL, Shakui P, Davidson BL. Gene transfer to rodent brain with recombinant adenoviral vectors: effects of infusion parameters, infectious titer, and virus concentration on transduction volume. *Exp Neurol*. 1998 Mar; 150(1): 136-42.

Bhorade R, Weissleder R, Nakakoshi T, Moore A, Tung CH. Macrocyclic chelators with paramagnetic cations are internalized into mammalian cells via a HIV-tat derived membrane translocation peptide. *Bioconjug Chem*. 2000 May-Jun; 11(3): 301-5.

Bobo RH, Laske DW, Akbasak A, Morrison PF, Dedrick RL, Oldfield EH. Convection-enhanced delivery of macromolecules in the brain. *Proc Natl Acad Sci U S A*. 1994 Mar 15; 91(6): 2076-80.

Bruce JN, Falavigna A, Johnson JP, Hall JS, Birch BD, Yoon JT, Wu EX, Fine RL, Parsa AT. Intracerebral clysis in a rat glioma model. *Neurosurgery*. 2000 Mar; 46(3): 683-91.

Cao YJ, Shibata T, Rainov NG. Liposome-mediated transfer of the bcl-2 gene results in neuroprotection after in vivo transient focal cerebral ischemia in an animal model. *Gene Ther*. 2002; 9: 415-419.

Carson BS Sr, Wu Q, Tyler B, Sukay L, Raychaudhuri R, DiMeco F, Clatterbuck RE, Olivi A, Guarnieri M. New approach to tumor therapy for inoperable areas of the brain: chronic intraparenchymal drug delivery. *J Neurooncol*. 2002 Nov; 60(2):151-8.

Chang HC, Samaniego F, Nair BC, Buonaguro L, Ensoli B. HIV-1 Tat protein exits from cells via a leaderless secretory pathway and binds to extracellular matrix-associated heparan sulfate proteoglycans through its basic region. *AIDS*. 1997; 11(12): 1421-1431.

Chen MY, Lonser RR, Morrison PF, Governale LS, Oldfield EH. Variables affecting convection-enhanced delivery to the striatum: a systematic examination of rate of infusion, cannula size, infusate concentration, and tissue-cannula sealing time. *J Neurosurg.* 1999 Feb; 90(2): 315-20.

Choi JS, MacKay JA, Szoka FC Jr. Low-pH-sensitive PEG-stabilized plasmid-lipid nanoparticles: preparation and characterization. *Bioconjug Chem.* 2003 Mar-Apr; 14(2): 420-9.

Cullis PR, Tilcock CP, Hope MJ. Lipid polymorphism. *Membrane Fusion.* Wilschut J, Hoekstra D, Eds. Marcel Dekker, Inc.: New York, 1991: 35-64.

Cunningham J, Oiwa Y, Nagy D, Podsakoff G, Colosi P, Bankiewicz KS. Distribution of AAV-TK following intracranial convection-enhanced delivery into rats. *Cell Transplant.* 2000 Sep-Oct; 9(5): 585-94.

Derossi D, Calvet S, Trembleau A, Brunissen A, Chassaing G, Prochiantz A. Cell internalization of the third helix of the Antennapedia homeodomain is receptor-independent. *J Biol Chem.* 1996; 271(30): 18188-18193.

Dodd CH, Hsu HC, Chu WJ, Yang P, Zhang HG, Mountz JD Jr, Zinn K, Forder J, Josephson L, Weissleder R, Mountz JM, Mountz JD. Normal T-cell response and in vivo magnetic resonance imaging of T cells loaded with HIV transactivator-peptide-derived superparamagnetic nanoparticles. *J Immunol Methods.* 2001; 256(1-2): 89-105.

Drummond DC, Zignani M, Leroux J. Current status of pH-sensitive liposomes in drug delivery. *Prog Lipid Res.* 2000 Sep; 39(5): 409-60.

Eguchi A, Akuta T, Okuyama H, Senda T, Yokoi H, Inokuchi H, Fujita S, Hayakawa T, Takeda K, Hasegawa M, Nakanishi M. Protein transduction domain of HIV-1 Tat protein promotes efficient delivery of DNA into mammalian cells. *J Biol Chem.* 2001; 276(28): 26204-26210.

Eliasz RE, Szoka FC Jr. Liposome-encapsulated doxorubicin targeted to CD44: a strategy to kill CD44-overexpressing tumor cells. *Cancer Res.* 2001 Mar 15; 61(6): 2592-601.

Ellens H, Bentz J, Szoka FC Jr. pH-induced destabilization of phosphatidylethanolamine-containing liposomes: role of bilayer contact. *Biochemistry.* 1984 Mar 27; 23(7): 1532-8.

Fenske DB, MacLachlan I, Cullis PR. Long-circulating vectors for the systemic delivery of genes. *Curr Opin Mol Ther.* 2001; 3: 153-158.

Fretz MM, Koning GA, Mastrobattista E, Jiskoot W, Storm G. OVCAR-3 cells internalize TAT-peptide modified liposomes by endocytosis. *Biochim Biophys Acta.* 2004 Oct 11; 1665(1-2): 48-56.

Futaki S, Nakase I, Suzuki T, Youjun Z, Sugiura Y. Translocation of branched-chain arginine peptides through cell membranes: flexibility in the spatial disposition of positive charges in membrane-permeable peptides. *Biochemistry*. 2002; 41(25): 7925-7930.

Groothuis DR. The blood-brain and blood-tumor barriers: a review of strategies for increasing drug delivery. *Neuro-oncol*. 2000 Jan; 2(1): 45-59.

Groothuis DR, Ward S, Itskovich AC, Dobrescu C, Allen CV, Dills C, Levy RM. Comparison of <sup>14</sup>C-sucrose delivery to the brain by intravenous, intraventricular, and convection-enhanced intracerebral infusion. *J Neurosurg*. 1999 Feb; 90(2): 321-31.

Groothuis DR, Ward S, Itskovich AC, Dobrescu C, Allen CV, Dills C, Levy RM. Comparison of <sup>14</sup>C-sucrose delivery to the brain by intravenous, intraventricular, and convection-enhanced intracerebral infusion. *J Neurosurg*. 1999 Feb;90(2): 321-31.

Guo X, Szoka FC Jr. Steric stabilization of fusogenic liposomes by a low-pH sensitive PEG--diortho ester--lipid conjugate. *Bioconjug Chem*. 2001 Mar-Apr; 12(2): 291-300.

Guo X, MacKay JA, Szoka FC Jr. Mechanism of pH-triggered collapse of phosphatidylethanolamine liposomes stabilized by an ortho ester polyethyleneglycol lipid. *Biophys J*. 2003 Mar; 84(3): 1784-95.

Guo X, Huang Z, Szoka FC Jr. Improved preparation of PEG-diortho ester-diacyl glycerol conjugates. *Methods Enzymol*. 2004; 387: 147-52.

Hamilton JF, Morrison PF, Chen MY, Harvey-White J, Pernaute RS, Phillips H, Oldfield E, Bankiewicz KS. Heparin coinfusion during convection-enhanced delivery (CED) increases the distribution of the glial-derived neurotrophic factor (GDNF) ligand family in rat striatum and enhances the pharmacological activity of neurturin. *Exp Neurol*. 2001 Mar; 168(1): 155-61.

Harvie P, Wong FM, Bally MB. Use of poly(ethylene glycol)-lipid conjugates to regulate the surface attributes and transfection activity of lipid-DNA particles. *J Pharm Sci*. 2000 May; 89(5): 652-63.

Hirko AC, Buethe DD, Meyer EM, Hughes JA. Plasmid delivery in the rat brain. *Biosci Rep*. 2002 Apr; 22(2): 297-308.

Hood JD, Bednarski M, Frausto R, Guccione S, Reisfeld RA, Xiang R, Cheresch DA. Tumor regression by targeted gene delivery to the neovasculature. *Science*. 2002 Jun 28; 296(5577): 2404-7.

Huang L, Hung M, Wagner E. Eds. *Nonviral Vectors for Gene Therapy*. Academic Press: San Diego, 1999.

Huang SY, Pooyan S, Wang J, Choudhury I, Leibowitz MJ, Stein S. A polyethylene glycol copolymer for carrying and releasing multiple copies of cysteine-containing peptides. *Bioconjug Chem.* 1998; 9(5): 612-617.

Huang Z, Li W, Mackay JA, Szoka FC Jr. Thiocholesterol-based lipids for ordered assembly of bioresponsive gene carriers. *Mol Ther.* 2005 Mar; 11(3): 409-17.

Imaoka T, Date I, Ohmoto T, Yasuda T, Tsuda M. In vivo gene transfer into the adult mammalian central nervous system by continuous injection of plasmid DNA-cationic liposome complex. *Brain Res.* 1998 Jan 5; 780(1): 119-28.

Jain RK. Delivery of molecular medicine to solid tumors: lessons from in vivo imaging of gene expression and function. *J Controlled Release.* 2001; 74: 7-25.

Josephson L, Tung CH, Moore A, Weissleder R. High-efficiency intracellular magnetic labeling with novel superparamagnetic-Tat peptide conjugates. *Bioconjug Chem.* 1999; 10(2): 186-191.

Kaiser MG, Parsa AT, Fine RL, Hall JS, Chakrabarti I, Bruce JN. Tissue distribution and antitumor activity of topotecan delivered by intracerebral clysis in a rat glioma model. *Neurosurgery.* 2000 Dec; 47(6): 1391-8, discussion 1398-9.

Kaneda Y. Virosomes: evolution of the liposome as a targeted drug delivery system. *Adv Drug Deliv Rev.* 2000 Sep 30; 43(2-3): 197-205.

Kaye AH, Laws ER Jr. *Brain Tumors.* Churchill Livingstone: New York, 1995.

Kroll RA, Pagel MA, Muldoon LL, Roman-Goldstein S, Neuwelt EA. Increasing volume of distribution to the brain with interstitial infusion: dose, rather than convection, might be the most important factor. *Neurosurgery.* 1996 Apr; 38(4): 746-52.

Leone P, Janson CG, Bilaniuk L, Wang Z, Sorgi F, Huang L, Matalon R, Kaul R, Zeng Z, Freese A, McPhee SW, Mee E, During MJ. Aspartoacylase gene transfer to the mammalian central nervous system with therapeutic implications for Canavan disease. *Ann Neurol.* 2000 Jul; 48(1): 27-38.

Levy RM, Major E, Ali MJ, Cohen B, Groothuis D. Convection-enhanced intraparenchymal delivery (CEID) of cytosine arabinoside (AraC) for the treatment of HIV-related progressive multifocal leukoencephalopathy (PML). *J Neurovirol.* 2001 Aug; 7(4): 382-5.

Lewin M, Carlesso N, Tung CH, Tang XW, Cory D, Scadden DT, Weissleder R. Tat peptide-derivatized magnetic nanoparticles allow in vivo tracking and recovery of progenitor cells. *Nat Biotechnol.* 2000; 18(4): 410-414.



Li W, Huang Z, MacKay JA, Grube S, Szoka FC Jr. Low-pH-sensitive poly(ethylene glycol) (PEG)-stabilized plasmid nanolipoparticles: effects of PEG chain length, lipid composition and assembly conditions on gene delivery. *J Gene Med.* 2005 Jan; 7(1): 67-79.

Lieberman DM, Laske DW, Morrison PF, Bankiewicz KS, Oldfield EH. Convection-enhanced distribution of large molecules in gray matter during interstitial drug infusion. *J Neurosurg.* 1995 Jun; 82(6): 1021-9.

Liu J, Zhang Q, Remsen EE, Wooley KL. Nanostructured materials designed for cell binding and transduction. *Biomacromolecules.* 2001; 2(2): 362-368.

Leifert JA, Harkins S, Whitton JL. Full-length proteins attached to the HIV tat protein transduction domain are neither transduced between cells, nor exhibit enhanced immunogenicity. *Gene Ther.* 2002; 9(21): 1422-1428.

Lonser RR, Corthesy ME, Morrison PF, Gogate N, Oldfield EH. Convection-enhanced selective excitotoxic ablation of the neurons of the globus pallidus internus for treatment of parkinsonism in nonhuman primates. *J Neurosurg.* 1999 Aug; 91(2): 294-302.

Lonser RR, Walbridge S, Garmestani K, Butman JA, Walters HA, Vortmeyer AO, Morrison PF, Brechbiel MW, Oldfield EH. Successful and safe perfusion of the primate brainstem: in vivo magnetic resonance imaging of macromolecular distribution during infusion. *J Neurosurg.* 2002 Oct; 97(4): 905-13.

Lundberg M, Johansson M. Is VP22 nuclear homing an artifact? *Nat Biotechnol.* 2001; 19(8): 713.

Lundberg M, Johansson M. Positively charged DNA-binding proteins cause apparent cell membrane translocation. *Biochem Biophys Res Commun.* 2002; 291(2): 367-371.

Mamot C, Nguyen JB, Pourdehnad M, Hadaczek P, Saito R, Bringas JR, Drummond DC, Hong K, Kirpotin DB, McKnight T, Berger MS, Park JW, Bankiewicz KS. Extensive distribution of liposomes in rodent brains and brain tumors following convection-enhanced delivery. *J Neurooncol.* 2004 May; 68(1): 1-9.

Mann DA, Frankel AD. Endocytosis and targeting of exogenous HIV-1 Tat protein. *EMBO J.* 1991; 10(7): 1733-1739.

Mardor Y, Roth Y, Lidar Z, Jonas T, Pfeffer R, Maier SE, Faibel M, Nass D, Hadani M, Orenstein A, Cohen JS, Ram Z. Monitoring response to convection-enhanced taxol delivery in brain tumor patients using diffusion-weighted magnetic resonance imaging. *Cancer Res.* 2001 Jul 1; 61(13): 4971-3.

Mi Z, Mai J, Lu X, Robbins PD. Characterization of a class of cationic peptides able to facilitate efficient protein transduction in vitro and in vivo. *Mol. Ther.* 2000; 2(4): 339-347.

Mok KW, Lam AM, Cullis PR. Stabilized plasmid-lipid particles: factors influencing plasmid entrapment and transfection properties. *Biochim Biophys Acta.* 1999 Jul 15; 1419(2): 137-50.

Monnard PA, Oberholzer T, Luisi P. Entrapment of nucleic acids in liposomes. *Biochim Biophys Acta.* 1997 Oct 2; 1329(1): 39-50.

Morris MC, Depollier J, Mery J, Heitz F, Divita G. A peptide carrier for the delivery of biologically active proteins into mammalian cells. *Nat Biotechnol.* 2001; 19(12): 1173-1176.

Morrison PF, Laske DW, Bobo H, Oldfield EH, Dedrick RL. High-flow microinfusion: tissue penetration and pharmacodynamics. *Am J Physiol.* 1994 Jan; 266(1 Pt 2): R292-305.

Nguyen JB, Sanchez-Pernaute R, Cunningham J, Bankiewicz KS. Convection-enhanced delivery of AAV-2 combined with heparin increases TK gene transfer in the rat brain. *Neuroreport.* 2001 Jul 3; 12(9): 1961-4.

Ono T, Fujino Y, Tsuchiya T, Tsuda M. Plasmid DNAs directly injected into mouse brain with lipofectin can be incorporated and expressed by brain cells. *Neurosci Lett.* 1990 Sep 18; 117(3): 259-63.

Paxinos G, Watson C. *The Rat Brain in Stereotaxic Coordinates.* Academic Press: New York, 1982.

Polfliet MM, Goede PH, van Kesteren-Hendriks EM, van Rooijen N, Dijkstra CD, van den Berg TK. A method for the selective depletion of perivascular and meningeal macrophages in the central nervous system. *J Neuroimmunol.* 2001 Jun 1; 116(2): 188-95.

Polyakov V, Sharma V, Dahlheimer JL, Pica CM, Luker GD, Piwnica-Worms D. Novel Tat-peptide chelates for direct transduction of technetium-99m and rhenium into human cells for imaging and radiotherapy. *Bioconjug Chem.* 2000 Nov-Dec; 11(6): 762-71.

Richard JP, Melikov K, Vives E, Ramos C, Verbeure B, Gait MJ, Chernomordik LV, Lebleu B. Cell-penetrating peptides: A re-evaluation of the mechanism of cellular uptake. *J Biol Chem.* 2003; 278(1): 585-590.

Roessler BJ, Davidson BL. Direct plasmid mediated transfection of adult murine brain cells in vivo using cationic liposomes. *Neurosci Lett.* 1994 Feb 14; 167(1-2): 5-10.

Ruan H, Deen DF. Use of hypoxia-regulated gene expression in tumor-specific gene therapy. *Curr Opin Investig Drugs*. 2001 Jun; 2(6): 839-43.

Rusnati M, Coltrini D, Oreste P, Zoppetti G, Albini A, Noonan D, d'Adda di Fagagna F, Giacca M, Presta M. Interaction of HIV-1 Tat protein with heparin. Role of the backbone structure, sulfation, and size. *J Biol Chem*. 1997; 272 (17): 11313-11320.

Rusnati M, Tulipano G, Spillmann D, Tanghetti E, Oreste P, Zoppetti G, Giacca M, Presta M. Multiple interactions of HIV-I Tat protein with size-defined heparin oligosaccharides. *J Biol Chem*. 1999; 274 (40): 28198-28205.

Saito R, Bringas JR, McKnight TR, Wendland MF, Mamot C, Drummond DC, Kirpotin DB, Park JW, Berger MS, Bankiewicz KS. Distribution of liposomes into brain and rat brain tumor models by convection-enhanced delivery monitored with magnetic resonance imaging. *Cancer Res*. 2004 Apr 1; 64(7): 2572-9.

Saltzman WM, Mak MW, Mahoney MJ, Duenas ET, Cleland JL. Intracranial delivery of recombinant nerve growth factor: release kinetics and protein distribution for three delivery systems. *Pharm Res*. 1999 Feb; 16(2): 232-40.

Sandberg DI, Edgar MA, Souweidane MM. Effect of hyperosmolar mannitol on convection-enhanced delivery into the rat brain stem. *J Neurooncol*. 2002 Jul; 58(3): 187-92.

Sandberg DI, Edgar MA, Souweidane MM. Convection-enhanced delivery into the rat brainstem. *J Neurosurg*. 2002 May; 96(5): 885-91.

Sandgren S, Cheng F, Belting M. Nuclear targeting of macromolecular polyanions by an HIV-Tat derived peptide. Role for cell-surface proteoglycans. *J Biol Chem*. 2002; 277(41): 38877-38883.

Schwarze SR, Ho A, Vocero-Akbani A, Dowdy SF. In vivo protein transduction: delivery of a biologically active protein into the mouse. *Science*. 1999 Sep 3; 285(5433): 1569-72.

Shukla D, Spear PG. Herpesviruses and heparan sulfate: an intimate relationship in aid of viral entry. *J Clin Invest*. 2001; 108: 503-510.

Shimada K, Miyagishima A, Sadzuka Y, Nozawa Y, Mochizuki Y, Ohshima H, Hirota S. Determination of the thickness of the fixed aqueous layer around polyethyleneglycol-coated liposomes. *J Drug Target*. 1995; 3(4): 283-9.

Silhol M, Tyagi M, Giacca M, Lebleu B, Vives E. Different mechanisms for cellular internalization of the HIV-1 Tat-derived cell penetrating peptide and recombinant proteins fused to Tat. *Eur J Biochem*. 2002; 269(2): 494-501.

Silva-Barcellos NM, Caligiorme S, dos Santos RA, Frezard F. Site-specific microinjection of liposomes into the brain for local infusion of a short-lived peptide. *J Control Release*. 2004 Mar 5; 95(2): 301-7.

Sonawane ND, Thiagarajah JR, Verkman AS. Chloride concentration in endosomes measured using a ratioable fluorescent Cl<sup>-</sup> indicator: evidence for chloride accumulation during acidification. *J Biol Chem*. 2002 Feb 15; 277(7): 5506-13

Stein S, Weiss A, Adermann K, Lazarovici P, Hochman J, Wellhoner H. A disulfide conjugate between anti-tetanus antibodies and HIV (37-72)Tat neutralizes tetanus toxin inside chromaffin cells. *FEBS Lett*. 1999 Sep 24; 458(3): 383-6.

Suzuki T, Futaki S, Niwa M, Tanaka S, Ueda K, Sugiura Y. Possible existence of common internalization mechanisms among arginine-rich peptides. *J Biol Chem*. 2002; 277(4): 2437-2443.

Tam P, Monck M, Lee D, Ludkovski O, Leng EC, Clow K, Stark H, Scherrer P, Graham RW, Cullis PR. Stabilized plasmid-lipid particles for systemic gene therapy. *Gene Ther*. 2000 Nov; 7(21): 1867-74.

Thorsell A, Fox E, Heilig M. Lipid mediated gene delivery in the adult rat brain: quantitative analysis of expression. *Neurochem Int*. 1999; 35: 65-71.

Torchilin VP. TAT peptide-modified liposomes for intracellular delivery of drugs and DNA. *Cell Mol Biol Lett*. 2002; 7(2): 265-267.

Torchilin VP, Rammohan R, Weissig V, Levchenko TS. TAT peptide on the surface of liposomes affords their efficient intracellular delivery even at low temperature and in the presence of metabolic inhibitors. *Proc Natl Acad Sci U S A*. 2001; 98(15): 8786-8791.

Tseng YL, Liu JJ, Hong RL. Translocation of liposomes into cancer cells by cell-penetrating peptides penetratin and tat: a kinetic and efficacy study. *Mol Pharmacol*. 2002 Oct; 62(4): 864-72.

Tyagi M, Rusnati M, Presta M, Giacca M. Internalization of HIV-1 tat requires cell surface heparan sulfate proteoglycans. *J Biol Chem*. 2001 Feb 2; 276(5): 3254-61.

Uyechi LS, Gagne L, Thurston G, Szoka FC Jr. Mechanism of lipoplex gene delivery in mouse lung: binding and internalization of fluorescent lipid and DNA components. *Gene Ther*. 2001 Jun; 8(11): 828-36.

Vander AJ, Sherman JH, Luciano DS. *Human Physiology: the Mechanisms of Body Function*. McGraw-Hill: New York, 1994.

Vives E, Brodin P, Lebleu B. A truncated HIV-1 Tat protein basic domain rapidly translocates through the plasma membrane and accumulates in the cell nucleus. *J Biol Chem.* 1997; 272(25): 16010-16017.

Voges J, Reszka R, Gossmann A, Dittmar C, Richter R, Garlip G, Kracht L, Coenen HH, Sturm V, Wienhard K, Heiss WD, Jacobs AH. Imaging-guided convection-enhanced delivery and gene therapy of glioblastoma. *Ann Neurol.* 2003 Oct; 54(4): 479-87.

Voges J, Weber F, Reszka R, Sturm V, Jacobs A, Heiss WD, Wiestler O, Kapp JF. Clinical protocol. Liposomal gene therapy with the herpes simplex thymidine kinase gene/ganciclovir system for the treatment of glioblastoma multiforme. *Hum Gene Ther.* 2002 Mar 20; 13(5): 675-85.

Viola JJ, Agbaria R, Walbridge S, Oshiro EM, Johns DG, Kelley JA, Oldfield EH, Ram Z. In situ cyclopentenyl cytosine infusion for the treatment of experimental brain tumors. *Cancer Res.* 1995 Mar 15; 55(6): 1306-9.

Watson K, Gooderham NJ, Davies DS, Edwards RJ. Interaction of the transactivating protein HIV-1 tat with sulphated polysaccharides. *Biochem Pharmacol.* 1999; 57(7): 775-783.

Wender PA, Mitchell DJ, Pattabiraman K, Pelkey ET, Steinman L, Rothbard JB. The design, synthesis, and evaluation of molecules that enable or enhance cellular uptake: peptoid molecular transporters. *Proc Natl Acad Sci U S A.* 2000; 97(24): 13003-13008.

Weyerbrock A, Oldfield EH. Gene transfer technologies for malignant gliomas. *Curr Opin Oncol.* 1999; 11: 168-73.

Wheeler JJ, Palmer L, Ossanlou M, MacLachlan I, Graham RW, Zhang YP, Hope MJ, Scherrer P, Cullis PR. Stabilized plasmid-lipid particles: construction and characterization. *Gene Ther.* 1999 Feb; 6(2): 271-81.

Wunderbaldinger P, Josephson L, Weissleder R. Tat peptide directs enhanced clearance and hepatic permeability of magnetic nanoparticles. *Bioconjug Chem.* 2002; 13(2): 264-268.

Wyman TB, Nicol F, Zelphati O, Scaria PV, Plank C, Szoka FC Jr. Design, synthesis, and characterization of a cationic peptide that binds to nucleic acids and permeabilizes bilayers. *Biochemistry.* 1997; 36: 3008 - 3017.

Xia H, Mao Q, Davidson BL. The HIV Tat protein transduction domain improves the biodistribution of beta-glucuronidase expressed from recombinant viral vectors. *Nat Biotechnol.* 2001; 19(7): 640-644.

Xu Y, Hui SW, Frederik P, Szoka FC Jr. Physicochemical characterization and purification of cationic lipoplexes. *Biophys J.* 1999 Jul; 77(1): 341-53.

Zhao M, Kircher MF, Josephson L, Weissleder R. Differential conjugation of tat peptide to superparamagnetic nanoparticles and its effect on cellular uptake. *Bioconjug Chem.* 2002; 13(4): 840-844.



# For reference

Not to be taken  
from the room.

8070990



3 1378 00807 0990



